THESIS FOR THE DEGREE OF DOCTOR OF PHILOSOPHY

Superconducting lumped-element travelling-wave parametric amplifiers

A theoretical and experimental study of superconducting travelling-wave parametric amplifiers for wideband microwave amplification with quantum-limited noise performance

Hampus Renberg Nilsson

CHALMERS
UNIVERSITY OF TECHNOLOGY

Department of Microtechnology and Nanoscience
Chalmers University of Technology
Gothenburg, Sweden, 2024

Superconducting lumped-element travelling-wave parametric amplifiers
A theoretical and experimental study of superconducting travelling-wave parametric amplifiers for wideband microwave amplification with quantum-limited noise performance

Hampus Renberg Nilsson

ISBN: 978-91-8103-104-1
Löpnummer: 5562
i serien Doktorsavhandlingar vid Chalmers tekniska högskola.
Ny serie (ISSN 0346-718X)
Acknowledgements, dedications, and similar personal statements in this thesis, reflect the author's own views.
This thesis has been prepared using LaTeX.

Department of Microtechnology and Nanoscience
Chalmers University of Technology
SE-412 96 Gothenburg, Sweden
Phone: +46 (0)31 772 1000
www.chalmers.se

The project was supported by the Knut and Alice Wallenberg foundation via the Wallenberg Centre for Quantum Technology

Cover
A TWPA wired to a box with an illustration of the amplification process

Printed by Chalmers Reproservice
Gothenburg, Sweden, August 2024

To my future children

Superconducting lumped-element travelling-wave parametric amplifiers

A theoretical and experimental study of superconducting travelling-wave parametric amplifiers for wideband microwave amplification with quantum-limited noise performance

Hampus Renberg Nilsson
Department of Microtechnology and Nanoscience
Gothenburg, Sweden, August 2024

Abstract

In this thesis we explore, theoretically and experimentally, the requirements of developing an ideal low-noise amplifier for amplifying signals close to the quantum limit, such as signals used in superconducting quantum systems. The work is focused on how to enable exponential amplification in a travelling-wave parametric amplifier (TWPA), especially the ones based on three-wave mixing (3WM), although four-wave mixing (4WM) is also treated. These amplifiers are composed of a long chain of cascaded nonlinear inductors and capacitors that form a lumped-element transmission line. The nonlinearity of the inductive element in each unitcell provides the possibility of frequency mixing between the input signal and a strong pump. As a result, some of the pump energy may be transferred to the signal (desired) and to up-converted frequencies (undesired). We extend the theory of the continuous three-mode model for 3WM, both for a discrete chain at frequencies close to the spectral cut-off, as well as for small frequencies with an arbitrary amount of up-converted modes included. In both cases we find that the gain is significantly reduced compared to the prediction by the continuous three-mode model. Based on our findings, we propose a prototype that uses frequencies close to the cut-off frequency to prevent up-conversion, resonant phase matching for phase matching and impedance matching networks for impedance matching. The developed prototype shows very promising results, presented in one of the appended papers, with the possibility of achieving a high gain of $\sim 20\,\mathrm{dB}$ in a wide band of several GHz, using only 200 unitcells. Finally we investigate the required peripheral circuitry to suppress leakage and provide isolation.

Keywords: Josephson junction, rf-SQUID, SNAIL, parametric amplifier, quantum-limited amplifier, parametric amplification, travelling-wave parametric amplifier, three-wave mixing, four-wave mixing, lumped-element, resonant phase matching, down-conversion, up-conversion.

List of Publications

This thesis is based on the following publications:

[A] **Hampus Renberg Nilsson**, Anita Fadavi Roudsari, Daryoush Shiri, Per Delsing, Vitaly Shumeiko, "High-Gain Traveling-Wave Parametric Amplifier Based on Three-Wave Mixing". Phys. Rev. Appl., **19**, 044056 (2023).

[B] Anita Fadavi Roudsari, Daryoush Shiri, **Hampus Renberg Nilsson**, Giovanna Tancredi, Amr Osman, Ida-Maria Svensson, Marina Kudra, Marcus Rommel, Jonas Bylander, Vitaly Shumeiko and Per Delsing, "Three-wave mixing traveling-wave parametric amplifier with periodic variation of the circuit parameters". Appl. Phys. Lett., **122**, 052601 (2023).

[C] **Hampus Renberg Nilsson**, Daryoush Shiri, Robert Rehammar, Anita Fadavi Roudsari, Per Delsing, "Peripheral circuits for ideal performance of a travelling-wave parametric amplifier". Phys. Rev. Appl., **21**, 064062 (2024).

[D] Daryoush Shiri, **Hampus Renberg Nilsson**, Pavan Telluri, Anita Fadavi Roudsari, Vitaly Shumeiko, Christian Fager, Per Delsing, "Modeling and Harmonic Balance Analysis of Parametric Amplifiers for Qubit Read-out". arXiv:2306.05177. Accepted for publication in IEEE Microwave Magazine.

[E] **Hampus Renberg Nilsson**, Liangyu Chen, Giovanna Tancredi, Robert Rehammar, Daryoush Shiri, Filip Nilsson, Amr Osman, Vitaly Shumeiko, Per Delsing, "A small footprint travelling-wave parametric amplifier with a high Signal-to-Noise Ratio improvement in a wide band". arXiv:2408.16366.

Other publications by the author, not included in this thesis, are:

[F] **Hampus Renberg Nilsson**, "Characterisation of a travelling-wave parametric amplifier for improved qubit measurements". *Master's thesis*, Chalmers University of Technology, Gothenburg, Sweden, June 2019.

[G] Yong Lu, Andreas Bengtsson, Jonathan J. Burnett, Baladitya Suri, Sankar Raman Sathyamoorthy, **Hampus Renberg Nilsson**, Marco Scigliuzzo, Jonas Bylander, Göran Johansson, Per Delsing, "Quantum efficiency, purity and stability of a tunable, narrowband microwave single-photon source". npj Quantum Information, **7**, 140 (2021).

[H] **Hampus Renberg Nilsson**, "Three-wave mixing in Josephson travelling-wave parametric amplifiers". *Licentiate thesis*, Chalmers University of Technology, Gothenburg, Sweden, May 2022.

Acknowledgements

This thesis and its corresponding publications are the result of six years of work at the Quantum Technology Laboratory at Chalmers University of Technology, funded by the Knut and Alice Wallenberg Foundation via Wallenberg Center for Quantum Technology, first during the work on my Master's thesis, and then as a doctoral student. During this time I have got help and support from multiple people, to whom I wish to show my gratitude.

First and foremost I would like to thank Prof. Per Delsing who has been my main supervisor, both during the work on my Master's thesis, and during the time as a doctoral student. With many meetings, insights, guidance, and support, you have helped me steer towards success.

Next I would like to thank Dr. Anita Fadavi Roudsari, who has been my assistant supervisor. With weekly meetings, discussions and guidance on fabrication, you have helped me a lot.

I would also like to show my gratitude to Prof. Vitaly Shumeiko, who has also been my assistant supervisor. I would not have gone as far without your help with theory and calculations.

Then I would like to thank Robert Rehammar, who has been like an inofficial supervisor to me. Your insights into microwave theory and all your ideas have both helped me and inspired me.

I would also like to show my gratitude to Dr. Daryoush Shiri. Your help with simulations have helped me a lot with understanding how TWPAs work.

There are more people that have helped in different ways: Avgust Yurgens, Liangyu Chen, Giovanna Tancredi, Amr Osman, Christopher Warren, Filip Nilsson, Christian Križan, Janka Biznárová, Hang-Xi Li, Lars Jönsson, Linda Brånell, Jonas Bylander, Yong Lu, Ida-Maria Svensson, Marco Scigliuzzo, Marina Kudra, David Niepce, Andreas Bengtsson and others.

Finally I would like to thank my family for the support through many stressful years: Gudrun Renberg, Martin Nilsson, Amanda Renberg, Anton Nilsson, Alvin Nilsson, Ella Nilsson, Emilia Renberg, Momo Renberg, Karin Renberg, Gudrun Nilsson, Bo Nilsson, Seline Renberg, Sammet Nilsson, Kasper Grenander Renberg and last, but not least, my heart's joy and eternal longing, my sunshine and bringer of happiness, Nicole Joseph.

Hampus Renberg Nilsson, Göteborg, August 2024

Acronyms

cQED:	circuit Quantum Electrodynamics
TWPA:	Travelling-wave parametric amplifier
3WM:	Three-wave mixing
4WM:	Four-wave mixing
JJ:	Josephson junction
SQUID:	Superconducting quantum interference device
rf-SQUID:	Radio-frequency SQUID
SNAIL:	Superconducting nonlinear asymmetric inductive element
c.c.:	Complex conjugate
LHS:	Left-hand side
RHS:	Right-hand side
RPM:	Resonant phase matching

List of Definitions

Name/Symbol	Value/Formula	Description
Φ_0	$\frac{h}{2e}$	The superconducting magnetic flux quantum.
φ_0	$\frac{\hbar}{2e}$	The reduced superconducting magnetic flux quantum.
I_c	–	The critical current of a Josephson junction.
Δ	$\phi_2 - \phi_1$	The phase difference between two neighbouring nodes.
I_J	$I_\mathrm{c} \sin \Delta$	The current through a Josephson junction.
U_J	$\varphi_0 \dot{\Delta}$	The voltage over a Josephson junction.
i	$\mathrm{i}^2 = -1$	The imaginary unit.
i	$\frac{I}{I_\mathrm{c}}$	A normalised and unitless current variable.
$L_{\mathrm{J}0}$	$\frac{\varphi_0}{I_\mathrm{c}}$	The inductance of a Josephson junction at zero bias.
L_J	$\frac{L_{\mathrm{J}0}}{\cos(\Delta_0)}$	The inductance of a Josephson junction.
L_0	See Table 4.3.	The series inductance of a TWPA.

Continued on next page

Continued from previous page

Name/Symbol	Value/Formula	Description
C_{J}	–	The intrinsic capacitance of a Josephson junction.
$C_{\circledcirc}$	$C_{\mathrm{J},1}\left(\frac{1}{\mathcal{N}}+\alpha\right)$	The capacitance of a SNAIL.
C	–	The parasitic capacitance of a TWPA.
C_0	–	The shunt capacitance of a TWPA.
$\tilde{C}$	$\frac{C}{C_0}$	The capacitance ratio between the parasitic and the shunt capacitances.
N	–	The number of unitcells.
$\mathcal{N}$	–	The number of junctions in arm 1 of a SNAIL.
$\tilde{x}$	$\frac{x}{a}$	A normalised spatial variable.
$\tilde{t}$	$t\omega_0$	A normalised time variable.
ω_0	$\frac{1}{\sqrt{L_0 C_0}}$	An important reference frequency of a TWPA.
ω_{pl}	$\frac{1}{\sqrt{L_0 C}}$	The plasma frequency of the unitcell of a TWPA.
ω_{c}	$\frac{2\omega_0}{\sqrt{1+4\tilde{C}}}$	The cutoff frequency of a TWPA.
ω_{p}	$2\pi f_{\mathrm{p}}$	The pump angular frequency.

Continued on next page

Continued from previous page

Name/Symbol	Value/Formula	Description
ω_s	$2\pi f_\mathrm{s}$	The signal angular frequency.
ω_i	$\omega_\mathrm{p} - \omega_\mathrm{s}$	The three-wave mixing idler angular frequency.
ω_i	$2\omega_\mathrm{p} - \omega_\mathrm{s}$	The four-wave mixing idler angular frequency.
$\omega_{m\mathrm{p}}$	$m\omega_\mathrm{p}$	The m:th harmonic of the pump.
$\omega_{\mathrm{s}+m\mathrm{p}}$	$\omega_\mathrm{s} + m\omega_\mathrm{p}$	Short notation for the m:th up-converted signal frequency.
$\omega_{\mathrm{i}+m\mathrm{p}}$	$\omega_\mathrm{i} + m\omega_\mathrm{p}$	Short notation for the m:th up-converted idler frequency.
$\tilde{\omega}_m$	$\frac{\omega_m}{\omega_0}$	The frequency ω_m normalised.
a	–	The unitcell physical length.
$\tilde{k}_m$	$k_m a$	The wave number k_m normalised.
c_3	See Table 4.3.	The three-wave mixing coefficient.
c_4	See Table 4.3.	The four-wave mixing coefficient.
A_m	–	The amplitude of mode m.
$A_{\mathrm{p}0}$	$A_\mathrm{p}(0)$	The initial amplitude of the pump.
$A_{\mathrm{s}0}$	$A_\mathrm{s}(0)$	The initial amplitude of the signal.

Continued on next page

Continued from previous page

Name/Symbol	Value/Formula	Description
$A_{\mathrm{i}0}$	$A_{\mathrm{i}}(0)$	The initial amplitude of the idler.
$\bar{A}$	–	The complex conjugate of A.
A'_m	$\dfrac{\partial A_m}{\partial \tilde{x}}$	The derivative of A_m with respect to $\tilde{x}$.
a_m	$\dfrac{\omega_m}{\omega_{\mathrm{p}}}\dfrac{A_m}{A_{\mathrm{p}0}}$	The rescaled amplitude of mode m.
g	–	The gain coefficient.
g_k	–	The k:th coefficient in a microwave filter or an impedance matching network.
G	$\left\lvert\dfrac{A_{\mathrm{s}}(N)}{A_{\mathrm{s}0}}\right\rvert^2$	The power gain.
M	–	The number of modes of each main mode (pump, signal or idler).
δ	$\dfrac{\omega_{\mathrm{s}}-\omega_{\mathrm{p}}/2}{\omega_{\mathrm{p}}/2}$	The 3WM signal detuning.
δ	$\dfrac{\omega_{\mathrm{s}}-\omega_{\mathrm{p}}}{\omega_{\mathrm{p}}}$	The 4WM signal detuning.

Contents

Part I

Thesis

CHAPTER 1

Introduction

During recent years, the interest for quantum computing and quantum processing has grown significantly. To build a large-scale, multiqubit quantum processor, high fidelity qubit readout is necessary. A promising kind of quantum computers are the quantum computers based on superconducting qubits. These quantum systems are very sensitive, typically work at sub-Kelvin temperatures and the results are read out with pulses that are very small in amplitude. Therefore there is a need for the ideal low-noise amplifier, an amplifier with not only a high gain, low added noise and a large bandwidth, but also with other properties. In this chapter we will outline the ideal low-noise amplifier for these applications, and discuss the focus of this thesis.

The work presented in this thesis is centred around the work presented in five publications [1]–[5]. These five publications are presented in Part II as paper [A], paper [B], paper [C], paper [D] and paper [E] respectively.

1.1 Parametric amplifiers

A parametric amplifier is a specific kind of amplifier that uses nonlinear elements. Superconducting parametric amplifiers, which are built with nonlinear,

superconducting lumped element oscillators or as transmission lines, demonstrate high gain and near quantum-limited noise performance [6]–[11] and have become an essential part of the circuit Quantum Electrodynamics (cQED) [12] toolbox.

The general principle of parametric amplification is having a system with a parameter that can be modulated. In a parametric amplifier, energy can under certain conditions be transferred into a signal by modulating the parameter, without any need for energy dissipation. The absence of dissipation removes additional fluctuations, which implies that parametric amplifiers have the potential to realise quantum-limited noise performance [13], [14]. This is a key difference between parametric amplifiers and transistor-based amplifiers, where the transistors are dissipative. Energy conversion from the energy source, the pump, to the signal in a parametric amplifier is provided by means of frequency mixing.

There are several ways of classifying different types of parametric amplifiers. One difference is whether the parametric amplifier is cavity-based, or a travelling-wave parametric amplifier (TWPA). In this work we will focus on the latter, due to its larger bandwidth. Another difference is the element it uses to provide the nonlinearity. For example, the nonlinearity can originate from the inductance of a Josephson junction [15]–[26] or the kinetic inductance of a thin superconducting film [27]–[34]. The third difference is what kind of nonlinear interaction it uses, typically either three-wave mixing (3WM) or four-wave mixing (4WM). For TWPAs, there is also a difference in what kind of dispersion engineering it uses, either periodic modulation (PM) [2], resonant phase matching (RPM) [19] or none [25].

The specific principle of amplification in a TWPA is based on the nonlinearity of a transmission line. Early works on TWPAs utilise the nonlinearity of capacitors, such as varactor diodes, as well inductors based on ferromagnetic materials [35], [36]. For cryogenic applications, the environment required for superconducting qubits, we are not aware of many nonlinear elements. While some work has been done on nonlinear capacitances [37], [38], this work will be limited to the use of nonlinear inductances based on Josephson junctions.

The nonlinear inductance allows a nonlinear interaction between the small-amplitude propagating signal with a large-amplitude copropagating wave known as the pump. Under a phase-matching condition this results in an exponential spatial growth of the signal amplitude [35], [36], [39]. In the quantum regime,

the TWPA is able to generate signal squeezing and photon entanglement [18], [40], but that is not investigated in this thesis.

1.2 Nonlinear interactions

There are two different kinds of nonlinear interactions commonly used in parametric amplifiers, three-wave mixing (3WM) and four-wave mixing (4WM).

In the 3WM interaction, three photons are involved in every interaction. The process uses the lowest order, cubic, nonlinearity of the inductive energy, which is similar to the $\chi^{(2)}$ nonlinearity in optical crystals [41]. Such a nonlinearity is associated with the broken time-reversal symmetry, which can be introduced by applying a current-bias [29], [31], or a magnetic flux-bias [7], [42]. The amplification occurs due to the down-conversion process of the pump into the signal and an idler, which is able to provide an efficient amplification within a large bandwidth in a weakly dispersive medium already at relatively small pump intensity [35]. An important property of this 3WM regime is the separation of the amplification band from the pump frequency, and also the possibility of phase-preserving as well as phase-sensitive amplification [43]–[45]. However, the amplification performance of 3WM devices with a weak frequency dispersion is compromised by the generation of pump harmonics [41] as well as signal and idler up-conversion [29], [46], [47].

In the 4WM interaction, there are four photons involved in every interaction. The process uses the next order, quartic, nonlinearity of the inductive energy, which is similar to the $\chi^{(3)}$ nonlinearity in optical fibers [41]. Amplification in this regime is less efficient since it is a higher order effect, and it also suffers from a phase mismatch due to Kerr effect that makes exponential amplification impossible without dispersion engineering [19]–[21], [48]. Furthermore, the pump position in the middle of the gain band is undesirable for certain applications. However, an advantage with 4WM is that it does not require any bias, and the generation of harmonics and upconversion is less of a problem.

1.3 Quantum noise limits

When amplifying, an amplifier typically adds noise. This does not only happen due to nonideal performance of the amplifier, but is a fundamental property of

any amplification process [6]. For any phase-preserving amplification process with gain G, it can be shown that the added number of noise photons N_{N} is

$$N_{\mathrm{N}} \geq \frac{|1 - 1/G|}{2}. \tag{1.1}$$

For small to no gain, $G \sim 1$, no noise has to be added. In the large gain limit $G \gg 1$, the number of added noise photons N_{N} approaches $1/2$.

The number of noise photons can be translated into a temperature, 'the noise temperature'. The total system noise temperature T_{sys} of a chain of N amplifiers, where the i:th amplifier has a gain G_i and a noise temperature $T_{\mathrm{N},i}$, is given by Friis' formula [49],

$$T_{\mathrm{sys}} = \sum_{i=1}^{N} \frac{T_{\mathrm{N},i}}{\prod_{j=1}^{i-1} G_j} = T_{\mathrm{N},1} + \frac{T_{\mathrm{N},2}}{G_1} + \frac{T_{\mathrm{N},3}}{G_1 G_2} + \ldots \xrightarrow{G_1 \to \infty} T_{\mathrm{N},1}. \tag{1.2}$$

As can be seen, if the first amplifier has a large gain, $G_1 \gg 1$, then the total system noise temperature is dominated by the first amplifiers noise performance. The aim of this work is thus to construct a quantum-limited amplifier with large enough gain to make the total noise temperature of the system approximately quantum-limited.

It is worth mentioning that loss of the signal between the signal source and the amplifier is equivalent to adding noise [11]. Therefore it is important to minimise the losses, and thus the number of contacts and components, between the signal source and the amplifier.

One can achieve noiseless amplification with phase-sensitive amplification. However, then only one quadrature is amplified, while the other is deamplified [6]. To be able to use phase-sensitive amplification, we hence need to both ensure that all the relevant information is coded in one quadrature, and that the phase of the signal is such that the correct quadrature is amplified. While phase-sensitive amplification is an interesting subject, we will not study it in this work.

1.4 Signal insensitivity

A continuous monochromatic wave is determined by three properties: its frequency, amplitude and phase. For pulses there is also a fourth property to

consider, the shape of the pulse. If we are going to use an amplifier for a large quantum system, with many different signals that need amplification, we do not want the amplifier to be sensitive to the different properties of the signals. In other words, we want the transfer function of the amplifier to be 'signal insensitive'.

For the transfer function to be insensitive to the signal frequency, we need a large bandwidth with ideally no gain ripples. This is why the focus of this work is on travelling-wave parametric amplifiers, and not the cavity-based ones, as the cavity-based ones typically have a much smaller bandwidth. We will discuss how to get a large bandwidth through the thesis, and how to minimise the gain ripples in Chapter 10.

For the transfer function to be insensitive to the signal amplitude, we need an amplifier with a high saturation power. The saturation power is the limit where the gain starts to decrease due to insufficient power in the amplifier to amplify the signal. We will discuss how to increase the saturation power in Sections 4.4 and 4.5.

For the transfer function to be insensitive to the signal phase, we simply need to implement phase-preserving amplification. Phase-preserving amplification, which is the focus of this work, is achieved when the signal and the idler frequencies are not equal and the initial idler amplitude is zero, see Chapter 3.

Finally, for the transfer function to be insensitive to the signal shape, we need to ensure that there is little to no distortion of pulses. This is, however, out of the scope of this thesis.

1.5 Leakage

When we use a parametric amplifier, the signal and the pump enter the amplifier. Ideally we would like to only have the amplified signal coming out of the amplifier, and nothing else. However, in reality both the pump and the idler exit together with the signal. There may also exist reflections of the pump, the signal and the idler, see Figure 1.1.

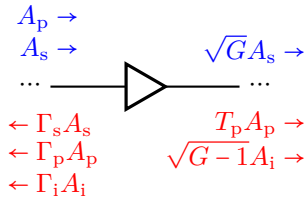

Figure 1.1: An illustration of leakage. The blue modes are the desired ones and the red ones are the undesired ones.

A transmitted pump may saturate the next amplifier in the chain since it typically has a large amplitude.

A transmitted idler can create problems in several ways. If the next amplifier in the chain is also a parametric amplifier, and it uses the same pump frequency, its gain becomes phase-sensitive. If the next amplifier in the chain is also a parametric amplifier, but uses another pump frequency, both the amplified signal and the idler will generate idlers of their own, and our single signal will become four signals. If the next amplifier in the chain is not a parametric amplifier, it will still amplify the idler, which increases the risk of saturating the next amplifier.

A reflected signal is a problem since it is a signal with the exact frequency of the signal source, and it can thus interfere with the source.

A reflected pump is a problem since, even though it may be well detuned in frequency from the signal source, it is still large in its amplitude and can interfere with the source to some extent.

A reflected idler is a problem since, even though it does not have the exact frequency of the signal source, it may be close in frequency to another signal source.

1.6 Isolation

Ideally we would like our amplifier to be directional, so that the noise entering at its output port does not propagate through the amplifier and to our signal sources. In reality, however, any unwanted wave of amplitude A_u entering at the output port typically propagates through the amplifier without getting amplified nor attenuated, see Figure 1.2.

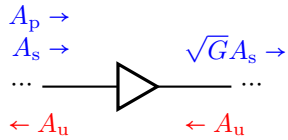

Figure 1.2: An amplifier without leakage but also without isolation. An unwanted wave of amplitude A_u propagates through the amplifier in the reverse direction.

1.6.1 Isolation by attenuation

The simplest approach to get isolation is by adding an attenuator after the amplifier, see Figure 1.3. Since the vacuum noise is amplified by the amplifier, the noise will also be attenuated by the attenuator, so this solution should not make the signal-to-noise ratio significantly worse.

While this approach could work in theory, it is challenging to deliver enough gain to compensate for the signal loss in the attenuator. We typically want a gain on the order of 20 dB and an isolation on the order of at least 30 dB. The gain of the amplifier with the attenuator hence needs to be on the order of 50 dB, which is a very challenging task to achieve.

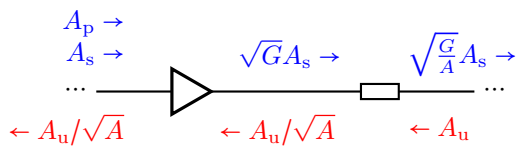

Figure 1.3: An amplifier followed by an attenuator.

1.6.2 Isolation by a second parametric process

An alternative way to get isolation is by using a second parametric process to up-convert unwanted modes to another frequency, see Figure 1.4. This is, at the time of writing, an actively researched technique [50], [51], but it is not the focus of this work.

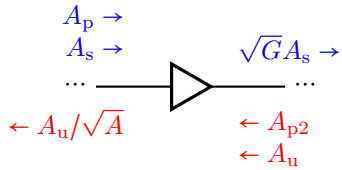

Figure 1.4: An amplifier with two pumps to get isolation. The first pump propagates with the signal and ensures amplification (blue). The second pump propagates in the reverse direction with the unwanted wave, and ensures that the unwanted wave is attenuated (red).

1.6.3 Isolation by idler filtering

A third and final approach is the one of idler filtering, see Figure 1.5. When using idler filtering, the amplifier is a four-port device, where the amplified signal propagates to one port while the idler propagates to another port. If we terminate the signal output and read out at the idler frequency, any unwanted wave at the output port can be dumped into the fourth port. This works since the idler contains the same information as the signal. This is the approach of this work and how to realise it will be studied in Chapter 10.

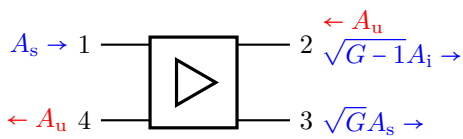

Figure 1.5: An amplifier setup implementing idler filtering for isolation. The signal propagates from port 1 to port 3 where it is terminated, while the generated idler exits at port 2 (blue), which is what the user detects. Any unwanted wave entering at port 2 exits at port 4 (red) where it is terminated.

1.7 Physical size

A final desired property of the amplifier is that it is not physically large. The space inside a cryostat, where these amplifiers are typically placed, is limited. If one is going to do large-scale quantum computing, typically requiring qubits on the order of millions, one will likely need more than tens of thousands of

quantum-limited amplifiers. Therefore it is important that each amplifier is as small as possible.

1.8 Thesis focus and outline

In this thesis we investigate how to build the ideal low-noise amplifier. We especially study, both theoretically and experimentally, travelling-wave parametric amplifiers based on three-wave mixing. However, some desired properties, like a high saturation power and a small signal distortion, have not been studied.

The thesis is organised as follows: In Chapters 2 to 4 we outline the basics of TWPAs. In Chapters 5 to 7 we study more complicated models for three-wave mixing, which are also presented in paper [A], as well as four-wave mixing. In Chapters 8 to 10 we look at more complicated techniques for phase matching, impedance matching, *etc.* This is also presented in paper [B] and paper [C]. Below is a more detailed outline of the chapters.

In Chapter 2 we derive the characteristics of both continuous and discrete transmission lines. The former is a regular transmission line while the latter is identical to a TWPA, except that the nonlinear interaction is neglected.

In Chapter 3 we study the discrete transmission line when the inductances are nonlinear, thus giving rise to the nonlinear interaction needed for amplification, and derive the discrete and continuous wave equations. The former is the exact wave equation in the discrete transmission line, while the latter is an approximation which is easier to solve.

In Chapter 4 we outline the different nonlinear inductors that can be used, with a focus on the rf-SQUID and the SNAIL. We derive the inductance, capacitance and mixing coefficients of these inductors.

In Chapter 5 we investigate three-wave mixing in the small frequency limit, also known as the quasilinear dispersion regime. We develop an extended model of the three-mode model by Tien [35] that captures the effects of upconversion.

In Chapter 6 we study what happens when the wavelengths become comparable with the unitcell. We develop an extended model of the three-mode model by Tien [35] that describes a discrete chain close to the spectral cutoff.

In Chapter 7 we derive the equations for four-wave mixing, and study the Kerr effect.

In Chapter 8 we look at ways to use dispersion engineering to solve the problems of phase matching we have encountered in the previous chapters.

In Chapter 9 we compare the TWPA with microwave filters, and see what techniques can be implemented to help the TWPA with impedance matching. We also discuss how microwave filter theory can be used to construct frequency multiplexers.

In Chapter 10 we investigate different peripheral circuits to solve different issues that prevent the TWPA from being the ideal low-noise amplifier. These issues are the issues of leakage and lack of isolation.

In Chapter 11 we discuss how we simulate our devices, how we fabricate them and how we measure them, including experimental data. The simulation models are also presented in paper [D]. The experimental data is also presented in paper [E].

In Chapter 12, we summarise the main conclusions made throughout the thesis: how to build a travelling-wave parametric amplifier based on three-wave mixing, how to build one based on four-wave mixing, and how to build the ideal low-noise amplifier, as outlined in this chapter. We also discuss future work to be done.

CHAPTER 2

Transmission lines

The amplifiers outlined in this thesis are nonlinear transmission lines. However, to understand how *nonlinear* transmission lines work, it is crucial to first understand how *linear* transmission lines work. In this chapter we will focus on the characteristics of discrete transmission lines. In Section 2.1 we will briefly go through transmission line theory for regular continuous tranmission lines. In Section 2.2 we will define the discrete transmission line and derive its wave equation. In Section 2.3 we will derive the dispersion relation and phase velocity of the discrete transmission line. In Section 2.4 we will derive the scattering parameters, the impedance and the resonance frequencies of the discrete transmission line. In Section 2.5 we will summarise the results of the discrete transmission line and the key differences from the continuous transmission line.

2.1 The continuous transmission line

In this section we will briefly outline the theory for regular continuous transmission lines. While the amplifiers outlined in this thesis are discrete lumped-element transmission lines, it is instructive to compare them with regular

continuous transmission lines, to identify similarities and differences.

The difference between circuit theory and transmission line theory is that in circuit theory, the circuits are assumed to be much smaller than the electrical lengths. In transmission line theory, no such assumption is made and the voltages and currents may change continuously over the length of the transmission line. We can still model a transmission line with lumped elements by studying an infinitesimally short piece of it, see Figure 2.1. Here R' is the series resistance per unit length, L' is the series inductance per unit length, G' is the shunt conductance per unit length and C' is the shunt capacitance per unit length.

For a lossless line, we have $R' = G' = 0$ and the line characteristics are fully determined by L' and C'. Following the derivation in Ref. [52], it can be shown that the characteristic impedance of such a line is given by

$$Z_0 = \sqrt{\frac{L'}{C'}} \tag{2.1a}$$

and its phase velocity by

$$v = \frac{1}{\sqrt{L'C'}}. \tag{2.1b}$$

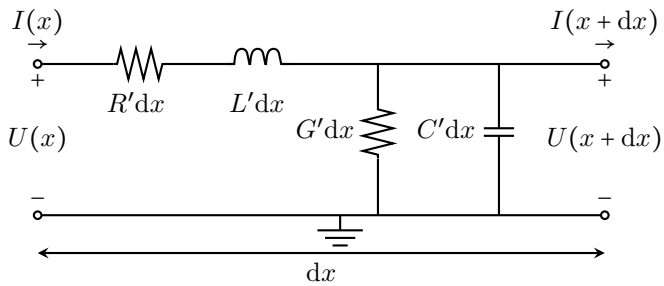

Figure 2.1: An infinitesimally short piece of a continuous transmission line.

2.2 The discrete transmission line

In this section we will define the discrete transmission line and derive its wave equation. The discrete transmission line is constructed from a chain of

lumped-element inductances and capacitances. The chain consists of a number of cascaded identical unitcells, see Figure 2.2. Each unitcell has a shunt capacitance C_0, to emulate the shunt capacitance per unit length C' of the continuous transmission line. Each unitcell also has a series inductance L_0, to emulate the series inductance per unit length L' of a continuous transmission line. Additionally, each unitcell has a capacitance C in parallel with the inductance to capture the effects of the intrinsic capacitances of the inductive elements. We will look closer at the inductive elements and their intrinsic capacitances in Chapter 4.

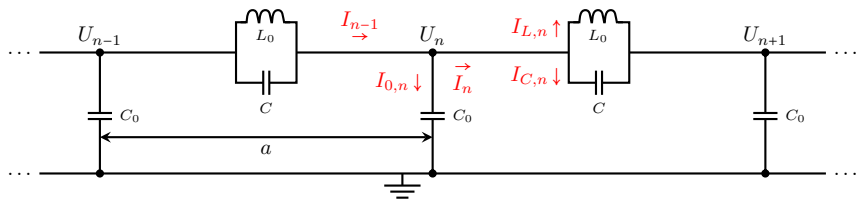

Figure 2.2: A discrete transmission line with definitions of currents, voltage U_n at the node n, and physical length a.

Each unitcell has the physical length a and a voltage U_n at node n. From Kirchhoff's current law it follows that, using the definitions in Figure 2.2, the current relations at node n are

$$I_{0,n} = I_{n-1} - I_n, \tag{2.2a}$$

$$I_n = I_{C,n} + I_{L,n}. \tag{2.2b}$$

We define the node fluxes as

$$\Phi_n(t) := \int U_n(t)\,\mathrm{d}t \tag{2.3}$$

and the node phases as $\phi_n := \Phi_n/\varphi_0$, where $\varphi_0 = \hbar/(2e)$ is the reduced superconducting magnetic flux quantum. The node fluxes are normalised with φ_0 for reasons that will become clear later. For now, let us simply consider it to be a normalisation factor.

The currents, which are time-dependent but we will skip writing the time-

dependence explicitly, can be expressed as

$$I_{0,n} = C_0 \frac{\mathrm{d}}{\mathrm{d}t}(U_n - 0) = C_0 \varphi_0 \frac{\mathrm{d}^2}{\mathrm{d}t^2}\phi_n, \tag{2.4a}$$

$$I_{C,n} = C \frac{\mathrm{d}}{\mathrm{d}t}(U_n - U_{n+1}) = -C\varphi_0 \frac{\mathrm{d}^2}{\mathrm{d}t^2}(\phi_{n+1} - \phi_n), \tag{2.4b}$$

$$L_0 \frac{\mathrm{d}I_{L,n}}{\mathrm{d}t} = U_n - U_{n+1} \implies I_{L,n} = -\frac{\varphi_0}{L_0}(\phi_{n+1} - \phi_n). \tag{2.4c}$$

Substituting the currents from Equations (2.4a) to (2.4c) into Equations (2.2a) and (2.2b) we get

$$\begin{aligned} &\overbrace{C_0\varphi_0 \frac{\mathrm{d}^2}{\mathrm{d}t^2}\phi_n}^{I_{0,n}} = \overbrace{-C\varphi_0 \frac{\mathrm{d}^2}{\mathrm{d}t^2}(2\phi_n - \phi_{n+1} - \phi_{n-1})}^{I_{C,n-1} - I_{C,n}} - \overbrace{\frac{\varphi_0}{L_0}(2\phi_n - \phi_{n+1} - \phi_{n-1})}^{I_{L,n-1} - I_{L,n}} \\ &\implies C_0\varphi_0 \frac{\mathrm{d}^2}{\mathrm{d}t^2}\phi_n - \left[C\varphi_0 \frac{\mathrm{d}^2}{\mathrm{d}t^2} + \frac{\varphi_0}{L_0}\right](\phi_{n+1} - 2\phi_n + \phi_{n-1}) = 0. \end{aligned} \tag{2.5}$$

This equation has the unit of current. By dividing it by φ_0/L_0 it becomes unitless and we get

$$L_0 C_0 \frac{\mathrm{d}^2}{\mathrm{d}t^2}\phi_n - \left[L_0 C \frac{\mathrm{d}^2}{\mathrm{d}t^2} + 1\right](\phi_{n+1} - 2\phi_n + \phi_{n-1}) = 0. \tag{2.6}$$

Finally, let us define the resonance frequency ω_0 and the plasma frequency ω_{pl} as

$$\omega_0 = \frac{1}{\sqrt{L_0 C_0}}, \quad \omega_{\mathrm{pl}} = \frac{1}{\sqrt{L_0 C}}. \tag{2.7}$$

Then Equation (2.6) becomes

$$\frac{1}{\omega_0^2}\frac{\mathrm{d}^2}{\mathrm{d}t^2}\phi_n - \left[\frac{1}{\omega_{\mathrm{pl}}^2}\frac{\mathrm{d}^2}{\mathrm{d}t^2} + 1\right](\phi_{n+1} - 2\phi_n + \phi_{n-1}) = 0. \tag{2.8}$$

We call this equation the linear, discrete wave equation.

2.3 The dispersion relation

In this section we will derive the dispersion relation for the discrete transmission line using Equation (2.8). We begin with the plane wave *ansatz* that the phase at each node n in Figure 2.2 is given by $\phi_n = A\mathrm{e}^{\mathrm{i}(\tilde{k}n-\omega t)}$, where $\tilde{k} = ka$ is the product of the wave number k and the length of the unitcell a. Inserting this *ansatz* into Equation (2.8) we get

$$\begin{aligned} 0 &= \frac{1}{\omega_0^2}(-\mathrm{i}\omega)^2\phi_n - \left(\frac{1}{\omega_{\mathrm{pl}}^2}(-\mathrm{i}\omega)^2 + 1\right)\left(\phi_{n+1} - 2\phi_n + \phi_{n-1}\right) \\ &= -\frac{\omega^2}{\omega_0^2}\phi_n + \left(\frac{\omega^2}{\omega_{\mathrm{pl}}^2} - 1\right)\left(\mathrm{e}^{\mathrm{i}\tilde{k}}\phi_n - 2\phi_n + \mathrm{e}^{-\mathrm{i}\tilde{k}}\phi_n\right) \end{aligned} \tag{2.9}$$

By dividing by ϕ_n this simplifies to

$$\begin{aligned} 0 &= -\frac{\omega^2}{\omega_0^2} + \left(\frac{\omega^2}{\omega_{\mathrm{pl}}^2} - 1\right)\left(\mathrm{e}^{\mathrm{i}\tilde{k}} - 2 + \mathrm{e}^{-\mathrm{i}\tilde{k}}\right) \\ &= -\frac{\omega^2}{\omega_0^2} + 2\left(\frac{\omega^2}{\omega_{\mathrm{pl}}^2} - 1\right)\left(\cos\left(\tilde{k}\right) - 1\right) \\ &= -\frac{\omega^2}{\omega_0^2} - 4\left(\frac{\omega^2}{\omega_{\mathrm{pl}}^2} - 1\right)\sin^2\left(\frac{\tilde{k}}{2}\right) \end{aligned} \tag{2.10}$$

which can be written as

$$\omega^2 = 4\omega_0^2\left(1 - \frac{\omega^2}{\omega_{\mathrm{pl}}^2}\right)\sin^2\left(\frac{\tilde{k}}{2}\right). \tag{2.11}$$

For $C \to 0 \implies \omega_{\mathrm{pl}} \to \infty$ we get the well-known dispersion for a discrete LC-chain, namely

$$\omega^2 = 4\omega_0^2\sin^2\left(\frac{\tilde{k}}{2}\right) \tag{2.12}$$

where the maximum frequency $\omega = 2\omega_0$ is trivially found for $\tilde{k} = \pi$. However, $C \neq 0$ gives rise to an additional term. Defining the dimensionless parameter

$\tilde{C} = \frac{C}{C_0} = \frac{\omega_0^2}{\omega_{\mathrm{pl}}^2}$, we solve for this term and get

$$\begin{aligned} \omega^2 + 4\tilde{C}\omega^2 \sin^2\left(\frac{\tilde{k}}{2}\right) &= 4\omega_0^2 \sin^2\left(\frac{\tilde{k}}{2}\right), \\ \implies \omega^2 &= \frac{4\omega_0^2 \sin^2\left(\frac{\tilde{k}}{2}\right)}{1 + 4\tilde{C}\sin^2\left(\frac{\tilde{k}}{2}\right)}. \end{aligned} \tag{2.13}$$

2.3.1 Unitless solution and cutoff frequency

Let us now normalise the frequency ω with ω_0. Then we can express Equation (2.13) with the unitless measure $\tilde{\omega}$,

$$\tilde{\omega}^2 := \frac{\omega^2}{\omega_0^2} = \frac{4\sin^2\left(\frac{\tilde{k}}{2}\right)}{1 + 4\tilde{C}\sin^2\left(\frac{\tilde{k}}{2}\right)} \tag{2.14}$$

We see in Equation (2.14) that $\tilde{\omega}$ can take values from 0 for $\tilde{k} = 0$ up to a maximum value $\tilde{\omega}_{\mathrm{c}}$, known as the cutoff frequency, for $\tilde{k} = \pi$. Letting $\tilde{k} = \pi$ we find the cutoff frequency to be

$$\tilde{\omega}_{\mathrm{c}}^2 := \frac{\omega_{\mathrm{c}}^2}{\omega_0^2} = \frac{4}{1 + 4\tilde{C}} \quad \implies \quad \tilde{\omega}_{\mathrm{c}} = \frac{2}{\sqrt{1 + 4\tilde{C}}}. \tag{2.15}$$

The cutoff frequency has the largest possible value $\tilde{\omega}_{\mathrm{c}} = 2$ when $\tilde{C} = 0$, but is reduced for larger values of $\tilde{C}$. For example, if $\tilde{C} = \frac{3}{4}$ then $\tilde{\omega}_{\mathrm{c}} = 1$, or if $\tilde{C} = 2$ then $\tilde{\omega}_{\mathrm{c}} = \frac{2}{3}$. If we let $\tilde{C} \to \infty$ then $\tilde{\omega}_{\mathrm{c}} \to 0$.

2.3.2 The dispersion relation as a function of frequency

To find the dispersion relation as a function of frequency, we solve Equation (2.14) for $\tilde{k}$. We have

$$\begin{aligned} \tilde{\omega}^2 \left(1 + 4\tilde{C}\sin^2\left(\frac{\tilde{k}}{2}\right)\right) &= 4\sin^2\left(\frac{\tilde{k}}{2}\right), \\ \implies \quad \sin\left(\frac{\tilde{k}}{2}\right) &= \frac{1}{2} \cdot \frac{\tilde{\omega}}{\sqrt{1 - \tilde{C}\tilde{\omega}^2}}. \end{aligned} \tag{2.16}$$

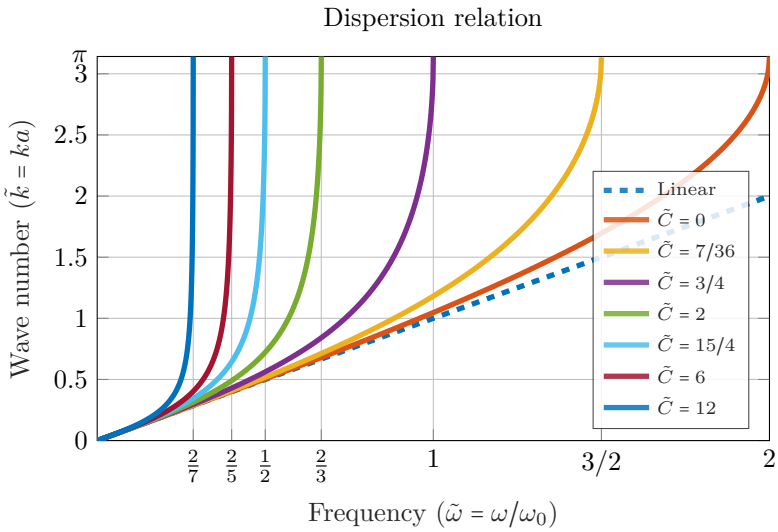

Figure 2.3: The dispersion relation of the discrete transmission line for different values of $\tilde{C}$. For small frequencies, $\omega \ll \omega_c$, the dispersion relation is linear regardless of $\tilde{C}$. For frequencies approaching the cutoff, $\omega \to \omega_c$, the wave number quickly increases to its maximum value π. The larger $\tilde{C}$ is, the more nonlinear the dispersion relation becomes.

The dispersion relation is hence

$$\tilde{k} = 2 \cdot \arcsin\left(\frac{1}{2} \cdot \frac{\tilde{\omega}}{\sqrt{1 - \tilde{C}\tilde{\omega}^2}}\right). \tag{2.17}$$

The dispersion relation is plotted for multiple values of $\tilde{C}$ in Figure 2.3. In this figure, the linear dispersion $\tilde{k} = \tilde{\omega}$, is the dispersion relation of the continuous transmission line.

2.3.3 Dispersion approximations

In the continuous limit, $a \ll \lambda \Leftrightarrow \tilde{k} \ll \pi$, we can simplify the dispersion relation with a first order Taylor expansion of the arcsin-function, see Table 2.1. If $\tilde{C}$ is small, *i.e.* if the frequency is much smaller than the plasma frequency, we can neglect the effects of the plasma frequency, which is also presented in Table 2.1. For very small frequencies $\tilde{\omega} \ll \tilde{\omega}_c$ we can approximate the disper-

sion relation with $\tilde{k} \approx \tilde{\omega}$, as shown in Table 2.1. This last approximation will be important in Chapter 5.

For frequencies that are not small enough to have the linear approximation, or in expressions where the first order terms cancel, we can add the next order term from the Taylor expansion. The dispersion relation then takes the form

$$\tilde{k}(\tilde{\omega}) \approx \tilde{\omega} + \frac{1 + 12\tilde{C}}{24}\tilde{\omega}^3 := \tilde{\omega} + b\tilde{\omega}^3. \tag{2.18}$$

Here b is the cubic order coefficient. Its smallest value is $1/24$ when $\tilde{C} = 0$, but increases as $\tilde{C}$ increases.

Table 2.1: The dispersion relation with different simplifications.

$\tilde{k}(\tilde{\omega})$	$\forall\omega_{\text{pl}} \Leftrightarrow \forall\tilde{C}$	$\omega \ll \omega_{\text{pl}} \Leftrightarrow \tilde{C}\tilde{\omega}^2 \ll 1$
Discrete	$2 \cdot \arcsin\left(\frac{1}{2} \cdot \frac{\tilde{\omega}}{\sqrt{1 - \tilde{C}\tilde{\omega}^2}}\right)$	$2 \cdot \arcsin\left(\frac{\tilde{\omega}}{2}\right)$
Continuous ($a \ll \lambda \Leftrightarrow \tilde{k} \ll \pi$)	$\frac{\tilde{\omega}}{\sqrt{1 - \tilde{C}\tilde{\omega}^2}}$	$\tilde{\omega}$

2.3.4 Phase velocity

Using the definitions of $\tilde{k}$ and $\tilde{\omega}$, we can write the phase velocity as

$$v = \frac{\omega}{k} = \omega_0 a \cdot \frac{\omega/\omega_0}{ka} = \omega_0 a \cdot \frac{\tilde{\omega}}{\tilde{k}}. \tag{2.19}$$

For small frequencies, where we can use the $\tilde{k} \approx \tilde{\omega}$ approximation, the phase velocity is $\omega_0 a$. With $L' = L_0/a$ and $C' = C_0/a$, we see that this is equivalent to the phase velocity of the continuous transmission line, recall Equation (2.1b). On the other hand, as the frequency increases and approaches the cutoff frequency, the phase velocity starts to decrease. This is a feature not observed in continuous transmission lines. Inserting the cutoff frequency into the dispersion relation we find the minimum phase velocity at the cutoff frequency to be

$$v_{\text{min}} = \omega_0 a \cdot \frac{2}{\pi} \frac{1}{\sqrt{1 + 4\tilde{C}}}. \tag{2.20}$$

2.4 Scattering parameters and impedance

In this section we will have a closer look at the scattering parameters of the discrete transmission line. This will in turn give a better understanding of the impedance of the line and its resonance frequencies. As we will see, the discrete transmission line is only fully impedance matched at its resonance frequencies. The discrete transmission line has, due to the asymmetry of the unitcell, an inductive side and a capacitive side, see Figure 2.4a. To improve impedance matching off-resonance, half of the capacitance from the capacitive side can be moved to the inductive side to form a symmetric π-structure, see Figure 2.4b, or half of the inductance from the inductive side can be moved to the capacitive side to form a symmetric T-structure, see Figure 2.4c.

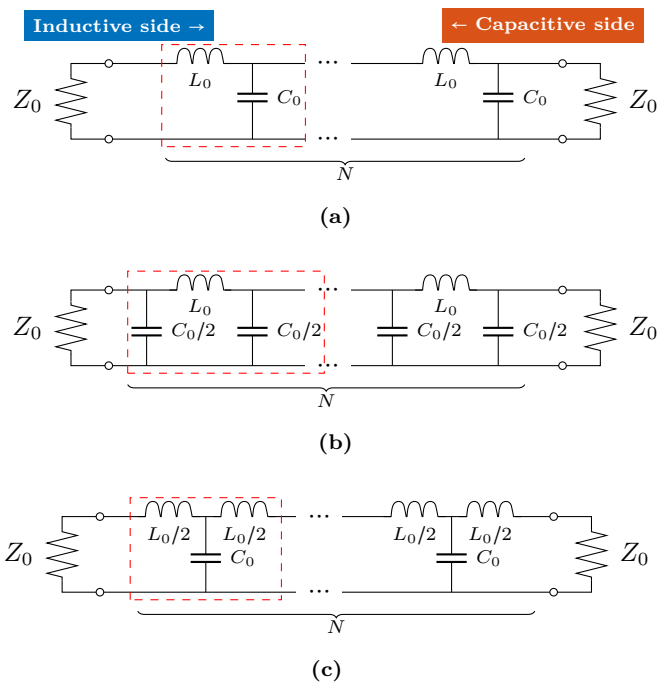

Figure 2.4: Different structures of the discrete transmission line, ignoring the series capacitance C. (**a**) The asymmetric structure. Note that it has both an inductive side and a capacitive side. (**b**) The π-symmetric structure. (**c**) The T-symmetric structure.

2.4.1 The transmission matrix

To find the reflection and transmission coefficients of the discrete transmission line, we can use the transmission ($ABCD$) matrix [52]. We begin by finding the transmission matrix of the unitcell. The transmission matrix depends on the unitcell structure. For the series impedance Z and the shunt admittance Y, given by

$$\begin{aligned} Z &= \frac{\mathrm{i}\omega L_0}{1-\omega^2 L_0 C}, \\ Y &= \mathrm{i}\omega C_0, \end{aligned} \tag{2.21}$$

the transmission matrix is either of

$$\begin{aligned} \boldsymbol{M}_{ZY} &= \begin{bmatrix} 1+ZY & Z \\ Y & 1 \end{bmatrix}, \quad \boldsymbol{M}_{\pi} = \begin{bmatrix} 1+\frac{1}{2}ZY & Z \\ Y+\frac{1}{4}ZY^2 & 1+\frac{1}{2}ZY \end{bmatrix}, \\ \boldsymbol{M}_{YZ} &= \begin{bmatrix} 1 & Z \\ Y & 1+ZY \end{bmatrix}, \quad \boldsymbol{M}_{T} = \begin{bmatrix} 1+\frac{1}{2}ZY & Z+\frac{1}{4}Z^2Y \\ Y & 1+\frac{1}{2}ZY \end{bmatrix} \end{aligned} \tag{2.22}$$

where $\boldsymbol{M}_{ZY}$ is the transmission matrix of the unitcell seen from the inductive side, $\boldsymbol{M}_{YZ}$ from the capacitive side, $\boldsymbol{M}_{\pi}$ for the π-symmetric unitcell and $\boldsymbol{M}_{T}$ for the T-symmetric unitcell. Inspired by the continuous transmission line impedance, recall Equation (2.1a), we initially set $L_0 = Z_0/\omega_0$ and $C_0 = Y_0/\omega_0$, where $Y_0 = Z_0^{-1}$.

The transmission matrix of the full chain is given by $\boldsymbol{M}^N$, where N is the number of unitcells. Defining the elements of $\boldsymbol{M}^N$ as

$$\boldsymbol{M}^N = \begin{bmatrix} A & B \\ C & D \end{bmatrix}, \tag{2.23}$$

the scattering parameters S_{11} and S_{21} in a Z_0-environment are given [52] by

$$S_{11} = \left(A + \frac{B}{Z_0} - CZ_0 - D\right)\left(A + \frac{B}{Z_0} + CZ_0 + D\right)^{-1}, \tag{2.24a}$$

$$S_{21} = 2\left(A + \frac{B}{Z_0} + CZ_0 + D\right)^{-1}. \tag{2.24b}$$

2.4.2 Discrete resonances

Using the appropriate transmission matrix from Equation (2.22), we can now find the transmission and the reflection of the different discrete transmission line structures, see the transmission for $\tilde{C} = 0$ and $N = 6$ in Figure 2.5.

It is clear that for small frequencies we have close to perfect transmission, but when we approach the cutoff frequency $2\omega_0$ we get large transmission ripples and only perfect transmission at certain resonance frequencies. The resonances happen at zero frequency and then for every frequency where the number of wavelengths over all the unitcells add up to a multiple of half of a wavelength, except for the cutoff frequency where $\tilde{k} = \pi$.

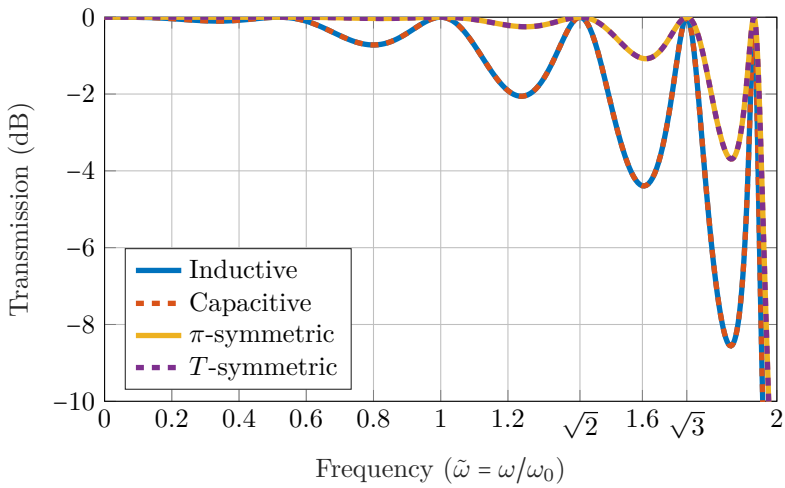

Figure 2.5: The transmission $|S_{21}|$ in dB for the discrete transmission line with inductance L_0 and capacitance C_0 in a $Z_0 = \sqrt{L_0/C_0}$ environment, with $\tilde{C} = 0$ and $N = 6$, for the asymmetric and symmetric structures.

In other words, the n:th resonance happens when

$$N\tilde{k}_{\mathrm{r},n} = (n-1)\pi \quad \Longrightarrow \quad \tilde{k}_{\mathrm{r},n} = (n-1)\frac{\pi}{N} \tag{2.25}$$

for $n \in [1, N] \cap \mathbb{N}$. Inserting these values of $\tilde{k}$ into Equation (2.13), we find the

resonance frequencies. Setting $\tilde{C} = 0$, the resonances simplify to

$$\tilde{\omega}_{\mathrm{r},n} = 2\sin\left((n-1)\frac{\pi}{2N}\right). \tag{2.26}$$

In Figure 2.5, where $\tilde{C} = 0$ and $N = 6$, the 3rd, 4th and 5th resonances are found at $1, \sqrt{2}$ and $\sqrt{3}$.

We can study the reflection coefficient and the input impedance of the line simultaneously in a Smith chart [53], see Figure 2.6. The chain is initially impedance matched, but is impedance mismatched for frequencies that are not equal to any of the resonance frequencies $\omega_{\mathrm{r},n}$. While the transmission in dB for the chain from the inductive and the capacitive sides were identical, we see in the Smith chart that the impedance off-resonance is always inductive for the inductive chain, and always capacitive for the capacitive chain.

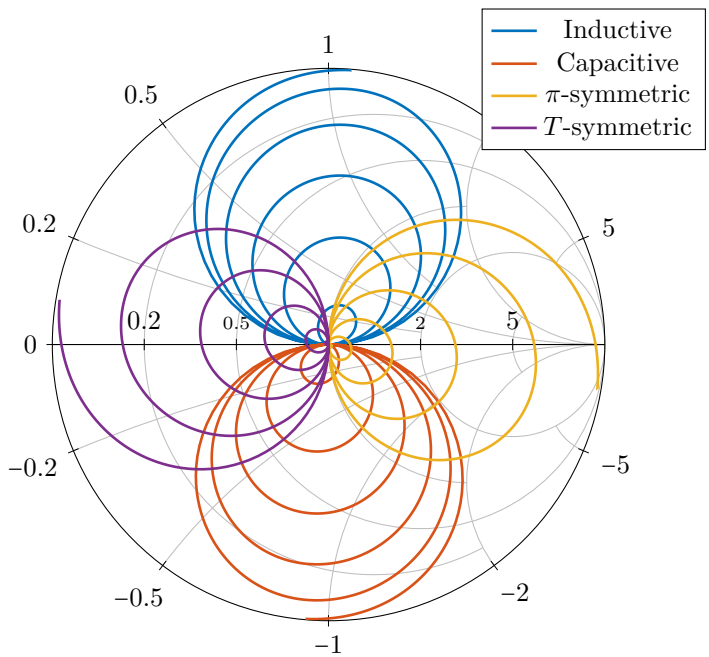

Figure 2.6: The reflection coefficient plotted in a Smith chart for the discrete transmission line with $\tilde{C} = 0$ and $N = 6$ in the frequency range 0 to $2\omega_0$ for the asymmetric and symmetric structures.

2.4.3 Adding an additional resonance

For the symmetric structures, we can add an additional resonance $\omega_{r'}$ to improve the transmission in a predetermined frequency band. This is achieved by ensuring that the unitcell itself is impedance matched at $\omega_{r'}$. In other words, we will modify L_0 and C_0 of the unitcell to introduce an additional resonance. Consider the T-symmetric unitcell, see Figure 2.7.

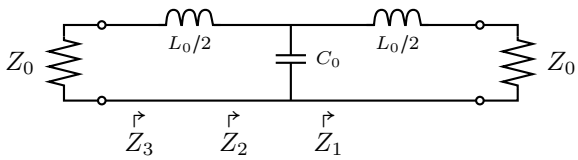

Figure 2.7: A single T-symmetric unitcell.

The impedance Z_1 at the resonance frequency $\omega_{r'}$ is given by

$$Z_1 = Z_0 + i\omega_{r'} L_0/2. \tag{2.27}$$

Taking the reciprocal gives us the admittance,

$$Y_1 = Z_1^{-1} = \frac{1}{Z_0 + i\omega_{r'} L_0/2} = \frac{Z_0 - i\omega_{r'} L_0/2}{Z_0^2 + \omega_{r'}^2 L_0^2/4} \tag{2.28}$$

To ensure impedance matching at the resonance frequency for the full unitcell, the admittance added by the capacitor must change the impedance Z_2 to a value such that the impedance of the last inductor $Z_3 = Z_2 + i\omega_{r'} L_0/2$ makes $Z_3 = Z_0$. Due to symmetry, this happens if the admittance $Y_2 = Z_2^{-1}$ is equal to Y_1 but with opposite sign of the imaginary part, *i.e.* when $\Im(Y_2) = -\Im(Y_1)$. In other words, we have that

$$i\omega_{r'} C_0 = 2 \cdot \frac{i\omega_{r'} L_0/2}{Z_0^2 + \omega_{r'}^2 L_0^2/4} \quad \Longrightarrow \quad C_0 = \frac{L_0}{Z_0^2 + \omega_{r'}^2 L_0^2/4}. \tag{2.29}$$

Now using $L_0 C_0 = \omega_0^{-2}$, we get that

$$\frac{L_0^2}{Z_0^2 + \omega_{r'}^2 L_0^2/4} = \frac{1}{\omega_0^2} \quad \Longrightarrow \quad L_0^2 \omega_0^2 = Z_0^2 + \omega_{r'}^2 L_0^2/4. \tag{2.30}$$

We can solve this for L_0, and in turn for C_0, and we get

$$L_0 = \frac{Z_0}{\omega_0} \cdot \frac{1}{\sqrt{1 - \tilde{\omega}_{r'}^2/4}}, \tag{2.31a}$$

$$C_0 = \frac{Y_0}{\omega_0} \cdot \sqrt{1 - \tilde{\omega}_{r'}^2/4}. \tag{2.31b}$$

Similarly we can solve the equations for the π-symmetric unitcell and find that

$$L_0 = \frac{Z_0}{\omega_0} \cdot \sqrt{1 - \tilde{\omega}_{r'}^2/4}, \tag{2.32a}$$

$$C_0 = \frac{Y_0}{\omega_0} \cdot \frac{1}{\sqrt{1 - \tilde{\omega}_{r'}^2/4}}. \tag{2.32b}$$

Note that setting $\tilde{\omega}_{r'} = 0$ retrieves the previous values of L_0 and C_0. Also note that these equations tell us that, to introduce this additional resonance frequency, the T-symmetric chain should be slightly more inductive than previously, while the π-symmetric chain should be slightly more capacitive.

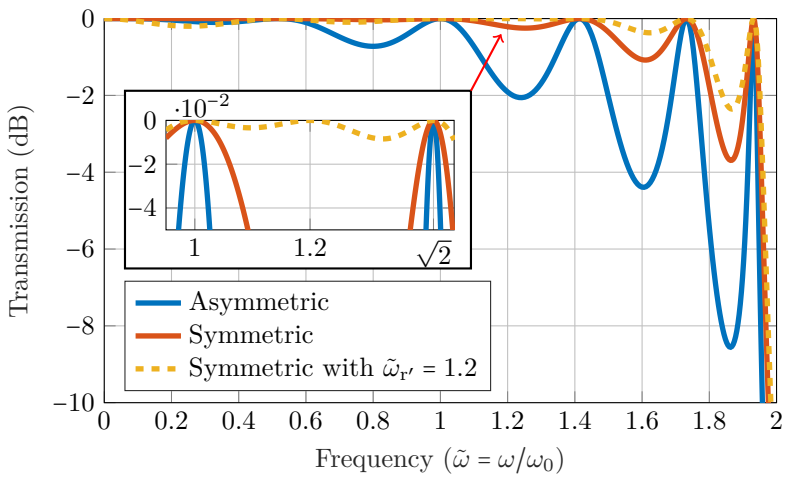

Figure 2.8: A comparison between the transmission for the asymmetric discrete chain, the symmetric chain and the symmetric chain with the additional resonance at $\tilde{\omega}_{r'} = 1.2$. The chain has $N = 6$ unitcells and $\tilde{C} = 0$.

Let us use the transmission matrix to calculate the transmission using these values of L_0 and C_0 to introduce this additional resonance, and compare the transmission for the different structures, see Figure 2.8. As we can see, the previous resonances are all there, but now there is an additional resonance at $\tilde{\omega}_{r'} = 1.2$, which improves the transmission and impedance matching for other frequencies close to this resonance as well. Simultaneously, the transmission and impedance matching for smaller frequencies is now worse.

2.5 Summary

In this chapter we have studied and compared the regular continuous transmission line and the discrete transmission line. There are some key differences. The lossless continuous transmission line has an inductance L' per unit length and a capacitance C' per unit length. The discrete transmission line has a unitcell length a and an inductance L_0 per unitcell and capacitance C_0 per unitcell. By letting $L' = L_0/a$ and $C' = C_0/a$, we can compare the two lines.

One difference is that, for the discrete transmission line, there is a parasitic capacitance C, giving rise to the plasma frequency ω_{pl}. However, the plasma frequency of our inductive elements is on the order of 100 GHz, while this work will mostly focus on frequencies below or around 10 GHz. Thus, the effects of the plasma frequency are of less importance and will mostly be neglected throughout this work.

Another difference is that of impedance and phase velocity. The lossless continuous line has a characteristic impedance $Z_0 = \sqrt{L'/C'}$ and a phase velocity $v = 1/\sqrt{L'C'}$ that both are independent of frequency. It supports propagating waves of any frequency. On the other hand, the discrete transmission line has a distinct cutoff frequency above which no waves can propagate indefinitely. It has the same impedance and phase velocity as the continuous transmission line for frequencies well below the cutoff frequency. However, when the frequencies approach the cutoff frequency, there are two key differences.

Firstly, the phase velocity goes down, which will give rise to a phase mismatch between propagating modes at different frequencies. We will discuss this phase mismatch more in the upcoming chapters.

Secondly, the impedance becomes complex-valued and varies with frequency, and is only impedance matched at certain resonance frequencies. Seen from the side beginning with a series inductor, 'the inductive side', the chain will

always have an inductive impedance off-resonance. Seen from the side beginning with a shunt capacitor, 'the capacitive side', it will always have a capacitive impedance off-resonance.

A way to understand why this change of impedance and phase velocity only occurs for the discrete transmission line and not for the continuous transmission line is to compare the wavelength with the unitcell length. For the discrete transmission line, the change of the phase velocity and the impedance happens when the wavelength $\lambda = 2\pi/k$ becomes comparable with the unitcell length a. For the continuous transmission line this never happens, since the unitcell has the infinitesimal length $\mathrm{d}x$.

Impedance matching for the discrete transmission line can be somewhat improved by creating a symmetric unitcell structure. It can be further improved by adding an additional resonance in the centre of the frequency band of interest. It cannot, however, be impedance matched in the full range from 0 to the cutoff frequency. To achieve that, we will need to implement more complicated impedance matching techniques, which we will discuss in Chapter 9.

CHAPTER 3

3

Travelling-wave parametric amplifiers

In this chapter we will study the travelling-wave parametric amplifier (TWPA). The TWPA is almost identical to the discrete transmission line presented in Chapter 2, but with one key difference: the inductance has a dependency on the phase difference between the nodes, see Figure 3.1. This gives the TWPA the possibility for wave mixing, which is required for the amplification process. We will study the inductors more closely in Chapter 4. For now, we will simply treat the inductors as general circuit elements with a nonlinear inductance.

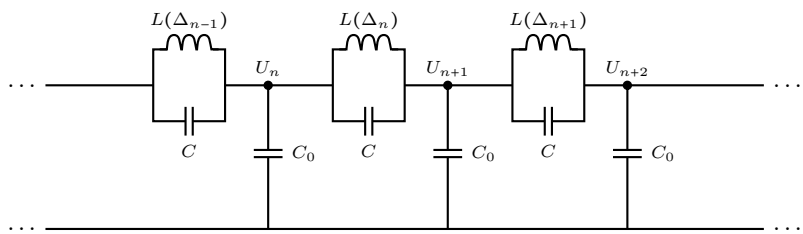

Figure 3.1: General schematic of a TWPA: a discrete transmission line with inductances that depend on the phase differences between the nodes.

3.1 TWPA discrete wave equation

In this section we will derive the wave equation for the TWPA, *i.e.* the equivalent version of Equation (2.8) with adjustments for the nonlinear inductors.

The only differences between Figures 2.2 and 3.1 are the inductive elements. Thus, Equation (2.5) is almost unchanged. The only difference is the expression for $I_{L,n}$, where there are now additional terms that reflect the nonlinearity of the inductance. Let us define the phase difference $\Delta_n = \phi_{n+1} - \phi_n$, where ϕ_n are the node phases defined in Section 2.2, and the static phase-bias Δ_0 such that $\Delta_n = \Delta_0 + \delta_n$. Using a Taylor expansion around Δ_0, we can in general describe the current as

$$I_{L,n} = \frac{\varphi_0}{L_0} f(\Delta_n) = I_0 \sum_{j=0}^{\infty} \frac{f^{(j)}(\Delta_0)}{j!} \delta_n^j. \tag{3.1}$$

The current $I_0 = \varphi_0/L_0$ is set by the static inductance L_0 of the inductive element, the function f is a general function describing the current phase relation of the inductive element, and the sum in the right hand side of the equation is the Taylor expansion of f around Δ_0.

Let us define the coefficients

$$b_j := \frac{f^{(j)}(\Delta_0)}{j!}. \tag{3.2}$$

Note that the static inductance per definition is such that $b_1 = 1$. In the absence of a bias current we also know that $b_0 = 0$. However, a more general relation is taking a bias current I_b into consideration, which gives the constraint $I_\mathrm{b} = I_0 b_0$. The inductance current difference thus becomes

$$I_{L,n-1} - I_{L,n} = I_0 \sum_{j=0}^{\infty} b_j \left(\delta_{n-1}^j - \delta_n^j\right). \tag{3.3}$$

The first term in the sum is trivially zero and, since $b_1 = 1$, the second term equals the same difference as in Equation (2.4c). The discrete wave equation

with a nonlinear inductance can be written as

$$\begin{aligned}&\frac{1}{\omega_0^2}\frac{\mathrm{d}^2}{\mathrm{d}t^2}\phi_n - \left[\frac{1}{\omega_{\mathrm{pl}}^2}\frac{\mathrm{d}^2}{\mathrm{d}t^2}+1\right](\phi_{n+1}-2\phi_n+\phi_{n-1})\\&=\sum_{j=2}^{\infty} b_j\left((\phi_{n+1}-\phi_n)^j-(\phi_n-\phi_{n-1})^j\right).\end{aligned} \tag{3.4}$$

Compared with the linear discrete wave equation, Equation (2.8), the only difference is the right-hand side of the equation, which arises from the nonlinear inductance. It is the right-hand side that allows different frequency mixing processes, as we will see in Section 3.3.

Finally we will assume small phase variations $\delta_n \ll 1$, which allows us to drop higher order terms. Due to conventions we define

$$c_3 = -2b_2, \quad c_4 = -3b_3. \tag{3.5}$$

In this work, c_3 and c_4 are called the 3-wave mixing (3WM) and 4-wave mixing (4WM) coefficients respectively [1] [2]. With these coefficients, we modify Equation (3.4) to reach the final form of the discrete wave equation,

$$\begin{aligned}&\frac{1}{\omega_0^2}\frac{\mathrm{d}^2}{\mathrm{d}t^2}\phi_n - \left[\frac{1}{\omega_{\mathrm{pl}}^2}\frac{\mathrm{d}^2}{\mathrm{d}t^2}+1\right](\phi_{n+1}-2\phi_n+\phi_{n-1})\\&\quad=-\frac{c_3}{2}\left((\phi_{n+1}-\phi_n)^2-(\phi_n-\phi_{n-1})^2\right)\\&\qquad-\frac{c_4}{3}\left((\phi_{n+1}-\phi_n)^3-(\phi_n-\phi_{n-1})^3\right).\end{aligned} \tag{3.6}$$

3.2 TWPA continuous wave equation

A common simplification of Equation (3.6) is the continuous wave approximation, where we assume that wavelengths are much longer than the unitcell length, $\lambda \gg a$. This is equivalent to have a small wave number, $\tilde{k} \ll \pi$. Then the node phase $\phi_n(t)$ can be replaced by a continuous phase variable $\phi(x,t)$

[1] Note: The c_3, c_4 here are not the same coefficients as c_3 and c_4 in Ref. [54].

[2] Note: In some literature [24], [26], [55], the mixing coefficients are expressed with $\beta = -b_2$ and $\gamma = -b_3$.

and the differences can be expressed with derivatives,

$$\phi_{n+1} - \phi_n = \sum_{j=1}^{\infty} \frac{(a\partial_x)^j}{j!}\phi(x,t) = \left[\mathrm{e}^{a\partial_x} - 1\right]\phi(x,t), \tag{3.7a}$$

$$\phi_n - \phi_{n-1} = \sum_{j=1}^{\infty} -\frac{(-a\partial_x)^j}{j!}\phi(x,t) = \left[1 - \mathrm{e}^{-a\partial_x}\right]\phi(x,t) \tag{3.7b}$$

where a is the physical length of the unitcell. For the linear part of the wave equation we can simplify the differential operator as

$$\left(\mathrm{e}^{a\partial_x} - 1\right) - \left(1 - \mathrm{e}^{-a\partial_x}\right) = 2\left(\frac{\mathrm{e}^{a\partial_x} + \mathrm{e}^{-a\partial_x}}{2} - 1\right) = -4\sin^2\left(\frac{1}{2}\mathrm{i}a\partial_x\right). \tag{3.8}$$

The continuous wave equation hence becomes

$$\begin{aligned}\frac{1}{\omega_0^2}\frac{\partial^2\phi}{\partial t^2} + 4\left[\frac{1}{\omega_{\mathrm{pl}}^2}\frac{\partial^2}{\partial t^2} + 1\right]\sin^2\left(\frac{1}{2}\mathrm{i}a\partial_x\right)\phi \\ = -\frac{c_3}{2}\left(\left(\left[\mathrm{e}^{a\partial_x} - 1\right]\phi\right)^2 - \left(\left[1 - \mathrm{e}^{-a\partial_x}\right]\phi\right)^2\right) \\ - \frac{c_4}{3}\left(\left(\left[\mathrm{e}^{a\partial_x} - 1\right]\phi\right)^3 - \left(\left[1 - \mathrm{e}^{-a\partial_x}\right]\phi\right)^3\right).\end{aligned} \tag{3.9}$$

We simplify Equation (3.9) by keeping only the lowest order terms with respect to the unitcell length a. For the linear part of the equation we get

$$4\sin^2\left(\frac{1}{2}\mathrm{i}a\partial_x\right)\phi \approx 4\left(\frac{1}{2}\mathrm{i}a\partial_x\right)^2\phi = -a^2\frac{\partial^2\phi}{\partial x^2}, \tag{3.10a}$$

for the quadratic part we get

$$\begin{aligned}\left(\left[\mathrm{e}^{a\partial_x} - 1\right]\phi\right)^2 &\approx \left(a\frac{\partial\phi}{\partial x}\right)^2 + a^3\frac{\partial\phi}{\partial x}\frac{\partial^2\phi}{\partial x^2} + \left(\frac{a^2}{2}\frac{\partial^2\phi}{\partial x^2}\right)^2, \\ \left(\left[1 - \mathrm{e}^{-a\partial_x}\right]\phi\right)^2 &\approx \left(a\frac{\partial\phi}{\partial x}\right)^2 - a^3\frac{\partial\phi}{\partial x}\frac{\partial^2\phi}{\partial x^2} + \left(\frac{a^2}{2}\frac{\partial^2\phi}{\partial x^2}\right)^2, \\ \left(\left[\mathrm{e}^{a\partial_x} - 1\right]\phi\right)^2 - \left(\left[1 - \mathrm{e}^{-a\partial_x}\right]\phi\right)^2 &\approx 2a^3\frac{\partial\phi}{\partial x}\frac{\partial^2\phi}{\partial x^2},\end{aligned} \tag{3.10b}$$

and for the cubic part we get

$$\begin{aligned}
\left(\left[\mathrm{e}^{a\partial_x}-1\right]\phi\right)^3 &\approx \left(a\frac{\partial\phi}{\partial x}\right)^3 + \frac{3}{2}a^4\left(\frac{\partial\phi}{\partial x}\right)^2\frac{\partial^2\phi}{\partial x^2} + \frac{3}{2}a^4\frac{\partial\phi}{\partial x}\left(\frac{\partial^2\phi}{\partial x^2}\right)^2 + \left(a^2\frac{\partial^2\phi}{\partial x^2}\right)^3,\\
\left(\left[1-\mathrm{e}^{-a\partial_x}\right]\phi\right)^3 &\approx \left(a\frac{\partial\phi}{\partial x}\right)^3 - \frac{3}{2}a^4\left(\frac{\partial\phi}{\partial x}\right)^2\frac{\partial^2\phi}{\partial x^2} + \frac{3}{2}a^4\frac{\partial\phi}{\partial x}\left(\frac{\partial^2\phi}{\partial x^2}\right)^2 - \left(a^2\frac{\partial^2\phi}{\partial x^2}\right)^3,\\
\left(\left[\mathrm{e}^{a\partial_x}-1\right]\phi\right)^3 - \left(\left[1-\mathrm{e}^{-a\partial_x}\right]\phi\right)^3 &\approx 3a^4\left(\frac{\partial\phi}{\partial x}\right)^2\frac{\partial^2\phi}{\partial x^2}.
\end{aligned} \tag{3.10c}$$

Now Equation (3.9) can be simplified to

$$\begin{aligned}
&\left[\frac{1}{\omega_0^2}\frac{\partial^2}{\partial t^2} - \frac{a^2}{\omega_{\mathrm{pl}}^2}\frac{\partial^2}{\partial t^2}\frac{\partial^2}{\partial x^2} - a^2\frac{\partial^2}{\partial x^2}\right]\phi\\
&= -c_3a^3\frac{\partial\phi}{\partial x}\frac{\partial^2\phi}{\partial x^2} - c_4a^4\left(\frac{\partial\phi}{\partial x}\right)^2\frac{\partial^2\phi}{\partial x^2}.
\end{aligned} \tag{3.11}$$

As a final step of simplification, let us introduce the normalised TWPA units $\tilde{t} = t\omega_0$ and $\tilde{x} = x/a$. These can either be thought of as unitless variables for time and space, normalised with ω_0 and a, or simply as time and space measured in units of ω_0^{-1} and a. With these, and the previously defined relation $\tilde{C} = C/C_0$, we reach the most simplified form of the continuous wave equation,

$$\left[\frac{\partial^2}{\partial\tilde{t}^2} - \tilde{C}\frac{\partial^2}{\partial\tilde{t}^2}\frac{\partial^2}{\partial\tilde{x}^2} - \frac{\partial^2}{\partial\tilde{x}^2}\right]\phi = -c_3\frac{\partial\phi}{\partial\tilde{x}}\frac{\partial^2\phi}{\partial\tilde{x}^2} - c_4\left(\frac{\partial\phi}{\partial\tilde{x}}\right)^2\frac{\partial^2\phi}{\partial\tilde{x}^2}. \tag{3.12}$$

This is the wave equation we will use for most of the analysis of mixing processes within the TWPA. It is worth remembering that this equation is an approximation of the exact discrete wave equation, Equation (3.6). It only holds as long as the wavelengths are much longer than the unitcell, which is equivalent to $\tilde{k} \ll \pi$, recall Section 2.3. If wavelengths are *not* much longer than a unitcell, one should use the discrete wave equation instead, which we will do in Chapter 6.

In the regime where the continuous wave equation can be used, the linear approximation of the dispersion relation holds most of the time. However, as we will show later, for the phase mismatches we will need to use the cubic approximation, recall Equation (2.18). Therefore we call this regime the *quasilinear* regime.

3.3 General three-wave mixing equations

In this section we will derive general expressions for the differential equations describing the 3WM processes in the quasilinear regime, which we will later use to predict gain and other 3WM characteristics. These equations are known as the propagation equations [14], or the coupled mode equations [46]. Four-wave mixing will be treated separately in Chapter 7. For now, we will assume that there is no four-wave mixing and set $c_4 = 0$. By doing so, the continuous wave equation (Equation (3.12)) now reads

$$\left[\frac{\partial^2}{\partial\tilde{t}^2} - \tilde{C}\frac{\partial^2}{\partial\tilde{t}^2}\frac{\partial^2}{\partial\tilde{x}^2} - \frac{\partial^2}{\partial\tilde{x}^2}\right]\phi = -c_3\frac{\partial\phi}{\partial\tilde{x}}\frac{\partial^2\phi}{\partial\tilde{x}^2}. \tag{3.13}$$

Furthermore, to solve the wave equation, we begin with the *ansatz* that the solutions are travelling waves given by the form

$$\phi = \sum_m \phi_m = \frac{1}{2}\sum_m A_m(\tilde{x})\mathrm{e}^{\mathrm{i}(\tilde{k}_m\tilde{x}-\tilde{\omega}_m\tilde{t})} + \bar{A}_m(\tilde{x})\mathrm{e}^{-\mathrm{i}(\tilde{k}_m\tilde{x}-\tilde{\omega}_m\tilde{t})} \tag{3.14}$$

where m is the index of each wave, the tilde-notation means units normalised as defined in the end of Section 3.2 and $\bar{A}_m$ is the complex conjugate of the amplitude A_m.

3.3.1 Simplifying the left-hand side

The left-hand side of Equation (3.13) comes from propagation of free waves in a linear medium, *i.e.* the discrete transmission line, as we know from Section 2.2. However, now that the right-hand side of the equation is not equal to zero, the derivatives of the amplitudes are not necessarily equal to zero either.

We begin by calculating each derivative of ϕ_m,

$$\frac{\partial^2 \phi_m}{\partial \tilde{t}^2} = -\tilde{\omega}_m^2 \phi_m, \tag{3.15a}$$

$$\frac{\partial \phi_m}{\partial \tilde{x}} = \frac{1}{2}\left[\left(A_m' + \mathrm{i}\tilde{k}_m A_m\right)\mathrm{e}^{\mathrm{i}\left(\tilde{k}_m\tilde{x}-\tilde{\omega}_m\tilde{t}\right)} + \text{c.c.}\right], \tag{3.15b}$$

$$\frac{\partial^2 \phi_m}{\partial \tilde{x}^2} = \frac{1}{2}\left[\left(A_m'' + 2\mathrm{i}\tilde{k}_m A_m' - \tilde{k}_m^2 A_m\right)\mathrm{e}^{\mathrm{i}\left(\tilde{k}_m\tilde{x}-\tilde{\omega}_m\tilde{t}\right)} + \text{c.c.}\right], \tag{3.15c}$$

$$\tilde{C}\frac{\partial^2}{\partial \tilde{t}^2}\frac{\partial^2 \phi_m}{\partial \tilde{x}^2} = -\tilde{C}\tilde{\omega}_m^2 \frac{\partial^2 \phi_m}{\partial \tilde{x}^2}, \tag{3.15d}$$

where "+c.c." refers to adding the complex conjugate of what was just written, and A_m' and A_m'' are the first and second derivatives with respect to $\tilde{x}$. Then we apply the slowly varying envelope approximation

$$\left|\frac{\partial^2 A_m}{\partial \tilde{x}^2}\right| \ll \left|\tilde{k}_m \frac{\partial A_m}{\partial \tilde{x}}\right| \tag{3.16}$$

to neglect the second derivative, and we can hence write the left-hand side of the equation for each wave m as

$$\begin{aligned}
\mathrm{LHS}_m^{(3.13)} &\approx -\tilde{\omega}_m^2\phi_m - \frac{1-\tilde{C}\tilde{\omega}_m^2}{2}\left[\left(2\mathrm{i}\tilde{k}_m A_m' - \tilde{k}_m^2 A_m\right)\mathrm{e}^{\mathrm{i}\left(\tilde{k}_m\tilde{x}-\tilde{\omega}_m\tilde{t}\right)} + \text{c.c.}\right] \\
&= \left(-\tilde{\omega}_m^2 - \tilde{C}\tilde{\omega}_m^2\tilde{k}_m^2 + \tilde{k}_m^2\right)\phi_m \\
&\quad + \left[\mathrm{i}\tilde{k}_m\left(\tilde{C}\tilde{\omega}_m^2 - 1\right)A_m'\mathrm{e}^{\mathrm{i}\left(\tilde{k}_m\tilde{x}-\tilde{\omega}_m\tilde{t}\right)} + \text{c.c.}\right].
\end{aligned} \tag{3.17}$$

Applying the continuous dispersion relation, recall Table 2.1, the first term equals zero. The second term can also be simplified using the continuous dispersion relation,

$$\mathrm{i}\tilde{k}_m\left(\tilde{C}\tilde{\omega}_m^2 - 1\right) = -\mathrm{i}\frac{\tilde{\omega}_m^2}{\tilde{k}_m}\frac{\tilde{k}_m^2}{\tilde{\omega}_m^2}\left(1 - \tilde{C}\tilde{\omega}_m^2\right) = -\mathrm{i}\frac{\tilde{\omega}_m^2}{\tilde{k}_m} \tag{3.18}$$

To summarise, the left-hand side of the wave equation can be simplified to

$$\mathrm{LHS}^{(3.13)} = \sum_m -\mathrm{i}\frac{\tilde{\omega}_m^2}{\tilde{k}_m}\left(A_m'\mathrm{e}^{\mathrm{i}\left(\tilde{k}_m\tilde{x}-\tilde{\omega}_m\tilde{t}\right)} - \bar{A}_m'\mathrm{e}^{-\mathrm{i}\left(\tilde{k}_m\tilde{x}-\tilde{\omega}_m\tilde{t}\right)}\right). \tag{3.19}$$

3.3.2 Simplifying the right-hand side

The right-hand side of Equation (3.13) is the part giving rise to the mixing between different waves and, potentially, gain. We have already calculated the derivatives that are on this side of the equation, recall Equations (3.15b) and (3.15c). However, on this side, the amplitudes without derivatives do not cancel and we can apply yet another approximation,

$$\left|\frac{\partial A_m}{\partial \tilde{x}}\right| \ll \left|\tilde{k}_m A_m\right|. \tag{3.20}$$

This allows us to approximate the derivatives as

$$\frac{\partial \phi_m}{\partial \tilde{x}} \approx \frac{\mathrm{i}}{2}\tilde{k}_m\left(A_m \mathrm{e}^{\mathrm{i}(\tilde{k}_m\tilde{x}-\tilde{\omega}_m\tilde{t})} - \bar{A}_m \mathrm{e}^{-\mathrm{i}(\tilde{k}_m\tilde{x}-\tilde{\omega}_m\tilde{t})}\right), \tag{3.21a}$$

$$\frac{\partial^2 \phi_m}{\partial \tilde{x}^2} \approx -\frac{1}{2}\tilde{k}_m^2\left(A_m \mathrm{e}^{\mathrm{i}(\tilde{k}_m\tilde{x}-\tilde{\omega}_m\tilde{t})} + \bar{A}_m \mathrm{e}^{-\mathrm{i}(\tilde{k}_m\tilde{x}-\tilde{\omega}_m\tilde{t})}\right). \tag{3.21b}$$

The full expression of the right-hand side of the wave equation is

$$\mathrm{RHS}^{(3.13)} = -c_3\left(\sum_m \frac{\partial \phi_m}{\partial \tilde{x}}\right)\left(\sum_m \frac{\partial^2 \phi_m}{\partial \tilde{x}^2}\right), \tag{3.22}$$

which, given that the total number of waves is M, is an expression with $4M^2$ terms and will be hard to fit on this page, and even harder to analyse completely.

However, not all terms are equally important. Given that we study wave m, only some of the terms will be resonant with this wave. In other words, we only care about the terms that have the frequency $\tilde{\omega}_m$ in the exponent, and neglect the rest.

Assume we have the three waves m, n, q, and that the frequencies have the relationship $\tilde{\omega}_m = \tilde{\omega}_n - \tilde{\omega}_q$, *i.e.* a down-conversion process. Then there are two terms in the right-hand side that will be resonant with m: one from $\phi_n' \cdot \phi_q''$, and the one from $\phi_q' \cdot \phi_n''$. The resulting terms are hence

$$\frac{\mathrm{i}}{2}\tilde{k}_n A_n \mathrm{e}^{\mathrm{i}(\tilde{k}_n\tilde{x}-\tilde{\omega}_n\tilde{t})} \cdot \left(-\frac{1}{2}\tilde{k}_q^2\right)\bar{A}_q \mathrm{e}^{-\mathrm{i}(\tilde{k}_q\tilde{x}-\tilde{\omega}_q\tilde{t})} = -\frac{\mathrm{i}}{4}\tilde{k}_n\tilde{k}_q^2 A_n \bar{A}_q \mathrm{e}^{\mathrm{i}[(\tilde{k}_n-\tilde{k}_q)\tilde{x}-\tilde{\omega}_m\tilde{t}]}$$

and

$$-\frac{\mathrm{i}}{2}\tilde{k}_q\bar{A}_q\mathrm{e}^{-\mathrm{i}(\tilde{k}_q\tilde{x}-\tilde{\omega}_q\tilde{t})}\cdot\left(-\frac{1}{2}\tilde{k}_n^2\right)A_n\mathrm{e}^{\mathrm{i}(\tilde{k}_n\tilde{x}-\tilde{\omega}_n\tilde{t})}=\frac{\mathrm{i}}{4}\tilde{k}_n^2\tilde{k}_qA_n\bar{A}_q\mathrm{e}^{\mathrm{i}[(\tilde{k}_n-\tilde{k}_q)\tilde{x}-\tilde{\omega}_m\tilde{t}]}.$$

Note the difference of the sign for the latter. If the relationship is instead $\tilde{\omega}_m=\tilde{\omega}_n+\tilde{\omega}_q$, *i.e.* an up-conversion process, the terms become

$$\frac{\mathrm{i}}{2}\tilde{k}_nA_n\mathrm{e}^{\mathrm{i}(\tilde{k}_n\tilde{x}-\tilde{\omega}_n\tilde{t})}\cdot\left(-\frac{1}{2}\tilde{k}_q^2\right)A_q\mathrm{e}^{\mathrm{i}(\tilde{k}_q\tilde{x}-\tilde{\omega}_q\tilde{t})}=-\frac{\mathrm{i}}{4}\tilde{k}_n\tilde{k}_q^2A_nA_q\mathrm{e}^{\mathrm{i}[(\tilde{k}_n+\tilde{k}_q)\tilde{x}-\tilde{\omega}_m\tilde{t}]}$$

and

$$\frac{\mathrm{i}}{2}\tilde{k}_qA_q\mathrm{e}^{\mathrm{i}(\tilde{k}_q\tilde{x}-\tilde{\omega}_q\tilde{t})}\cdot\left(-\frac{1}{2}\tilde{k}_n^2\right)A_n\mathrm{e}^{\mathrm{i}(\tilde{k}_n\tilde{x}-\tilde{\omega}_n\tilde{t})}=-\frac{\mathrm{i}}{4}\tilde{k}_n^2\tilde{k}_qA_nA_q\mathrm{e}^{\mathrm{i}[(\tilde{k}_n+\tilde{k}_q)\tilde{x}-\tilde{\omega}_m\tilde{t}]}.$$

The last case is for addition with degeneracy, *i.e.* when $\tilde{\omega}_m=2\tilde{\omega}_n$. Then there will only be one term, given by

$$\frac{\mathrm{i}}{2}\tilde{k}_nA_n\mathrm{e}^{\mathrm{i}(\tilde{k}_n\tilde{x}-\tilde{\omega}_n\tilde{t})}\cdot\left(-\frac{1}{2}\tilde{k}_n^2\right)A_n\mathrm{e}^{\mathrm{i}(\tilde{k}_n\tilde{x}-\tilde{\omega}_n\tilde{t})}=-\frac{\mathrm{i}}{4}\tilde{k}_n^3A_n^2\mathrm{e}^{\mathrm{i}(2\tilde{k}_n\tilde{x}-\tilde{\omega}_m\tilde{t})}. \tag{3.23}$$

3.3.3 Constructing the propagation equations

Now that we have simplified both sides of Equation (3.13), we can construct the differential equations describing wave propagation, *i.e.* the propagation equations. On the left-hand side of the wave equation, each amplitude derivative A'_m has the prefactor $-\mathrm{i}\frac{\tilde{\omega}_m^2}{\tilde{k}_m}$ and on the right hand-side each term has the prefactor $\mp c_3\frac{\mathrm{i}}{4}$. Solving for A'_m, the prefactors on the right-hand side become $\pm\frac{c_3}{4}\frac{\tilde{k}_m}{\tilde{\omega}_m^2}$. When solving for A'_m the time dependence will disappear, since we have only kept the resonant terms. The propagation equation for each wave m hence becomes

$$\begin{aligned}A'_m=&\sum_{n,q:\ \tilde{\omega}_m=\tilde{\omega}_n-\tilde{\omega}_q}\frac{c_3}{4}\mathcal{C}_-(m,n,q)A_n\bar{A}_q\mathrm{e}^{\mathrm{i}(\tilde{k}_n-\tilde{k}_q-\tilde{k}_m)\tilde{x}}\\&-\frac{1}{2}\sum_{n,q:\ \tilde{\omega}_m=\tilde{\omega}_n+\tilde{\omega}_q}\frac{c_3}{4}\mathcal{C}_+(m,n,q)A_nA_q\mathrm{e}^{-\mathrm{i}(\tilde{k}_m-\tilde{k}_n-\tilde{k}_q)\tilde{x}}.\end{aligned} \tag{3.24}$$

where

$$\mathcal{C}_{-}(m,n,q) = \frac{\tilde{k}_m \tilde{k}_n \tilde{k}_q \left(\tilde{k}_n - \tilde{k}_q\right)}{\tilde{\omega}_m^2} \approx \tilde{\omega}_n \tilde{\omega}_q, \tag{3.25a}$$

$$\mathcal{C}_{+}(m,n,q) = \frac{\tilde{k}_m \tilde{k}_n \tilde{k}_q \left(\tilde{k}_n + \tilde{k}_q\right)}{\tilde{\omega}_m^2} \approx \tilde{\omega}_n \tilde{\omega}_q \tag{3.25b}$$

are the coupling factors. The factor $\frac{1}{2}$ adjusts for the degeneracy problem raised in Equation (3.23), since for every $a \neq b$ there will be two terms in the sum for $(n,q) = (a,b)$ and $(n,q) = (b,a)$, while for every $a = b$, only the term$(n,q) = (a,a)$ will exist. The approximation of the coupling coefficient is based on the fact that we are working with the continuous limit. We can hence approximate the wave numbers with linear dispersion, *i.e.* $\tilde{k} \approx \tilde{\omega}$. However, we do not use this approximation for the phase mismatches, as they would then be equal to zero. If all the phase mismatches are neglected, the propagation equations will not converge for any number of modes [47].

3.4 The three-wave mixing single idler model

In this section we will go through how to solve the propagation equations for three waves: the pump, which serves as the energy source, the signal, which is what we want to amplify, and the idler, a necessary third wave that is generated by the mixing process.

We will later show that this case is a highly idealised scenario which is not particularly accurate. However, it still serves as a benchmark showing what 3WM is capable of, if the necessary requirements are fulfilled.

3.4.1 The propagation equations

To begin let us assume we have three waves, the pump 'p', the signal 's' fulfilling $\tilde{\omega}_\mathrm{s} < \tilde{\omega}_\mathrm{p}$ and the idler 'i' given by $\tilde{\omega}_\mathrm{i} = \tilde{\omega}_\mathrm{p} - \tilde{\omega}_\mathrm{s}$. The full propagation

equations, using the form in Equation (3.24), for these three waves are

$$A_\mathrm{p}' = -\frac{c_3}{4}\mathcal{C}_+(\mathrm{p,s,i})A_\mathrm{s}A_\mathrm{i}\mathrm{e}^{-\mathrm{i}(\tilde{k}_\mathrm{p}-\tilde{k}_\mathrm{s}-\tilde{k}_\mathrm{i})\tilde{x}} \approx -\frac{c_3}{4}\tilde{\omega}_\mathrm{s}\tilde{\omega}_\mathrm{i}A_\mathrm{s}A_\mathrm{i}\mathrm{e}^{-\mathrm{i}(\tilde{k}_\mathrm{p}-\tilde{k}_\mathrm{s}-\tilde{k}_\mathrm{i})\tilde{x}}, \tag{3.26a}$$

$$A_\mathrm{s}' = \frac{c_3}{4}\mathcal{C}_-(\mathrm{s,p,i})A_\mathrm{p}\bar{A}_\mathrm{i}\mathrm{e}^{\mathrm{i}(\tilde{k}_\mathrm{p}-\tilde{k}_\mathrm{s}-\tilde{k}_\mathrm{i})\tilde{x}} \approx \frac{c_3}{4}\tilde{\omega}_\mathrm{p}\tilde{\omega}_\mathrm{i}A_\mathrm{p}\bar{A}_\mathrm{i}\mathrm{e}^{\mathrm{i}(\tilde{k}_\mathrm{p}-\tilde{k}_\mathrm{s}-\tilde{k}_\mathrm{i})\tilde{x}}, \tag{3.26b}$$

$$A_\mathrm{i}' = \frac{c_3}{4}\mathcal{C}_-(\mathrm{i,p,s})A_\mathrm{p}\bar{A}_\mathrm{s}\mathrm{e}^{\mathrm{i}(\tilde{k}_\mathrm{p}-\tilde{k}_\mathrm{s}-\tilde{k}_\mathrm{i})\tilde{x}} \approx \frac{c_3}{4}\tilde{\omega}_\mathrm{p}\tilde{\omega}_\mathrm{s}A_\mathrm{p}\bar{A}_\mathrm{s}\mathrm{e}^{\mathrm{i}(\tilde{k}_\mathrm{p}-\tilde{k}_\mathrm{s}-\tilde{k}_\mathrm{i})\tilde{x}}. \tag{3.26c}$$

Now let us define the phase mismatch $\Delta\tilde{k} = \tilde{k}_\mathrm{p} - \tilde{k}_\mathrm{s} - \tilde{k}_\mathrm{i}$ and the pumping strength $\chi = \frac{1}{4}c_3\tilde{\omega}_\mathrm{p}A_\mathrm{p}$. Let us also assume that the signal and idler amplitudes are much smaller than the pump amplitude, $A_\mathrm{s}, A_\mathrm{i} \ll A_\mathrm{p}$, which makes the pump equation $A_\mathrm{p}' = 0$, *i.e.* a constant pump, throughout the TWPA, which is also known as the *stiff pump approximation* [56]. Then we get the equations

$$A_\mathrm{s}' = \chi\tilde{\omega}_\mathrm{i}\bar{A}_\mathrm{i}\mathrm{e}^{\mathrm{i}\Delta\tilde{k}\tilde{x}}, \tag{3.27a}$$

$$A_\mathrm{i}' = \chi\tilde{\omega}_\mathrm{s}\bar{A}_\mathrm{s}\mathrm{e}^{\mathrm{i}\Delta\tilde{k}\tilde{x}}. \tag{3.27b}$$

3.4.2 Solving the propagation equations

To solve these differential equations, we first do a transformation to remove the exponential dependency. Then we get a matrix equation which can be solved by finding the eigenvalues and eigenvectors of the matrix of that equation. These steps are all outlined in Ref. [47]. Here we will only present the solution. Assuming that the initial amplitudes are $A_\mathrm{s0} = A_\mathrm{s}(0)$ and $A_\mathrm{i0} = A_\mathrm{i}(0)$, the solution is given by

$$A_\mathrm{s}(\tilde{x}) = \left[A_\mathrm{s0}\left(\cosh(g\tilde{x}) - \frac{\mathrm{i}\Delta\tilde{k}}{2g}\sinh(g\tilde{x})\right) + \frac{\tilde{\omega}_\mathrm{i}\chi}{g}\bar{A}_\mathrm{i0}\sinh(g\tilde{x})\right]\mathrm{e}^{\mathrm{i}\Delta\tilde{k}\tilde{x}/2}, \tag{3.28a}$$

$$A_\mathrm{i}(\tilde{x}) = \left[A_\mathrm{i0}\left(\cosh(g\tilde{x}) - \frac{\mathrm{i}\Delta\tilde{k}}{2g}\sinh(g\tilde{x})\right) + \frac{\tilde{\omega}_\mathrm{s}\chi}{g}\bar{A}_\mathrm{s0}\sinh(g\tilde{x})\right]\mathrm{e}^{\mathrm{i}\Delta\tilde{k}\tilde{x}/2}. \tag{3.28b}$$

where g is the gain coefficient, given by

$$g = \sqrt{\tilde{\omega}_\mathrm{s}\tilde{\omega}_\mathrm{i}\left|\chi\right|^2 - \left(\frac{\Delta\tilde{k}}{2}\right)^2}. \tag{3.29}$$

To obtain the gain we assume a zero initial idler, *i.e.* $A_{i0} = 0$ in Equation (3.28a), and we get that the power gain G is given by

$$G := \left|\frac{A_s(\tilde{x})}{A_{s0}}\right|^2 = \cosh^2(g\tilde{x}) + \frac{\Delta\tilde{k}^2}{4g^2}\sinh^2(g\tilde{x})\,. \tag{3.30}$$

3.4.3 Analysis in the purely linear dispersion regime

The purely linear regime is the regime where the dispersion relation is fully linear. In this regime the phase mismatch is zero ($\Delta\tilde{k} \approx 0$), or more accurately, negligibly small. Then we get

$$G = \cosh^2(g\tilde{x})\,, \quad \text{and} \quad g = \chi\sqrt{\tilde{\omega}_s\tilde{\omega}_i}. \tag{3.31}$$

In other words, we obtain exponential growth of the signal set by the gain coefficient g. By expressing the frequencies as

$$\tilde{\omega}_s = \frac{1+\delta}{2}\tilde{\omega}_p, \quad \tilde{\omega}_i = \frac{1-\delta}{2}\tilde{\omega}_p, \quad \delta = \frac{\tilde{\omega}_s - \tilde{\omega}_p/2}{\tilde{\omega}_p/2} \in (-1,1), \tag{3.32}$$

where δ is the signal detuning from half of the pump frequency, we can express the gain coefficient as

$$g = \chi\sqrt{\frac{1+\delta}{2}\frac{1-\delta}{2}\tilde{\omega}_p^2} = \frac{\chi\tilde{\omega}_p}{2}\sqrt{1-\delta^2}. \tag{3.33}$$

The gain coefficient has the shape of a semicircle with radius $\frac{1}{2}\chi\tilde{\omega}_p$ and its maximum at $\delta = 0$, *i.e.* when the signal frequency is equal to half of the pump frequency.

3.4.4 Further analysis of the pump

It is clear from Equation (3.33) that the larger the pump frequency is, the larger the gain coefficient becomes. However, if we increase the pump frequency enough, we will no longer be in the purely linear regime and the phase mismatch can no longer be neglected. If we keep increasing the pump frequency, at some point the phase mismatch becomes too large and the gain coefficient becomes imaginary. Then the exponential gain is replaced by oscillations as a function of the length of the TWPA. The pump frequency at

the threshold where this happens is known as the critical pump frequency.

If we instead fix the pump frequency and assume a pump amplitude large enough for exponential gain, and then decrease the pump amplitude, the same problem will arise. At some point, the phase mismatch will become too large and the gain coefficient becomes imaginary. This is known as the critical pumping strength.

Finally, given a certain pumping strength, there is a certain pump frequency where the gain coefficient has reached its largest value before the phase mismatch becomes too large. This is known as the optimal pump frequency.

The critical pump frequency, the critical pumping strength and the optimal pump frequency are all analysed and determined in Ref. [47].

3.5 Summary

In this chapter we have looked at what happens when the inductance in the discrete transmission line is nonlinear. We showed that it gives rise to frequency mixing, especially three-wave mixing and four-wave mixing. We derived the discrete wave equation and showed how it, under an assumption of long wavelengths, can be approximated by the continuous wave equation. We determined the general mixing equations for pure three-wave mixing. Then we solved the mixing equations for pure three-wave mixing between three modes: the pump, the signal and the idler. Finally we showed that under these assumptions, three modes in the continuous dispersion regime, one should expect an exponential spatial growth of the signal.

CHAPTER 4

Superconducting nonlinear inductive elements

In this chapter we will explore the different nonlinear elements we will use to build our TWPAs. While a TWPA can be built with nonlinear capacitors [35], this work is entirely focused on nonlinear inductors. To avoid losses, all the nonlinear inductors in this chapter are superconducting.

4.1 The Josephson junction

The simplest inductive element is the Josephson junction, which is also the basic building block for other inductive elements. The Josephson junction consists of two superconductors separated by a thin insulating barrier, see Figure 4.1.

For an ideal Josephson junction the Josephson relations [57] are

$$I_\mathrm{J} = I_\mathrm{c} \sin \Delta \qquad \text{“Josephson I”}, \tag{4.1a}$$

$$U_\mathrm{J} = \varphi_0 \dot{\Delta} \qquad \text{“Josephson II”}, \tag{4.1b}$$

where U_J is the voltage over the junction, I_J is the current passing through the junction, I_c is the junction critical current, $\varphi_0 = \hbar/(2e)$ is the reduced

superconducting magnetic flux quantum and Δ is the phase difference across the junction.

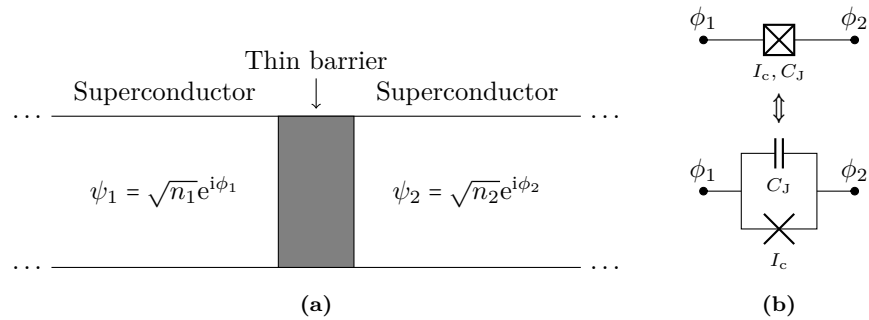

Figure 4.1: Illustrations of a Josephson junction. (**a**) Sketch of the superconductors with the wave functions ψ_i with the densities n_i and the phases ϕ_i, and the thin barrier that make the junction with the phase difference $\Delta := \phi_2 - \phi_1$. (**b**) Pictogram for a real Josephson junction (top) and pictogram for an ideal junction in parallel with a capacitance equal to the junction intrinsic capacitance (bottom).

Using the Josephson junction as the inductor in Figure 3.1 and utilising Equation (3.1), we can approximate the current through the junction at each node n of the TWPA as

$$\begin{aligned} I_{J,n} &= I_c \sin(\Delta_n) = I_c \sin(\Delta_0 + \delta_n) \\ &= I_c \sin\Delta_0 \cos\delta_n + I_c \sin\delta_n \cos\Delta_0 \\ &\approx I_c \sin\Delta_0 \left(1 - \frac{1}{2}\delta_n^2\right) + I_c \cos\Delta_0 \left(\delta_n - \frac{1}{6}\delta_n^3\right) \\ &= I_c \cos\Delta_0 \left[\tan\Delta_0 \left(1 - \frac{1}{2}\delta_n^2\right) + \left(\delta_n - \frac{1}{6}\delta_n^3\right)\right]. \end{aligned} \tag{4.2}$$

Let us define normalised currents as $i = I/I_c$. Then the phase-bias Δ_0 is determined by the normalised bias current $i_b = I_b/I_c$ as

$$i_b = \sin\Delta_0 \quad \Longrightarrow \quad \Delta_0 = \arcsin(i_b)\,. \tag{4.3}$$

The reference current is $I_0 = I_c \cos\Delta_0$, therefore the static inductance is given

by

$$L_{\mathrm{J}} = \frac{\varphi_0}{I_0} = \frac{\varphi_0}{I_{\mathrm{c}} \cos \Delta_0} = \frac{L_{\mathrm{J0}}}{\sqrt{1 - i_{\mathrm{b}}^2}} \tag{4.4}$$

where $L_{\mathrm{J0}} = \varphi_0 / I_{\mathrm{c}}$ is the junction inductance at zero bias. The line capacitance is equal to the junction intrinsic capacitance, $C = C_{\mathrm{J}}$.

The quadratic and cubic coefficients, as defined in Equation (3.2), are $b_2 = -\frac{1}{2} \tan \Delta_0$ and $b_3 = -\frac{1}{6}$. The mixing coefficients, as defined in Equation (3.5), are hence

$$c_3 = \tan \Delta_0, \quad c_4 = \frac{1}{2}. \tag{4.5}$$

The 4WM coefficient c_4 is fixed, *i.e.* 4WM is unaffected by the bias current. The 3WM coefficient on the other hand is

$$c_3 = \tan \Delta_0 = \frac{\sin \Delta_0}{\cos \Delta_0} = \frac{i_{\mathrm{b}}}{\sqrt{1 - i_{\mathrm{b}}^2}}. \tag{4.6}$$

In words, without a bias current there is 4WM but no 3WM. When increasing the bias current, the 3WM increases while 4WM is fixed. For a bias current close to the critical current, the 3WM coefficient diverges towards infinity. However, this does not mean that we can get an arbitrarily strong 3WM process, since the pumping strength χ is a function of both the mixing coefficient and the pump amplitude. Since the total current through the junction should not exceed the critical current, we get the constraint $I_{\mathrm{b}} + I_{\mathrm{p}} < I_{\mathrm{c}}$, which ensures that $\chi < 1/8$. See Ref. [47] for details.

4.2 Radio-frequency SQUID

Another superconducting nonlinear inductive element is the rf-SQUID [24]. It consists of a superconducting loop where one arm has an inductor with linear inductance L and another arm has a Josephson junction with critical current I_{c}. The linear inductance should be smaller than the junction inductance at zero bias, *i.e.* $L \leq L_{\mathrm{J0}}$, to avoid a hysteretic behaviour of the SQUID. There may also be a static external magnetic field applying a magnetic flux bias Φ_{b}, and/or a bias current I_{b}. The rf-SQUID is depicted in Figure 4.2.

The phase drop over the upper arm is $\Delta_{L,n}$ and the phase drop over the lower arm is Δ_n. To relate the magnetic flux bias Φ_{b} to the phase, let us define $F \coloneqq 2\pi \Phi_{\mathrm{b}} / \Phi_0$. This gives the constraint that $\Delta_n - \Delta_{L,n} = F$.

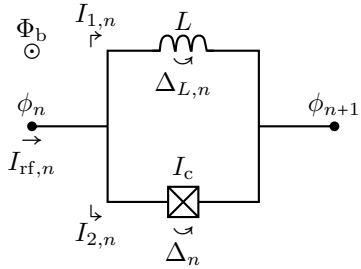

Figure 4.2: The rf-SQUID.

The rf-SQUID current is given by

$$\begin{aligned} I_{\mathrm{rf},n}(F,\Delta_n) = I_{1,n} + I_{2,n} &= \frac{\varphi_0}{L}\left(F+\Delta_n\right) + I_\mathrm{c}\sin(\Delta_n) \\ \implies i_{\mathrm{rf},n} &= \frac{L_{\mathrm{J}0}}{L}\left(\Delta_n - F\right) + \sin(\Delta_n)\,. \end{aligned} \tag{4.7a}$$

where $i_{\mathrm{rf},n} = I_{\mathrm{rf},n}/I_\mathrm{c}$ is the normalised rf-SQUID current and $L_{\mathrm{J}0} = \varphi_0/I_\mathrm{c}$ is the unbiased junction inductance. Let us define the inductance ratio $\bar{L} = L/L_{\mathrm{J}0}$. Since $L \leq L_{\mathrm{J}0}$, we know that $\bar{L} \in [0,1]$. By inserting the small phase variation, $\Delta_n = \Delta_0 + \delta_n$, the current becomes

$$\begin{aligned} i_{\mathrm{rf},n} &= \frac{\Delta_0+\delta_n-F}{\bar{L}} + \sin(\Delta_0+\delta_n) \\ &= \frac{\Delta_0+\delta_n-F}{\bar{L}} + \sin(\Delta_0)\cos(\delta_n) + \sin(\delta_n)\cos(\Delta_0) \\ &\approx \frac{\Delta_0+\delta_n-F}{\bar{L}} + \sin(\Delta_0)\left(1-\frac{1}{2}\delta_n^2\right) + \left(\delta_n - \frac{1}{6}\delta_n^3\right)\cos(\Delta_0)\,. \end{aligned} \tag{4.7b}$$

Rearranging the equation so that the different orders of small phase variation are gathered we get

$$\begin{aligned} i_{\mathrm{rf},n} = 1 \cdot &\left[\frac{\Delta_0 - F}{\bar{L}} + \sin(\Delta_0)\right] \\ &+ \delta_n \cdot \left[\frac{1}{\bar{L}} + \cos(\Delta_0)\right] \\ &- \frac{1}{2}\delta_n^2 \cdot \sin(\Delta_0) - \frac{1}{6}\delta_n^3 \cdot \cos(\Delta_0)\,. \end{aligned} \tag{4.7c}$$

We factor out the $1/\bar{L} + \cos(\Delta_0)$ factor to ensure that $b_1 = 1$, following the definition of the b_j-coefficients. The first term in Equation (4.7c) is the normalised bias current i_b and gives the constraint

$$i_\mathrm{b} = \frac{\Delta_0 - F}{\bar{L}} + \sin(\Delta_0)\,, \tag{4.8}$$

which, given a value of the flux bias F and of the bias current i_b, lets us find the value of Δ_0 numerically. Typically we use $i_\mathrm{b} = 0$, although an rf-SQUID could be biased with a bias current instead of a magnetic flux bias [24]. From Equation (4.7c) we extract the inductance of the rf-SQUID to be

$$L_0 = L_\mathrm{rf} = \frac{L_\mathrm{J0}}{\bar{L}^{-1} + \cos(\Delta_0)} = \frac{L}{1 + \bar{L}\cos(\Delta_0)}. \tag{4.9}$$

The capacitance of the rf-SQUID is simply given by the capacitance of the junction, *i.e.* $C = C_\mathrm{J}$. We can also extract the mixing coefficients, as defined in Equation (3.5), as

$$c_3 = \frac{\sin(\Delta_0)}{\bar{L}^{-1} + \cos(\Delta_0)} = \frac{\bar{L}\sin(\Delta_0)}{1 + \bar{L}\cos(\Delta_0)}, \tag{4.10a}$$

$$c_4 = \frac{1}{2} \cdot \frac{\cos(\Delta_0)}{\bar{L}^{-1} + \cos(\Delta_0)} = \frac{1}{2} \cdot \frac{\bar{L}\cos(\Delta_0)}{1 + \bar{L}\cos(\Delta_0)}. \tag{4.10b}$$

Now let us analyse the inductance and the mixing coefficients. Note that there exists a bias point where $c_3 \neq 0, c_4 = 0$. There are hence three fluxes of interest in particular: zero flux $\Phi_\mathrm{b} = 0$, half of a flux quantum $\Phi_\mathrm{b}/\Phi_0 = 0.5$ and the flux of pure three-wave mixing $\Phi_\mathrm{b}/\Phi_0 = \phi_3$, also known as the Kerr-free point.

At the Kerr-free point we have that $c_4 = 0$ and thus $\cos(\Delta_0) = 0$. The first positive value of Δ_0 to fulfill this is $\Delta_0 = \pi/2$. By solving Equation (4.8) for F using $\Delta_0 = \pi/2$, we can show that

$$\phi_3 = \frac{1}{4} + \frac{\bar{L}}{2\pi}\,(1 - i_\mathrm{b})\,. \tag{4.11a}$$

For zero bias current, the Kerr-free point is thus somewhere in the interval

$$\phi_3 \in \left[\frac{1}{4}, \frac{1}{4} + \frac{1}{2\pi}\right] \approx \left[0.25, 0.41\right]. \tag{4.11b}$$

since $\bar{L} \in [0, 1]$. If instead we want to apply a bias current and no flux bias, we set $\phi_3 = 0$ in Equation (4.11a) and solve for i_b. We get

$$i_\mathrm{b} = 1 + \frac{\pi}{2\bar{L}}, \tag{4.11c}$$

i.e. the bias current needs to be at least $1 + \pi/2 \approx 2.57$ times larger than the junction critical current, which is possible because most of the bias current goes through the linear inductor L.

The inductance and mixing coefficients at these points can be found analytically and are presented in Table 4.1. Plots for the inductance and mixing coefficients for all fluxes are presented in Figures 4.3 and 4.4.

Table 4.1: The inductance L_0 in terms of L and the mixing coefficients c_3, c_4 for different flux biases Φ_b of an rf-SQUID at zero bias current.

Φ_b/Φ_0	0	ϕ_3	0.5
L_0/L	$\dfrac{1}{1+\bar{L}}$	1	$\dfrac{1}{1-\bar{L}}$
c_3	0	$\bar{L}$	0
c_4	$\dfrac{1}{2}\cdot\dfrac{\bar{L}}{1+\bar{L}}$	0	$-\dfrac{1}{2}\cdot\dfrac{\bar{L}}{1-\bar{L}}$

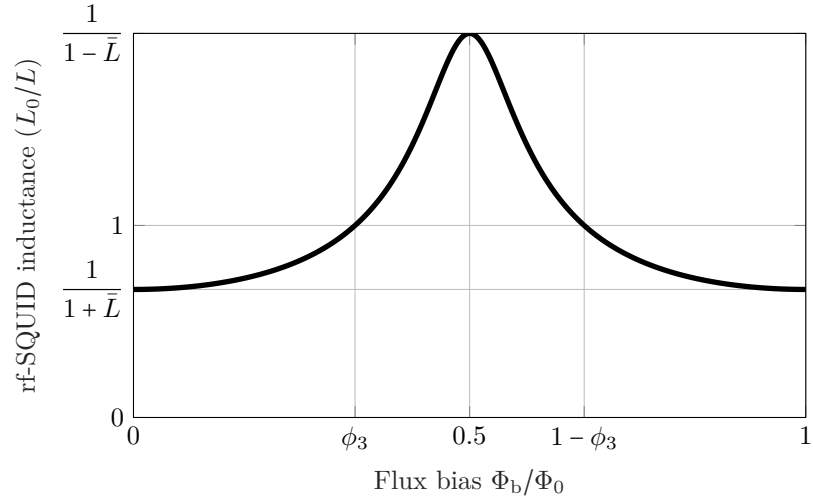

Figure 4.3: The inductance of an rf-SQUID at zero bias current in terms of the linear inductor L as a function of magnetic flux bias.

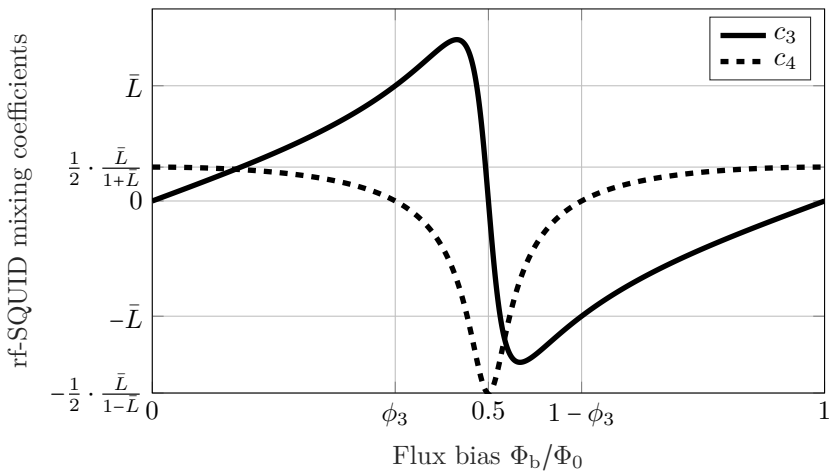

Figure 4.4: The mixing coefficients c_3, c_4 of an rf-SQUID at zero bias current as a function of magnetic flux bias.

4.3 The SNAIL

Another nonlinear inductive element is the SNAIL, which is an acronym for the Superconducting Nonlinear Asymmetric Inductive eLement [16]. It consists of a loop, where one arm has $\mathcal{N}$ identical Josephson junctions with critical current I_c, while the other arm has a single Josephson junction with critical current αI_c where $\alpha < 1$. There may also be a static external magnetic field applying a magnetic flux bias Φ_b. The SNAIL is depicted in Figure 4.5.

Further limitations to α can be made. We want $\alpha \leq 1/\mathcal{N}$ to be free of hysteresis, similar to the rf-SQUID where $\bar{L}$ had to be smaller than 1 for the same reason. We also want $\alpha > 1/\mathcal{N}^3$ to ensure that there exists a flux ϕ_3 with pure three-wave mixing.

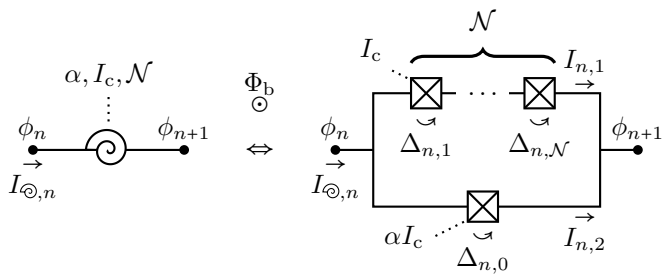

Figure 4.5: The Superconducting Nonlinear Asymmetric Inductive eLement.

In Figure 4.5, let us call the lone junction "junction 0", and those on the top arm "junction 1", ..., "junction $\mathcal{N}$". Since the same current that flows through junction 1 will also flow through junction 2 to junction $\mathcal{N}$, and they have the same critical currents, the phase differences over these junctions are identical. If we call the total phase drop over these junctions Δ_n, the phase drop over one of them is hence $\Delta_n/\mathcal{N}$.

The phase difference over the upper arm is Δ_n and the phase difference over the lower arm is $\Delta_{n,0}$. To relate the magnetic flux Φ_b to the phase difference, let us use the same definition as in Section 4.2, $F \coloneqq 2\pi\Phi_b/\Phi_0$. This gives us the constraint $\Delta_{n,0} - \Delta_n = F$, or in other words, that the phase difference over junction 0 is $\Delta_{n,0} = F + \Delta_n$.

The SNAIL current is given by

$$\begin{aligned} I_{\circledcirc,n} &= I_{n,1} + I_{n,2} = \alpha I_\mathrm{c} \sin(\Delta_{n,0}) + I_\mathrm{c} \sin(\Delta_{n,1}) \\ &= I_\mathrm{c} \left[\alpha \sin(F + \Delta_n) + \sin\left(\frac{\Delta_n}{\mathcal{N}}\right)\right]. \end{aligned} \tag{4.12a}$$

To make the equations cleaner, let us define the normalised SNAIL current $i_{\circledcirc,n} = I_{\circledcirc,n}/I_\mathrm{c}$. Let us also insert the small phase variation $\Delta_n = \Delta_0 + \delta_n$. The current becomes

$$\begin{aligned} i_{\circledcirc,n} &= \alpha \sin(F + \Delta_0 + \delta_n) + \sin\left(\frac{\Delta_0 + \delta_n}{\mathcal{N}}\right) \\ &= \alpha\big[\sin(F + \Delta_0)\cos(\delta_n) + \sin(\delta_n)\cos(F + \Delta_0)\big] \\ &+ \sin\left(\frac{\Delta_0}{\mathcal{N}}\right)\cos\left(\frac{\delta_n}{\mathcal{N}}\right) + \sin\left(\frac{\delta_n}{\mathcal{N}}\right)\cos\left(\frac{\Delta_0}{\mathcal{N}}\right). \end{aligned} \tag{4.12b}$$

Then, using Taylor expansion, we can approximate the current as

$$\begin{aligned} i_{\circledcirc,n} \approx \alpha &\left[\sin(F + \Delta_0)\left(1 - \frac{1}{2}\delta_n^2\right) + \left(\delta_n - \frac{1}{6}\delta_n^3\right)\cos(F + \Delta_0)\right] \\ &+ \sin\left(\frac{\Delta_0}{\mathcal{N}}\right)\left(1 - \frac{1}{2}\left(\frac{\delta_n}{\mathcal{N}}\right)^2\right) + \left(\frac{\delta_n}{\mathcal{N}} - \frac{1}{6}\left(\frac{\delta_n}{\mathcal{N}}\right)^3\right)\cos\left(\frac{\Delta_0}{\mathcal{N}}\right). \end{aligned} \tag{4.12c}$$

Rearranging the equation so that the different orders of small phase variation are gathered we get

$$\begin{aligned} i_{\circledcirc,n} \approx\ & 1 \cdot \left[\alpha \sin(F + \Delta_0) + \sin\left(\frac{\Delta_0}{\mathcal{N}}\right)\right] \\ &+ \delta_n \cdot \left[\alpha \cos(F + \Delta_0) + \frac{1}{\mathcal{N}}\cos\left(\frac{\Delta_0}{\mathcal{N}}\right)\right] \\ &- \frac{1}{2}\delta_n^2 \cdot \left[\alpha \sin(F + \Delta_0) + \frac{1}{\mathcal{N}^2}\sin\left(\frac{\Delta_0}{\mathcal{N}}\right)\right] \\ &- \frac{1}{6}\delta_n^3 \cdot \left[\alpha \cos(F + \Delta_0) + \frac{1}{\mathcal{N}^3}\cos\left(\frac{\Delta_0}{\mathcal{N}}\right)\right]. \end{aligned} \tag{4.12d}$$

We factor out the factor multiplied with δ_n, to ensure that $b_1 = 1$ as we have previously mentioned follows from the definition of the b_j-coefficients. The first term in Equation (4.12d) is the normalised bias current i_b which gives

the constraint

$$i_\mathrm{b} = \alpha \sin(F + \Delta_0) + \sin\left(\frac{\Delta_0}{\mathcal{N}}\right), \tag{4.13}$$

which in turn lets us find the value of Δ_0 numerically, given the value of the flux bias F and the bias current i_b. Typically we use $i_\mathrm{b} = 0$, although a SNAIL, just like the rf-SQUID, can be biased with a bias current instead of magnetic flux bias. We extract the inductance of the SNAIL from Equation (4.12d) as

$$L_0 = L_{\circledcirc} = \frac{L_{\mathrm{J}0}}{\alpha \cos(F + \Delta_0) + \frac{1}{\mathcal{N}} \cos\left(\frac{\Delta_0}{\mathcal{N}}\right)} \tag{4.14}$$

The capacitance of the SNAIL is given by

$$C = C_{\circledcirc} = \frac{C_{\mathrm{J},1}}{\mathcal{N}} + C_{\mathrm{J},2} \overset{!}{=} \frac{C_{\mathrm{J},1}}{\mathcal{N}} + \alpha C_{\mathrm{J},1} = C_{\mathrm{J},1}\left(\frac{1}{\mathcal{N}} + \alpha\right). \tag{4.15}$$

where $C_{\mathrm{J},1}$ is the capacitance of each junction in the upper arm in Figure 4.5 and $C_{\mathrm{J},2}$ is the capacitance of the single junction. In the middle equality, marked with an exclamation mark, we used the fact that junctions made with the same process will have the same plasma frequency, regardless of their size. In other words, both C_J and I_c scale equally with the junction area.

We can also extract the mixing coefficients, as defined in Equation (3.5), as

$$c_3 = \frac{\alpha \sin(F + \Delta_0) + \frac{1}{\mathcal{N}^2} \sin\left(\frac{\Delta_0}{\mathcal{N}}\right)}{\alpha \cos(F + \Delta_0) + \frac{1}{\mathcal{N}} \cos\left(\frac{\Delta_0}{\mathcal{N}}\right)}, \tag{4.16a}$$

$$c_4 = \frac{1}{2} \cdot \frac{\alpha \cos(F + \Delta_0) + \frac{1}{\mathcal{N}^3} \cos\left(\frac{\Delta_0}{\mathcal{N}}\right)}{\alpha \cos(F + \Delta_0) + \frac{1}{\mathcal{N}} \cos\left(\frac{\Delta_0}{\mathcal{N}}\right)}. \tag{4.16b}$$

Now let us analyse the inductance and the mixing coefficients. Note that, similarly to the rf-SQUID, there exists a bias point where $c_3 \neq 0, c_4 = 0$. There are hence three fluxes of interest in particular: zero flux $\Phi_\mathrm{b} = 0$, half of a flux quantum $\Phi_\mathrm{b}/\Phi_0 = 0.5$ and the flux of pure three-wave mixing $\Phi_\mathrm{b}/\Phi_0 = \phi_3$. The inductance and mixing coefficients at these points are presented in Table 4.2. Plots for the inductance and mixing coefficients for all fluxes are presented in Figures 4.6 and 4.7.

Let us begin with analysing the inductance, see Figure 4.6. If the junctions 1 to $\mathcal{N}$ were linear inductors, the SNAIL would be identical to an rf-SQUID

and the inductance at ϕ_3 would be $\mathcal{N}L_{J0}$. However, the nonlinearity of the junctions increases the four-wave mixing coefficient, which in turn shifts the Kerr-free point from $\phi_3' = 1/4 + \alpha\mathcal{N}/(2\pi)$ where it would have been if the junctions were linear (recall and *cf.* with Equation (4.11a)), to $\phi_3 > \phi_3'$. Since ϕ_3 is closer to half of a flux quantum than ϕ_3', the inductance is increased.

By solving Equation (4.14) for $i_b = 0$ and $c_4 = 0$, the inductance at ϕ_3 for the SNAIL can be shown to be

$$L_{\circledcirc}(\phi_3) = \frac{\mathcal{N}L_{J0}}{1-\mathcal{N}^{-2}} \cdot \sqrt{\frac{1-\mathcal{N}^{-6}}{1-\alpha^2}} \approx \frac{\mathcal{N}L_{J0}}{1-\mathcal{N}^{-2}}. \tag{4.17}$$

As we can see, for $\mathcal{N} = 2$ the inductance of the SNAIL at the Kerr-free point is clearly larger than the inductance of the rf-SQUID at the Kerr-free point. For $\mathcal{N} > 2$ the denominator quickly becomes negligible and the SNAIL has a comparable inductance to the rf-SQUID. Furthermore, at the flux bias ϕ_3', the SNAIL has approximately the same inductance as the rf-SQUID, see the inductance at ϕ_3' in Figure 4.6. By solving Equation (4.16a) for $i_b = 0$ and $c_4 = 0$, the three-wave mixing coefficient at ϕ_3 can be shown to be

$$c_3(\phi_3) = \alpha\mathcal{N}\sqrt{\frac{1-\alpha^{-2}\mathcal{N}^{-6}}{1-\alpha^2}} \approx \alpha\mathcal{N}. \tag{4.18}$$

Note that the approximation $\alpha\mathcal{N}$ will underestimate the coefficient for $\alpha > 1/\mathcal{N}^{3/2}$, and overestimate it for $\alpha < 1/\mathcal{N}^{3/2}$, especially when $\alpha \to 1/\mathcal{N}^3$.

Table 4.2: The inductance L_0 in terms of $\mathcal{N}L_{J0}$ and the mixing coefficients c_3, c_4 for different flux biases Φ_b of a SNAIL at zero bias current.

Φ_b/Φ_0	0	ϕ_3	0.5
$L_0/(\mathcal{N}L_{J0})$	$\dfrac{1}{1+\alpha\mathcal{N}}$	$\approx \dfrac{1}{1-\mathcal{N}^{-2}}$	$\dfrac{1}{1-\alpha\mathcal{N}}$
c_3	0	$\approx \alpha\mathcal{N}$	0
c_4	$\dfrac{1}{2}\cdot\dfrac{\alpha\mathcal{N}+\mathcal{N}^{-2}}{1+\alpha\mathcal{N}}$	0	$-\dfrac{1}{2}\cdot\dfrac{\alpha\mathcal{N}-\mathcal{N}^{-2}}{1-\alpha\mathcal{N}}$

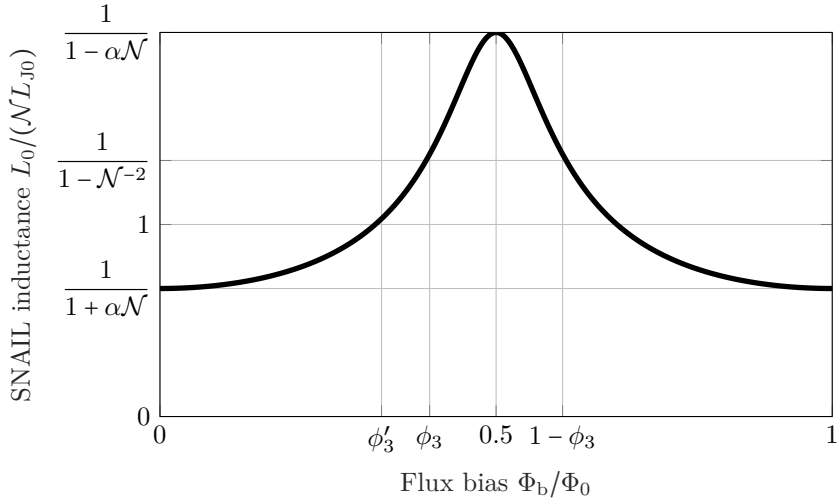

Figure 4.6: The inductance L_0 of a SNAIL at zero bias current, in terms of $\mathcal{N}L_{J0}$, as a function of magnetic flux bias.

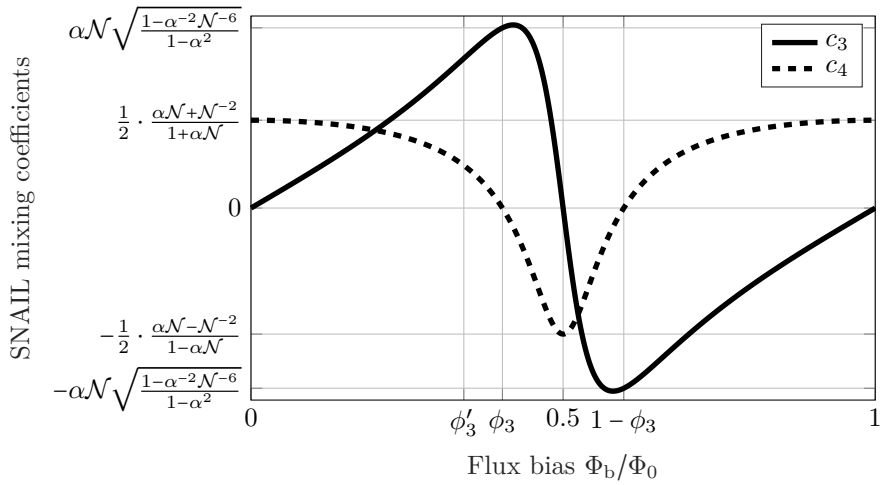

Figure 4.7: The mixing coefficients c_3, c_4 of a SNAIL at zero bias current as a function of magnetic flux bias.

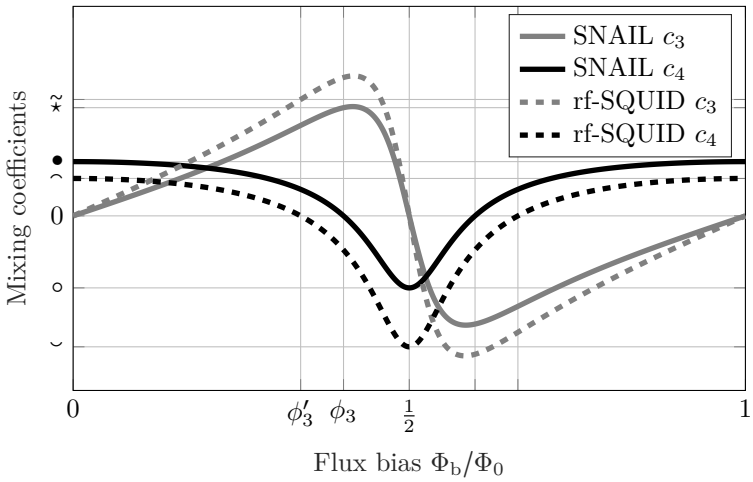

Figure 4.8: The mixing coefficients for the rf-SQUID and the SNAIL as a function of flux bias for $\alpha < 1/\mathcal{N}^{3/2}$. The symbols are explained in Section 4.3.1.

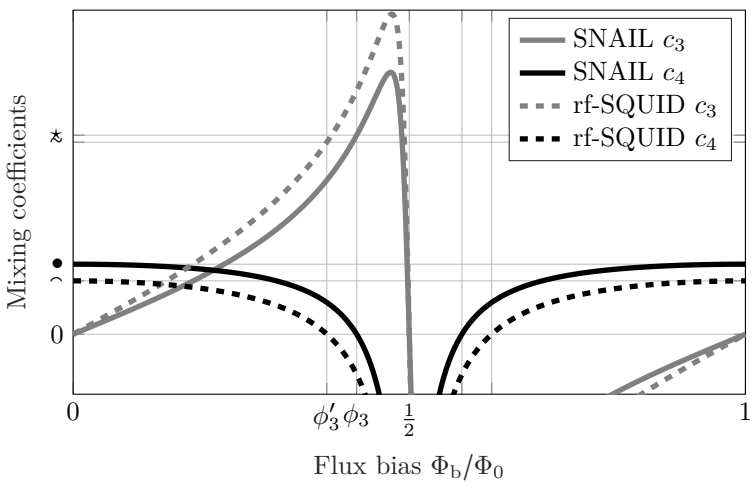

Figure 4.9: The mixing coefficients for the rf-SQUID and the SNAIL as a function of flux bias for $\alpha > 1/\mathcal{N}^{3/2}$. The symbols are explained in Section 4.3.1.

4.3.1 Comparison between the SNAIL and the rf-SQUID

Due to the similarities between the rf-SQUID and the SNAIL, it is instructive to compare the two. To be able to compare the two, one needs to find relevant measures for comparing.

As we discussed previously, for the inductance the relevant comparison is found by setting $L = \mathcal{N} L_{\mathrm{J0}}$. The inductance at a given flux is essentially the same between the two, but due to the shift of the Kerr-free point, the SNAIL has a larger inductance than the rf-SQUID at the Kerr-free point, recall Equation (4.17). The mixing coefficients can be compared by letting $\bar{L} = \alpha\mathcal{N}$.

Study Figures 4.8 and 4.9. Here '$\star$' denotes the three-wave mixing coefficient at the Kerr-free point for the SNAIL, '$\sim$' the three-wave mixing coefficient at the Kerr-free point for the rf-SQUID, '$\bullet$' the four-wave mixing coefficient at zero flux for the SNAIL, '$\frown$' the four-wave mixing coefficient at zero flux for the rf-SQUID, '$\circ$' the four-wave mixing coefficient at half a flux quantum for the SNAIL, and '$\smile$' the four-wave mixing coefficient at half a flux quantum for the rf-SQUID. Recall Figures 4.3, 4.4, 4.6 and 4.7 for the exact values.

As can be seen in Figures 4.8 and 4.9, the four-wave mixing coefficient is always larger for the SNAIL than for the rf-SQUID, but this increase becomes negligible for large $\mathcal{N}$. Furthermore, for each flux bias, the absolute value of the three-wave mixing coefficient is always smaller for the SNAIL than for the rf-SQUID. However, this does not mean that the three-wave mixing coefficient at the Kerr-free point is smaller for the SNAIL. Due to the shape of the curve, and the fact that $\phi_3 > \phi_3'$, the three-wave mixing coefficient at the Kerr-free point will be larger for the SNAIL than the one of the rf-SQUID when $\alpha > 1/\mathcal{N}^{3/2}$, and smaller when $\alpha < 1/\mathcal{N}^{3/2}$, recall Equation (4.18) and compare Figures 4.8 and 4.9.

4.4 Kinetic inductance

Similarly to a Josephson junction, a thin superconducting wire also behaves like a nonlinear inductor with an inductance modulated by the current. The inductance can be approximated as $L(I) \approx L(0)\left(1 + I^2/I_*^2\right)$ [27] for currents $I \ll I_*$, where I_* plays a similar role as the critical current I_c of a Josephson junction. There are two main differences between the Josephson junction and the kinetic inductor:

Firstly, the kinetic inductor is a distributed element, while the junction is a discrete element. It is hence possible to make an actual continuous transmission line, instead of a lumped-element one which we use in the discrete transmission line. This has both advantages and disadvantages, as we will see in later chapters. One can still make the kinetic inductor appearing like a lumped-element by ensuring that the wavelengths of all propagating modes are much longer than the kinetic inductor.

Secondly, the current I_* is typically orders of magnitude larger than the critical current I_c of a junction. This makes no difference except that the pump, and the potential bias current, must be increased with the factor I_*/I_c in order to get the same gain characteristics. This has one clear advantage and one clear disadvantage. The advantage is that the kinetic inductance TWPA thus typically has a much larger saturation power, since the pump has a much larger amplitude. The disadvantage is that, since the pump has a much larger amplitude, the kinetic inductance TWPA also has a much worse pump leakage.

A material with a kinetic inductance is aluminium, but it has a fairly weak kinetic inductance. A way of increasing the kinetic inductance of aluminium is by making granular aluminium (grAl). Granular aluminium consists of pure aluminium grains separated by thin aluminium oxide barriers [58]. This essentially builds a network of Josephson junctions inside the material, which increases the kinetic inductance significantly.

4.5 Arrays of inductive elements

An alternative approach to increase the saturation power without having to use a kinetic inductor is to use an array of inductive elements. This means that, instead of using a single Josephson junction, a single rf-SQUID or a single SNAIL, one uses several in series. To get the appropriate inductance, one simply increases the critical currents with the same factor as the number of elements in the chain.

As an example, if a TWPA design has a single junction with critical current I_c, one replaces with single junction with N junctions with the critical current NI_c. The required pump current to get the same gain as the original TWPA scales with the same factor, $I_p \mapsto NI_p$, and the saturation power is thus increased with a factor N^2. Simultaneously, the pump leakage is also increased

with a factor N^2. It is thus a tradeoff, where the user needs to decide what is more important, a higher saturation power or a lower pump leakage.

4.6 Summary

In conclusion, there are several different nonlinear inductive elements that we can use to build a TWPA, each with their own pros and cons. The Josephson junction has the advantage that it is the simplest one, but it can never fully eliminate four-wave mixing. The rf-SQUID can fully eliminate four-wave mixing if biased properly and it is more resilient to electrostatic discharges (ESDs) than a single junction, but it requires two different kinds of inductors. The SNAIL only requires one kind of inductor, the Josephson junction, but it lacks the resilience against ESDs that the rf-SQUID has. The kinetic inductors, including granular aluminium, can give a higher saturation power, but they also increase the pump leakage. A summary of the equations for the Josephson junction, the rf-SQUID and the SNAIL is presented in Table 4.3.

Table 4.3: The capacitance, phase-bias equation, inductance and the mixing coefficients for the Josephson junction, the rf-SQUID and the SNAIL.

	JJ	rf-SQUID	SNAIL
C	C_J	C_J	$C_{\mathrm{J},1}\left(\frac{1}{\mathcal{N}}+\alpha\right)$
i_b	$\sin(\Delta_0)$	$\frac{\Delta_0 - F}{\bar{L}} + \sin(\Delta_0)$	$\alpha\sin(F+\Delta_0)+\sin\left(\frac{\Delta_0}{\mathcal{N}}\right)$
L_0	$\frac{L_{\mathrm{J}0}}{\cos(\Delta_0)}$	$\frac{L}{1+\bar{L}\cos(\Delta_0)}$	$\frac{L_{\mathrm{J}0}}{\alpha\cos(F+\Delta_0)+\frac{1}{\mathcal{N}}\cos\left(\frac{\Delta_0}{\mathcal{N}}\right)}$
c_3	$\tan(\Delta_0)$	$\frac{\bar{L}\sin(\Delta_0)}{1+\bar{L}\cos(\Delta_0)}$	$\frac{\alpha\sin(F+\Delta_0)+\frac{1}{\mathcal{N}^2}\sin\left(\frac{\Delta_0}{\mathcal{N}}\right)}{\alpha\cos(F+\Delta_0)+\frac{1}{\mathcal{N}}\cos\left(\frac{\Delta_0}{\mathcal{N}}\right)}$
c_4	$\frac{1}{2}$	$\frac{1}{2}\cdot\frac{\bar{L}\cos(\Delta_0)}{1+\bar{L}\cos(\Delta_0)}$	$\frac{1}{2}\cdot\frac{\alpha\cos(F+\Delta_0)+\frac{1}{\mathcal{N}^3}\cos\left(\frac{\Delta_0}{\mathcal{N}}\right)}{\alpha\cos(F+\Delta_0)+\frac{1}{\mathcal{N}}\cos\left(\frac{\Delta_0}{\mathcal{N}}\right)}$

CHAPTER 5

Three-wave mixing in the quasilinear dispersion regime

In this chapter we will study multimode theory for three-wave mixing in the quasilinear dispersion regime. One could study three-wave mixing in the purely linear dispersion regime, where all phase mismatches are zero, $\Delta k = 0$. However, as outlined in Section 4.3 of Ref. [47], in the purely linear dispersion regime there is an infinite number of up-converted modes generated, and the transmission never converges. Therefore we will study the quasilinear regime, which more accurately describes reality.

5.1 Single input multimode study

In Section 3.3 we outlined the general mixing equations for three-wave mixing for any number of waves and mixing processes, recall Equation (3.24). In this section we will assume that there is only one input. Thus, the only waves present inside the TWPA are the input and its harmonics. Then we will use certain transformations on the propagation equations such that there is only one parameter left in the equations.

5.1.1 The propagation equations

If we assume the frequency of the input is $\tilde{\omega}_1$, the mixing products are thus at the frequencies $\tilde{\omega}_m = m\tilde{\omega}_1$ for $m \in \mathbb{Z}_+$. Let us assume that the number of harmonics is M. For each wave $m \in [1, M] \cap \mathbb{N}$, it can up-convert to any of the higher frequencies $n \in [m+1, M] \cap \mathbb{N}$, or down-convert into any of the lower frequencies $n \in [1, m-1] \cap \mathbb{N}$. The propagation equations for this case, recall Equation (3.24), are hence

$$\begin{aligned} A'_m = &\sum_{n=m+1}^{M} \frac{c_3}{4} \tilde{\omega}_n \tilde{\omega}_{n-m} A_n \bar{A}_{n-m} \mathrm{e}^{\mathrm{i}(\tilde{k}_n - \tilde{k}_m - \tilde{k}_{n-m})\tilde{x}} \\ &-\frac{1}{2} \sum_{n=1}^{m-1} \frac{c_3}{4} \tilde{\omega}_n \tilde{\omega}_{m-n} A_n A_{m-n} \mathrm{e}^{-\mathrm{i}(\tilde{k}_m - \tilde{k}_n - \tilde{k}_{m-n})\tilde{x}}. \end{aligned} \tag{5.1}$$

Since all frequencies are harmonics of the first one, we can write the frequency product as a number times $\tilde{\omega}_1^2$. Furthermore, we can approximate the phase mismatches within the cubic approximation of the dispersion relation,

$$\begin{aligned} \tilde{k}_n - \tilde{k}_m - \tilde{k}_{n-m} &\approx b\tilde{\omega}_n^3 - b\tilde{\omega}_m^3 - b\tilde{\omega}_{n-m}^3 \\ &= b\left(n\tilde{\omega}_1\right)^3 - b\left(m\tilde{\omega}_1\right)^3 - b\big((n-m)\tilde{\omega}_1\big)^3 \\ &= b\tilde{\omega}_1^3\left(n^3 - m^3 - (n-m)^3\right) \\ &= 3b\tilde{\omega}_1^3 mn(n-m) \end{aligned} \tag{5.2}$$

where b is the cubic coefficient in Equation (2.18). For the first phase mismatch this is hence

$$\tilde{k}_2 - 2\tilde{k}_1 \approx 3b\tilde{\omega}_1^3 \cdot 2 \cdot 1 \cdot (2-1) = 6b\tilde{\omega}_1^3. \tag{5.3}$$

We can find the fraction of the general phase mismatch and the first one as

$$\frac{\tilde{k}_n - \tilde{k}_m - \tilde{k}_{n-m}}{\tilde{k}_2 - 2\tilde{k}_1} = \frac{3b\tilde{\omega}_1^3 mn(n-m)}{6b\tilde{\omega}_1^3} = \frac{1}{2} mn(n-m) := d_{n,m}. \tag{5.4}$$

We can hence write the propagation equations as

$$\begin{aligned} A'_m = &\sum_{n=m+1}^{M} \frac{c_3\tilde{\omega}_1^2}{4} n(n-m) A_n \bar{A}_{n-m} \mathrm{e}^{\mathrm{i}(\tilde{k}_2-2\tilde{k}_1)\tilde{x}d_{n,m}} \\ &-\frac{1}{2}\sum_{n=1}^{m-1} \frac{c_3\tilde{\omega}_1^2}{4} n(m-n) A_n A_{m-n} \mathrm{e}^{-\mathrm{i}(\tilde{k}_2-2\tilde{k}_1)\tilde{x}d_{m,n}}. \end{aligned} \tag{5.5}$$

5.1.2 Rescaling the propagation equations

Now we will rescale the propagation equations for reasons that will soon become apparent. First let us note that, since energy is conserved and all initial energy is in the first harmonic, if we rescale each amplitude according to

$$b_m(\tilde{x}) = m\frac{A_m(\tilde{x})}{A_1(0)} \tag{5.6}$$

the sum of the absolute value of all amplitudes squared must always be 1, which is convenient. Then the propagation equations become

$$\begin{aligned} \frac{A_1(0)}{m} b'_m = &\sum_{n=m+1}^{M} \frac{c_3\tilde{\omega}_1^2}{4} A_1^2(0) b_n \bar{b}_{n-m} \mathrm{e}^{\mathrm{i}(\tilde{k}_2-2\tilde{k}_1)\tilde{x}d_{n,m}} \\ &-\frac{1}{2}\sum_{n=1}^{m-1} \frac{c_3\tilde{\omega}_1^2}{4} A_1^2(0) b_n b_{m-n} \mathrm{e}^{-\mathrm{i}(\tilde{k}_2-2\tilde{k}_1)\tilde{x}d_{m,n}}. \end{aligned} \tag{5.7}$$

If we now introduce the rescaled length ξ and the transformed amplitude a_m as

$$\xi(\tilde{x}) = \frac{c_3\tilde{\omega}_1^2}{4} A_1(0)\cdot\tilde{x}, \quad a_m\big(\xi(\tilde{x})\big) = b_m(\tilde{x}) \tag{5.8}$$

we get that

$$\frac{\mathrm{d}}{\mathrm{d}\tilde{x}} b_m(\tilde{x}) = \frac{\mathrm{d}}{\mathrm{d}\xi} a_m\big(\xi(\tilde{x})\big)\cdot\frac{\mathrm{d}}{\mathrm{d}\tilde{x}}\xi(\tilde{x}) \quad \Longrightarrow \quad \frac{\mathrm{d}}{\mathrm{d}\xi} a_m = \frac{\mathrm{d}}{\mathrm{d}\tilde{x}} b_m \cdot \frac{4}{A_1(0) c_3\tilde{\omega}_1^2}. \tag{5.9}$$

Finally, by defining the dimensionless parameter

$$\mu = 4\frac{\tilde{k}_2 - 2\tilde{k}_1}{c_3\tilde{\omega}_1^2 A_1(0)} \tag{5.10}$$

we can write the propagation equations as a function of only this one parameter μ and the rescaled length ξ,

$$a'_m(\xi) = m\left(\sum_{n=m+1}^{M} a_n \bar{a}_{n-m} \mathrm{e}^{\mathrm{i}\mu\xi d_{n,m}} - \frac{1}{2}\sum_{n=1}^{m-1} a_n a_{m-n} \mathrm{e}^{-\mathrm{i}\mu\xi d_{m,n}}\right). \tag{5.11}$$

This is a set of M equations, one for each harmonic $m \in [1, M] \cap \mathbb{N}$. Here we have reduced all values of $c_3, A_1(0), \tilde{\omega}_1, \tilde{C}$ in the quasilinear regime into a set of equations dependent on the single scaling parameter μ. Regardless of actual initial amplitudes, the *rescaled* initial amplitudes are 1 for the first harmonic and 0 for the others. Furthermore, we can simplify the expression of the scaling parameter as

$$\mu \approx 4\frac{b\tilde{\omega}_2^3 - b\tilde{\omega}_1^3}{c_3\tilde{\omega}_1^2 A_1(0)} = \frac{24b\tilde{\omega}_1^3}{c_3\tilde{\omega}_1^2 A_1(0)} = \frac{24b\tilde{\omega}_1}{c_3 A_1(0)} = \frac{24b\tilde{\omega}_1^2}{c_3\dot{\Delta}_1(0)} \overset{!}{=} \frac{\tilde{\omega}_1^2}{c_3\dot{\Delta}_1(0)} \tag{5.12}$$

where $\dot{\Delta}_1(0) = \tilde{\omega}_1 A_1(0)$ is the rate of change of the superconducting phase difference induced by the first harmonic. The last equality, marked with the exclamation mark, is only valid for $\tilde{C} = 0$, recall the definition of the cubic coefficient b in Equation (2.18). Now that we have a generalised description dependent only on the parameter μ, we can solve the propagation equations for different number of harmonics M and study the results.

An important question is: what do the rescaled amplitudes a_m, the parameter μ and the rescaled length ξ represent?

- **Normalised amplitudes:** The rescaled amplitudes are simply the amplitudes normalised with respect to energy and initial amplitude such that 1 represents the total injected energy. Expressing the amplitudes this way ensures that the absolute value of each amplitude will always be a number between 0 and 1, and that the sum of the absolute values squared will always be 1.

- **Effective phase mismatch:** The dimensionless parameter μ describes the relation between phase mismatch and the pump strength, *i.e.* the "effective phase mismatch". As we know from Section 3.4, and especially Equation (3.29), it is not the value of the phase mismatch on its own that determines the behaviour of the propagating waves, but the relation between the phase mismatch and the pump strength. The

parameter μ captures this relation and puts a number to it. A large number ($\mu \gtrsim 10$) represents a large phase mismatch compared with the pump strength, while a small number ($\mu \lesssim 1$) represents a small phase mismatch compared with the pump strength.

- **Effective length:** The rescaled length ξ describes the "effective length" of the TWPA. It is not the specific number of unitcells $\tilde{x} = N$ on its own that determines whether the TWPA is long enough to reach a certain gain, but rather the physical length combined with the pump strength, which is what ξ captures.

5.1.3 Single input analysis

We can solve the explicit expressions of Equation (5.11) for different number of M. For example, for $M = 2$ we have

$$a_1' = a_2\bar{a}_1 e^{i\mu\xi}, \tag{5.13a}$$
$$a_2' = -a_1^2 e^{-i\mu\xi}. \tag{5.13b}$$

which can be solved numerically for any value of μ. In fact, the equations for two harmonics have been solved analytically [41]. For $M = 3$ we have

$$a_1' = a_2\bar{a}_1 e^{i\mu\xi} + a_3\bar{a}_2 e^{3i\mu\xi}, \tag{5.14a}$$
$$a_2' = 2a_3\bar{a}_1 e^{3i\mu\xi} - a_1^2 e^{-i\mu\xi}, \tag{5.14b}$$
$$a_3' = -3a_2 a_1 e^{-3i\mu\xi}. \tag{5.14c}$$

which can also be solved numerically for any value of μ, and so on.

However, a more important question is: How many harmonics M should be included to get a convergent result? In other words, at what number of harmonics M_c will adding another harmonic not make a difference for the transmission of the first harmonic?

As we showed in Ref. [47] and in paper [A], it depends on the value of μ. For large values of $\mu \gtrsim 10$, corresponding to a large phase mismatch and/or a weak coupling between the harmonics, very few harmonics are needed, while for small values of $\mu \lesssim 2$, corresponding to a strong coupling between the harmonics and/or small phase mismatches, many harmonics are needed. The exact number of harmonics for each value of μ is harder to predict, as it

depends on the required accuracy of the solution. As $\mu \to 0$, $M_c \to \infty$, which is why the transmission never converges in the purely linear dispersion regime, as already mentioned.

Since the more interesting scenario is the one with two inputs, where amplification can occur, we will move onto that for now. For those who are interested in the details of the single input analysis, we recommend to read Ref. [47] and paper [A].

5.2 Multimode study of two inputs

In this section we will develop a generalised model to capture all up- and down-conversion processes when inserting both a pump and a signal into a TWPA. The generalisation steps will very closely follow the steps taken in Section 5.1, so it is recommended to read that section first.

The *ansatz* of tones we will develop this model with is the pump-mediated tones *ansatz* [46], where the waves have frequencies

$$\begin{aligned} \tilde{\omega}_{mp} &= m\tilde{\omega}_p, \quad m \in [1, M] \cap \mathbb{N} \\ \tilde{\omega}_{s+mp} &= \tilde{\omega}_s + m\tilde{\omega}_p, \quad m \in [0, M-1] \cap \mathbb{N}, \\ \tilde{\omega}_{i+mp} &= \tilde{\omega}_i + m\tilde{\omega}_p, \quad m \in [0, M-1] \cap \mathbb{N}, \end{aligned} \tag{5.15}$$

where M is the number of modes for the pump, the signal and the idler.

5.2.1 Possible mixing processes

First we must identify what mixing processes can take place, as this is the foundation when deriving the propagation equations. We know from the definition of the idler that $\tilde{\omega}_s + \tilde{\omega}_i = \tilde{\omega}_p$. However, we can also go to higher modes of both signal and idler, and their sum will still be a pump harmonic. All the possible mixing processes of these transitions can be summarised as

$$\{m, n \in [0, M-1] \cap \mathbb{N} : m + n < M\} : \tilde{\omega}_{s+mp} + \tilde{\omega}_{i+np} = \tilde{\omega}_{(m+n+1)p}. \tag{5.16}$$

We also know that the signal and its up-converted modes can be up-converted by the pump, $\tilde{\omega}_{s+mp} + \tilde{\omega}_p = \tilde{\omega}_{s+(m+1)p}$. However, now that we include harmonics of the pump, every pump harmonic can induce similar processes. All these

possible mixing processes can be summarised as

$$\begin{aligned}\{m \in [0, M-1] \cap \mathbb{N}, n \in [1, M] \cap \mathbb{N} : m + n < M\} : \\ \tilde{\omega}_{\mathrm{s}+m\mathrm{p}} + \tilde{\omega}_{n\mathrm{p}} = \tilde{\omega}_{\mathrm{s}+(m+n)\mathrm{p}}.\end{aligned} \tag{5.17}$$

The same is valid for the idler, simply replace s→i in the equation above.

5.2.2 The propagation equations

Now that we have identified the possible mixing processes, let us determine what the propagation equations are. The equation for the pump is

$$\begin{aligned}A'_{m\mathrm{p}} = &\sum_{n=m+1}^{M} \frac{c_3}{4} \tilde{\omega}_{n\mathrm{p}} \tilde{\omega}_{(n-m)\mathrm{p}} A_{n\mathrm{p}} \bar{A}_{(n-m)\mathrm{p}} \mathrm{e}^{\mathrm{i}\left(\tilde{k}_{n\mathrm{p}} - \tilde{k}_{m\mathrm{p}} - \tilde{k}_{(n-m)\mathrm{p}}\right)\tilde{x}} \\ &- \frac{1}{2} \sum_{n=1}^{m-1} \frac{c_3}{4} \tilde{\omega}_{n\mathrm{p}} \tilde{\omega}_{(m-n)\mathrm{p}} A_{n\mathrm{p}} A_{(m-n)\mathrm{p}} \mathrm{e}^{-\mathrm{i}\left(\tilde{k}_{m\mathrm{p}} - \tilde{k}_{n\mathrm{p}} - \tilde{k}_{(m-n)\mathrm{p}}\right)\tilde{x}} \\ &+ \sum_{n=m}^{M-1} \frac{c_3}{4} \tilde{\omega}_{\mathrm{s}+n\mathrm{p}} \tilde{\omega}_{\mathrm{s}+(n-m)\mathrm{p}} A_{\mathrm{s}+n\mathrm{p}} \bar{A}_{\mathrm{s}+(n-m)\mathrm{p}} \mathrm{e}^{\mathrm{i}\left(\tilde{k}_{\mathrm{s}+n\mathrm{p}} - \tilde{k}_{n\mathrm{p}} - \tilde{k}_{\mathrm{s}+(n-m)\mathrm{p}}\right)\tilde{x}} \\ &+ \sum_{n=m}^{M-1} \frac{c_3}{4} \tilde{\omega}_{\mathrm{i}+n\mathrm{p}} \tilde{\omega}_{\mathrm{i}+(n-m)\mathrm{p}} A_{\mathrm{i}+n\mathrm{p}} \bar{A}_{\mathrm{i}+(n-m)\mathrm{p}} \mathrm{e}^{\mathrm{i}\left(\tilde{k}_{\mathrm{i}+n\mathrm{p}} - \tilde{k}_{n\mathrm{p}} - \tilde{k}_{\mathrm{i}+(n-m)\mathrm{p}}\right)\tilde{x}} \\ &- \sum_{n=0}^{m-1} \frac{c_3}{4} \tilde{\omega}_{\mathrm{s}+n\mathrm{p}} \tilde{\omega}_{\mathrm{i}+(m-n-1)\mathrm{p}} A_{\mathrm{s}+n\mathrm{p}} A_{\mathrm{i}+(m-n-1)\mathrm{p}} \mathrm{e}^{-\mathrm{i}\left(\tilde{k}_{m\mathrm{p}} - \tilde{k}_{\mathrm{s}+n\mathrm{p}} - \tilde{k}_{\mathrm{i}+(m-n-1)\mathrm{p}}\right)\tilde{x}}.\end{aligned} \tag{5.18a}$$

If we assume that the amplitudes of the signal and idler modes are much smaller than the pump amplitude, we can neglect the three latter sums where we have products of amplitudes of signal and idler modes. We call this the *back-action* as it describes the action the signal and idler modes exert back on the pump harmonics when being amplified. Neglecting back-action when there are no pump harmonics other than the first is usually called *the stiff pump approximation*. Then we get the same equations for the pump harmonics as in the single input study, Section 5.1, and we can use the results from that section to describe the propagation of the pump harmonics.

For the signal modes we get the equation

$$\begin{aligned}A'_{\mathrm{s}+m\mathrm{p}} = &\sum_{n=m+1}^{M} \frac{c_3}{4} \tilde{\omega}_{n\mathrm{p}} \tilde{\omega}_{\mathrm{s}+(n-m-1)\mathrm{p}} A_{n\mathrm{p}} \bar{A}_{\mathrm{i}+(n-m-1)\mathrm{p}} \mathrm{e}^{\mathrm{i}\left(\tilde{k}_{n\mathrm{p}} - \tilde{k}_{\mathrm{s}+m\mathrm{p}} - \tilde{k}_{\mathrm{i}+(n-m-1)\mathrm{p}}\right)\tilde{x}} \\ &+ \sum_{n=m+1}^{M-1} \frac{c_3}{4} \tilde{\omega}_{\mathrm{s}+n\mathrm{p}} \tilde{\omega}_{(n-m)\mathrm{p}} A_{\mathrm{s}+n\mathrm{p}} \bar{A}_{(n-m)\mathrm{p}} \mathrm{e}^{\mathrm{i}\left(\tilde{k}_{\mathrm{s}+n\mathrm{p}} - \tilde{k}_{\mathrm{s}+m\mathrm{p}} - \tilde{k}_{(n-m)\mathrm{p}}\right)\tilde{x}} \\ &- \sum_{n=1}^{m} \frac{c_3}{4} \tilde{\omega}_{n\mathrm{p}} \tilde{\omega}_{\mathrm{s}+(m-n)\mathrm{p}} A_{n\mathrm{p}} A_{\mathrm{s}+(m-n)\mathrm{p}} \mathrm{e}^{-\mathrm{i}\left(\tilde{k}_{\mathrm{s}+m\mathrm{p}} - \tilde{k}_{n\mathrm{p}} - \tilde{k}_{\mathrm{s}+(m-n)\mathrm{p}}\right)\tilde{x}}.\end{aligned} \tag{5.18b}$$

The equations for the idler modes are the same as in Equation (5.18b) with replacement s↔i.

5.2.3 Rescaling the propagation equations

Now we will rescale the propagation equations above in the same way as we did in Section 5.1.2, to get the generalised propagation equations. We express the frequencies as

$$\begin{aligned}\tilde{\omega}_{m\mathrm{p}} &= m\tilde{\omega}_{\mathrm{p}},\\ \tilde{\omega}_{\mathrm{s}+m\mathrm{p}} &= \tilde{\omega}_{\mathrm{s}} + m\tilde{\omega}_{\mathrm{p}} = \left(m + \frac{1+\delta}{2}\right)\tilde{\omega}_{\mathrm{p}},\\ \tilde{\omega}_{\mathrm{i}+m\mathrm{p}} &= \tilde{\omega}_{\mathrm{i}} + m\tilde{\omega}_{\mathrm{p}} = \left(m + \frac{1-\delta}{2}\right)\tilde{\omega}_{\mathrm{p}}\end{aligned} \tag{5.19}$$

where δ is the detuning (recall Equation (3.32)). The rescaled amplitudes are hence

$$\begin{aligned}a_{m\mathrm{p}} &= m\frac{A_{\mathrm{p}}}{A_{\mathrm{p}0}},\\ a_{\mathrm{s}+m\mathrm{p}} &= \left(m + \frac{1+\delta}{2}\right)\frac{A_{\mathrm{s}+m\mathrm{p}}}{A_{\mathrm{p}0}},\\ a_{\mathrm{i}+m\mathrm{p}} &= \left(m + \frac{1-\delta}{2}\right)\frac{A_{\mathrm{i}+m\mathrm{p}}}{A_{\mathrm{p}0}}\end{aligned} \tag{5.20}$$

where $A_{\mathrm{p}0}$ is the initial pump amplitude. We rescale length in the same way as in Section 5.1. With the replacements $\tilde{\omega}_1 \to \tilde{\omega}_{\mathrm{p}}, \tilde{k}_1 \to \tilde{k}_{\mathrm{p}}$ and $A_1 \to A_{\mathrm{p}}$, recall Equations (5.8) and (5.10), and ξ and μ become

$$\xi = \frac{c_3\tilde{\omega}_{\mathrm{p}}^2}{4}A_{\mathrm{p}0}\cdot\tilde{x} \approx \frac{1}{4}c_3\tilde{\omega}_{\mathrm{p}}\dot{\Delta}_{\mathrm{p}0}\tilde{x} \tag{5.21}$$

and

$$\mu = 4\frac{\tilde{k}_{2\mathrm{p}} - 2\tilde{k}_{\mathrm{p}}}{c_3\tilde{\omega}_{\mathrm{p}}^2 A_{\mathrm{p}0}} \approx \frac{\tilde{\omega}_{\mathrm{p}}^2}{c_3\dot{\Delta}_{\mathrm{p}0}}. \tag{5.22}$$

All that remains is finding a way to approximate the phase mismatches with numerical factors. We once again expand the dispersion relation to its cubic order and divide each phase mismatch by $\tilde{k}_{2\mathrm{p}} - 2\tilde{k}_{\mathrm{p}}$. Then we get the numerical

factors

$$d_{\mathrm{p}:n,m} = \frac{1}{6}\left(n^3 - \left(m + \frac{1+\delta}{2}\right)^3 - \left(n - m - 1 + \frac{1-\delta}{2}\right)^3\right), \tag{5.23a}$$

$$d_{\mathrm{s}:n,m} = \frac{1}{6}\left(\left(n + \frac{1+\delta}{2}\right)^3 - \left(m + \frac{1+\delta}{2}\right)^3 - (n-m)^3\right), \tag{5.23b}$$

$$d_{\mathrm{i}:n,m} = \frac{1}{6}\left(\left(n + \frac{1-\delta}{2}\right)^3 - \left(m + \frac{1-\delta}{2}\right)^3 - (n-m)^3\right), \tag{5.23c}$$

in addition to $d_{n,m}$ defined in Equation (5.4). The propagation equations, recall Equation (5.18), neglecting back-action of signal and idler modes on the pump harmonics (as discussed in Section 5.2.2), can then be written as

$$a'_{m\mathrm{p}} = m\left(\sum_{n=m+1}^{M} a_{n\mathrm{p}}\bar{a}_{(n-m)\mathrm{p}}\mathrm{e}^{\mathrm{i}\mu\xi d_{n,m}} - \frac{1}{2}\sum_{n=1}^{m-1} a_{n\mathrm{p}}a_{(m-n)\mathrm{p}}\mathrm{e}^{-\mathrm{i}\mu\xi d_{m,n}}\right), \tag{5.24a}$$

$$\begin{aligned} a'_{\mathrm{s}+m\mathrm{p}} = \left(m + \frac{1+\delta}{2}\right) \times \Bigg(& \sum_{n=m+1}^{M} a_{n\mathrm{p}}\bar{a}_{\mathrm{i}+(n-m-1)\mathrm{p}}\mathrm{e}^{\mathrm{i}\mu\xi d_{\mathrm{p}:n,m}} \\ & + \sum_{n=m+1}^{M-1} a_{\mathrm{s}+n\mathrm{p}}\bar{a}_{(n-m)\mathrm{p}}\mathrm{e}^{\mathrm{i}\mu\xi d_{\mathrm{s}:n,m}} - \sum_{n=1}^{m} a_{n\mathrm{p}}a_{\mathrm{s}+(m-n)\mathrm{p}}\mathrm{e}^{-\mathrm{i}\mu\xi d_{\mathrm{s}:m,m-n}}\Bigg), \end{aligned} \tag{5.24b}$$

$$\begin{aligned} a'_{\mathrm{i}+m\mathrm{p}} = \left(m + \frac{1-\delta}{2}\right) \times \Bigg(& \sum_{n=m+1}^{M} a_{n\mathrm{p}}\bar{a}_{\mathrm{s}+(n-m-1)\mathrm{p}}\mathrm{e}^{\mathrm{i}\mu\xi d_{\mathrm{p}:n,n-m-1}} \\ & + \sum_{n=m+1}^{M-1} a_{\mathrm{i}+n\mathrm{p}}\bar{a}_{(n-m)\mathrm{p}}\mathrm{e}^{\mathrm{i}\mu\xi d_{\mathrm{i}:n,m}} - \sum_{n=1}^{m} a_{n\mathrm{p}}a_{\mathrm{i}+(m-n)\mathrm{p}}\mathrm{e}^{-\mathrm{i}\mu\xi d_{\mathrm{i}:m,m-n}}\Bigg). \end{aligned} \tag{5.24c}$$

Due to the rescaling, the initial condition is $a_{\mathrm{p}0} = 1$, $a_{\mathrm{s}0} = A_{\mathrm{s}0}/A_{\mathrm{p}0} \ll 1$ and 0 for all other amplitudes. However, if back-action is neglected, as done in the equations above, the value of $a_{\mathrm{s}0}$ makes no difference and can be set to 1 for convenience, which simplifies the gain to $|a_{\mathrm{s}}/a_{\mathrm{s}0}|^2 = |a_{\mathrm{s}}|^2$. Another way to phrase this: the value of the initial signal amplitude only makes a difference for the back-action terms, so once the back-action terms are neglected, we can freely set the value of the initial signal amplitude to whatever value we wish, without it having any impact on the transmission of the signal, and 1 is a convenient starting value.

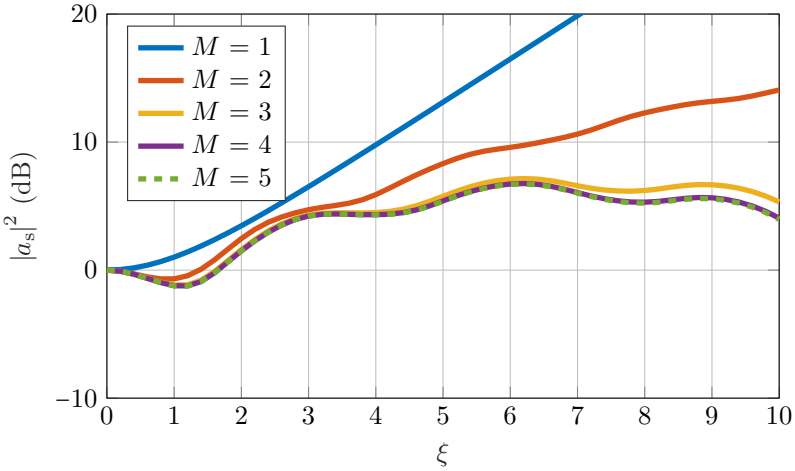

Figure 5.1: Transmission of the signal for $\mu = 5$ at zero detuning for several values of M up to $M_c + 1$.

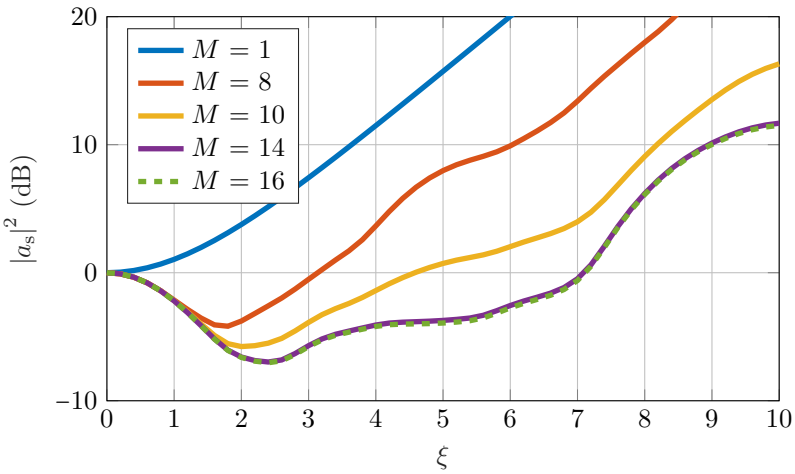

Figure 5.2: Transmission of the signal for $\mu = 0.5$ at zero detuning for several values of M up to $M_c + 1$.

To investigate the transmission of a signal with a frequency larger than the pump, we instead set the initial amplitude of the appropriate up-converted mode of the signal to 1. For example, if $\tilde{\omega}_\mathrm{s} = 2.5\tilde{\omega}_\mathrm{p}$, we set $a_{\mathrm{s}0} = 0$ and $a_{\mathrm{s}+2\mathrm{p}}(0) = 1$. At this frequency the gain is given by $|a_{\mathrm{s}+2\mathrm{p}}|^2$.

5.2.4 Analysis of the solution

Now that we have the generalised propagation equations, Equations (5.24a) to (5.24c), we can numerically find the solution for a given value of μ. The single idler model, $M = 1$, predicts exponential gain [35], [47] if

$$\mu < \frac{8}{1-\delta^2}. \tag{5.25}$$

But just as in the single input case, the needed number of harmonics M_c depends on the value of μ.

As we can see in Figure 5.1, plotted for $\mu = 5$, the gain grows quickly for $M = 1$. When we include the up-converted modes, the gain quickly goes down, even though we only need $M = 4$ for convergence.

If we go to smaller values of μ, the gain grows even quicker according to the single idler model, study Figure 5.2 where $\mu = 0.5$. Now the gain still grows quickly for $M = 8$. However, for this small value of μ, we need as much as $M = 15$ for convergence. When all these up-converted modes are included, the gain is severely reduced.

5.3 Summary

In this chapter we have looked at three-wave mixing for the standard TWPA in the quasilinear dispersion regime. This is the regime where we assume linear dispersion for the coupling coefficients, but we use a third-order approximation of the dispersion relation for the phase mismatches. By using these approximations, we could transform the regular propagation equations, which have several different parameters in them, into a new set of differential equations with only one parameter μ. The parameter μ captures the relation between the phase mismatches and the nonlinear interaction, also known as the pumping strength. It turns out that for large values of μ, there is little to no up-conversion. However, then there is no exponential gain due to a too

large phase mismatch. For small values of μ, there is a small phase mismatch. However, then there is no exponential gain due to too much up-conversion processes. In short, there is never exponential gain for the standard TWPA in the quasilinear regime, due to either too much phase mismatch, too many up-conversion processes, or both.

CHAPTER 6

Three-wave mixing for arbitrary frequencies

Until now we have studied wave propagation via the propagation equations, which were developed using the continuous wave approximation. Therefore, this theory is only valid as long as all wavelengths are much longer than the length of the unitcell, or equivalently, as long as all frequencies are well below the cutoff frequency. This weak spot of the theory has two major problems. Firstly, we saw in Chapter 5 that for large pump strengths in the quasilinear dispersion regime, there is a lot of up-conversion. At some point the highest pump harmonics and up-converted signal and idler modes will reach the cutoff frequency, where the theory breaks down. Secondly, we cannot study the propagation of a signal when the signal frequency is close to the cutoff frequency to begin with.

In this chapter we will develop a theory that is built on the discrete propagation equations which describe the propagation of waves with any frequency within the spectrum. However, it is complicated to make an equivalent model of the discrete propagation equations for multiple modes to the general small frequency theory developed in Chapter 5. Therefore, we limit the study to the simplest case of three modes, as a discrete equivalent to the continuous three-mode model [35]. This allows us to investigate whether the pump and

the signal can be placed close to the cutoff frequency in order to completely eliminate up-conversion.

6.1 Eliminating up-conversion

In Chapter 5 we concluded that it is very challenging to achieve a high gain for a 3WM TWPA in the small frequency limit, *i.e.* when the pump and the signal are well below the cutoff frequency ω_c, due to the large amount of up-conversion processes. Before doing more complicated measures to hinder up-conversion, such as dispersive engineering [20], we want to investigate if we can use the natural cutoff frequency of the TWPA itself to stop up-conversion, at least for some signal frequencies, and get exponential gain. To find the required pump and signal frequencies to stop up-conversion, we simply assume that the sum of the signal and pump frequencies equal the cutoff and find ω_p/ω_c with respect to ω_s/ω_p, and likewise for the idler. We get

$$\omega_p + \omega_s = \omega_c \quad \Longrightarrow \quad \frac{\omega_p}{\omega_c} = \frac{1}{1 + \frac{\omega_s}{\omega_p}}, \tag{6.1a}$$

$$\omega_p + \omega_i = \omega_c \quad \Longrightarrow \quad \frac{\omega_p}{\omega_c} = \frac{1}{2 - \frac{\omega_s}{\omega_p}}, \tag{6.1b}$$

which is illustrated in Figure 6.1. Here we see that if the pump frequency is smaller than half of the cutoff frequency, the pump, the signal and the idler can all up-convert at least once. If the pump is larger than half of the cutoff, the pump itself cannot up-convert, but the signal, the idler or both may still up-convert. However, once the pump frequency becomes larger than 2/3 of the cutoff frequency, there opens up a band around half of the pump frequency where no up-conversion at all is possible, see the green area in Figure 6.1. To find the width of this band, we solve Equations (6.1a) and (6.1b) for ω_s/ω_p with respect to ω_p/ω_c, and find that the band is given by

$$\frac{\omega_c}{\omega_p} - 1 < \frac{\omega_s}{\omega_p} < 2 - \frac{\omega_c}{\omega_p}. \tag{6.2}$$

Expressed in terms of the detuning δ, recall Equation (3.32), we can write this as

$$|\delta| < 3 - 2\frac{\omega_c}{\omega_p} \quad \text{or} \quad \frac{\omega_p}{\omega_c} > \frac{2}{3 - |\delta|}. \tag{6.3}$$

To find the pump frequency to retrieve 1/3 or 2/3 of the full band, we set $|\delta|$ equal to 1/3 or 2/3 and solve Equation (6.3) for ω_p. These bands are also shown in Figure 6.1.

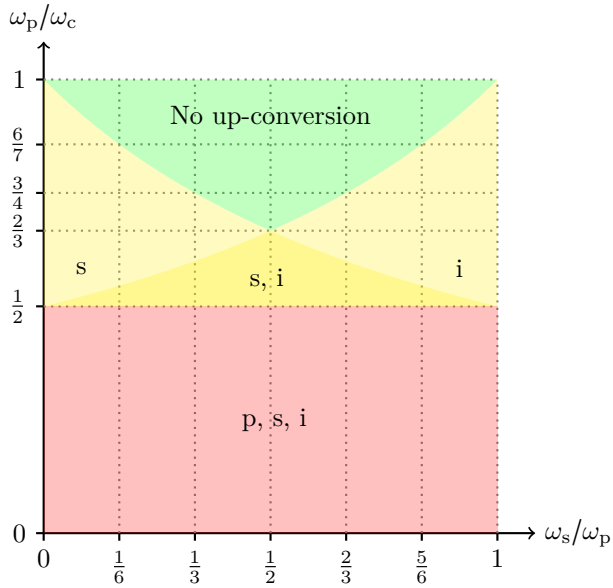

Figure 6.1: The regions of the presence/absence of up-conversion of pump, signal and idler. In the light red region all three modes can be up-converted, in the yellow region both signal and idler are up-converted but pump is not, in the light yellow regions only up-conversion of either signal or idler is possible, and in the green region no up-conversion takes place.

In short, the pump frequency must be larger than 2/3 of the cutoff frequency in order to get a band without up-conversion, and specifically larger than 3/4 of the cutoff in order to get at least 1/3 of the full band without up-conversion.

If we try to use the continuous single idler model, described in Section 3.4, to analyse what the gain would be for a pump at any of these large frequencies, we encounter 2 problems. The first problem is that there is more and more phase mismatch the closer to the cutoff we get. From Chapter 3 we know that phase mismatch suppresses, and might prevent, exponential gain. The second problem is that to work with the continuous wave equation, instead of

the discrete wave equation, we assumed that all wavelengths are much larger than the unitcell length, or equivalently all frequencies are well below the cutoff frequency, recall Figure 2.3. Hence, we cannot use the continuous wave equation to analyse the propagation and transmission in the up-conversion-free regime; instead we must use the discrete wave equation.

6.2 General mixing equations

In this section we will derive general expressions for the mixing equations in the discrete regime. We begin with the discrete wave equation, recall Equation (3.6), but we ignore the four-wave mixing term and implement the unitless definitions used in Chapter 3. The discrete wave equation then reads

$$\begin{aligned}\frac{\mathrm{d}^2}{\mathrm{d}\tilde{t}^2}\phi_n - \left[\tilde{C}\frac{\mathrm{d}^2}{\mathrm{d}\tilde{t}^2} + 1\right](\phi_{n+1} - 2\phi_n + \phi_{n-1}) \\ = -\frac{c_3}{2}\left((\phi_{n+1} - \phi_n)^2 - (\phi_n - \phi_{n-1})^2\right).\end{aligned} \tag{6.4}$$

Now we use the *ansatz* that the node phases ϕ_n are given by

$$\phi_n\left(\tilde{t}\right) = \sum_m \phi_{m,n}\left(\tilde{t}\right) = \frac{1}{2}\sum_m A_{m,n}\mathrm{e}^{\mathrm{i}(\tilde{k}_m n - \tilde{\omega}_m \tilde{t})} + \bar{A}_{m,n}\mathrm{e}^{-\mathrm{i}(\tilde{k}_m n - \tilde{\omega}_m \tilde{t})} \tag{6.5}$$

where $\phi_{m,n}$ is the node phase of mode m at node n.

6.2.1 Simplifying the left-hand side

First let us simplify the left-hand side of Equation (6.4). As we know from the derivation of the dispersion relation, recall Section 2.3, Equation (6.4) describes the propagation of the free waves if the right-hand side of the equation is equal to zero. However, since the right-hand side is not equal to zero we can no longer assume constant amplitudes, just as in Chapter 3. Further analysis is hence needed.

When applying the second time derivative to the node phases we get

$$\frac{\mathrm{d}^2\phi_n}{\mathrm{d}\tilde{t}^2} = \sum_m -\tilde{\omega}_m^2\phi_{m,n}, \tag{6.6}$$

and the left-hand side can hence be written as

$$\mathrm{LHS}^{(6.4)} = \sum_m -\tilde{\omega}_m^2 \phi_{m,n} - \left(1 - \tilde{C}\tilde{\omega}_m^2\right) \underbrace{\left(\phi_{m,n+1} - 2\phi_{m,n} + \phi_{m,n-1}\right)}_{\star} \tag{6.7}$$

where the last parenthesis can be written as

$$\star = A_{m,n} \mathrm{e}^{\mathrm{i}\left(\tilde{k}_m n - \tilde{\omega}_m \tilde{t}\right)} \left(\frac{A_{m,n+1}}{A_{m,n}} \mathrm{e}^{\mathrm{i}\tilde{k}_m} - 2 + \frac{A_{m,n-1}}{A_{m,n}} \mathrm{e}^{-\mathrm{i}\tilde{k}_m} \right) + \text{c.c.}, \tag{6.8}$$

where the amplitude fractions would be unity in a linear medium, but will differ when there is frequency mixing.

6.2.2 Simplifying the right-hand side

Now let us simplify the right-hand side of Equation (6.4). Just as for the continuous analogue in Chapter 3, the full expression of the right-hand side will contain multiple terms and will be hard to fit on this page, and hard to fully analyse. However, we can apply the same technique as before, and only study the mixing terms resonant with each wave while neglecting the rest, recall Section 3.3.2.

Assume we have the three waves m, q, r, and that the frequencies have the relationship $\tilde{\omega}_m = \tilde{\omega}_q - \tilde{\omega}_r$. There will be two terms from $\left(\phi_{n+1} - \phi_n\right)^2$ and another two terms from $\left(\phi_n - \phi_{n-1}\right)^2$ that will resonate with m. The contribution for this mixing process for $\left(\phi_{n+1} - \phi_n\right)^2$ is hence

$$\begin{aligned}
&\frac{1}{2}\left(A_{q,n+1}\mathrm{e}^{\mathrm{i}\left(\tilde{k}_q(n+1) - \tilde{\omega}_q\tilde{t}\right)} - A_{q,n}\mathrm{e}^{\mathrm{i}\left(\tilde{k}_q n - \tilde{\omega}_q\tilde{t}\right)}\right) \\
\times&\frac{1}{2}\left(\bar{A}_{r,n+1}\mathrm{e}^{-\mathrm{i}\left(\tilde{k}_r(n+1) - \tilde{\omega}_r\tilde{t}\right)} - \bar{A}_{r,n}\mathrm{e}^{-\mathrm{i}\left(\tilde{k}_r n - \tilde{\omega}_r\tilde{t}\right)}\right) \\
+&\frac{1}{2}\left(\bar{A}_{r,n+1}\mathrm{e}^{-\mathrm{i}\left(\tilde{k}_r(n+1) - \tilde{\omega}_r\tilde{t}\right)} - \bar{A}_{r,n}\mathrm{e}^{-\mathrm{i}\left(\tilde{k}_r n - \tilde{\omega}_r\tilde{t}\right)}\right) \\
\times&\frac{1}{2}\left(A_{q,n+1}\mathrm{e}^{\mathrm{i}\left(\tilde{k}_q(n+1) - \tilde{\omega}_q\tilde{t}\right)} - A_{q,n}\mathrm{e}^{\mathrm{i}\left(\tilde{k}_q n - \tilde{\omega}_q\tilde{t}\right)}\right) \\
=&\frac{1}{2}\mathrm{e}^{\mathrm{i}\left(\left(\tilde{k}_q - \tilde{k}_r\right)n - \tilde{\omega}_m\tilde{t}\right)}\left(A_{q,n+1}\mathrm{e}^{\mathrm{i}\tilde{k}_q} - A_{q,n}\right)\left(\bar{A}_{r,n+1}\mathrm{e}^{-\mathrm{i}\tilde{k}_r} - \bar{A}_{r,n}\right)
\end{aligned} \tag{6.9}$$

and analogously for $\left(\phi_n - \phi_{n-1}\right)^2$. For the transition $\tilde{\omega}_m = \tilde{\omega}_q + \tilde{\omega}_r$ we instead

get

$$\begin{aligned}
&\frac{1}{2}\left(A_{q,n+1}\mathrm{e}^{\mathrm{i}\left(\tilde{k}_q(n+1)-\tilde{\omega}_q\tilde{t}\right)}-A_{q,n}\mathrm{e}^{\mathrm{i}\left(\tilde{k}_q n-\tilde{\omega}_q\tilde{t}\right)}\right)\\
\times&\frac{1}{2}\left(A_{r,n+1}\mathrm{e}^{\mathrm{i}\left(\tilde{k}_r(n+1)-\tilde{\omega}_r\tilde{t}\right)}-A_{r,n}\mathrm{e}^{\mathrm{i}\left(\tilde{k}_r n-\tilde{\omega}_r\tilde{t}\right)}\right)\\
+&\frac{1}{2}\left(A_{r,n+1}\mathrm{e}^{\mathrm{i}\left(\tilde{k}_r(n+1)-\tilde{\omega}_r\tilde{t}\right)}-A_{r,n}\mathrm{e}^{\mathrm{i}\left(\tilde{k}_r n-\tilde{\omega}_r\tilde{t}\right)}\right)\\
\times&\frac{1}{2}\left(A_{q,n+1}\mathrm{e}^{\mathrm{i}\left(\tilde{k}_q(n+1)-\tilde{\omega}_q\tilde{t}\right)}-A_{q,n}\mathrm{e}^{\mathrm{i}\left(\tilde{k}_q n-\tilde{\omega}_q\tilde{t}\right)}\right)\\
=&\frac{1}{2}\mathrm{e}^{\mathrm{i}\left((\tilde{k}_q+\tilde{k}_r)n-\tilde{\omega}_m\tilde{t}\right)}\left(A_{q,n+1}\mathrm{e}^{\mathrm{i}\tilde{k}_q}-A_{q,n}\right)\left(A_{r,n+1}\mathrm{e}^{\mathrm{i}\tilde{k}_r}-A_{r,n}\right)
\end{aligned}\tag{6.10}$$

but if it is degenerate, $\tilde{\omega}_m = 2\tilde{\omega}_q$, we only get

$$\begin{aligned}
&\frac{1}{2}\left(A_{q,n+1}\mathrm{e}^{\mathrm{i}\left(\tilde{k}_q(n+1)-\tilde{\omega}_q\tilde{t}\right)}-A_{q,n}\mathrm{e}^{\mathrm{i}\left(\tilde{k}_q n-\tilde{\omega}_q\tilde{t}\right)}\right)\\
\times&\frac{1}{2}\left(A_{q,n+1}\mathrm{e}^{\mathrm{i}\left(\tilde{k}_q(n+1)-\tilde{\omega}_q\tilde{t}\right)}-A_{q,n}\mathrm{e}^{\mathrm{i}\left(\tilde{k}_q n-\tilde{\omega}_q\tilde{t}\right)}\right)\\
=&\frac{1}{4}\mathrm{e}^{\mathrm{i}\left(2\tilde{k}_q n-\tilde{\omega}_m\tilde{t}\right)}\left(A_{q,n+1}\mathrm{e}^{\mathrm{i}\tilde{k}_q}-A_{q,n}\right)^2.
\end{aligned}\tag{6.11}$$

6.2.3 Constructing the discrete propagation equations

Now that we have simplified both sides of Equation (6.4), we can retrieve the discrete analogue of the continuous propagation equations, Equation (3.24) in Chapter 3. In the continuous limit we got differential equations, but now taking the discreteness of the TWPA into consideration we instead get difference equations.

For each wave, we begin by only retrieving the resonant terms and then divide the left-hand side with its exponential factor. The propagation equation

for the amplitude of each wave m becomes

$$\begin{aligned}
&A_{m,n}\left[\tilde{\omega}_m^2+\left(1-\tilde{C}\tilde{\omega}_m^2\right)\left(\frac{A_{m,n+1}}{A_{m,n}}\mathrm{e}^{\mathrm{i}\tilde{k}_m}-2+\frac{A_{m,n-1}}{A_{m,n}}\mathrm{e}^{-\mathrm{i}\tilde{k}_m}\right)\right]\\
&=\sum_{q,r:\ \tilde{\omega}_m=\tilde{\omega}_q-\tilde{\omega}_r}\frac{c_3}{2}\mathrm{e}^{\mathrm{i}(\tilde{k}_q-\tilde{k}_r-\tilde{k}_m)n}A_{q,n}\bar{A}_{r,n}\\
&\times\left[\left(\frac{A_{q,n+1}}{A_{q,n}}\mathrm{e}^{\mathrm{i}\tilde{k}_q}-1\right)\left(\frac{\bar{A}_{r,n+1}}{\bar{A}_{r,n}}\mathrm{e}^{-\mathrm{i}\tilde{k}_r}-1\right)-\left(1-\frac{A_{q,n-1}}{A_{q,n}}\mathrm{e}^{-\mathrm{i}\tilde{k}_q}\right)\left(1-\frac{\bar{A}_{r,n-1}}{\bar{A}_{r,n}}\mathrm{e}^{\mathrm{i}\tilde{k}_r}\right)\right]\\
&+\frac{1}{2}\sum_{q,r:\ \tilde{\omega}_m=\tilde{\omega}_q+\tilde{\omega}_r}\frac{c_3}{2}\mathrm{e}^{-\mathrm{i}(\tilde{k}_m-\tilde{k}_q-\tilde{k}_r)n}A_{q,n}A_{r,n}\\
&\times\left[\left(\frac{A_{q,n+1}}{A_{q,n}}\mathrm{e}^{\mathrm{i}\tilde{k}_q}-1\right)\left(\frac{A_{r,n+1}}{A_{r,n}}\mathrm{e}^{\mathrm{i}\tilde{k}_r}-1\right)-\left(1-\frac{A_{q,n-1}}{A_{q,n}}\mathrm{e}^{-\mathrm{i}\tilde{k}_q}\right)\left(1-\frac{A_{r,n-1}}{A_{r,n}}\mathrm{e}^{-\mathrm{i}\tilde{k}_r}\right)\right].
\end{aligned}\tag{6.12}$$

6.3 The discrete single idler model

In this section we will study the single idler model, just as in Section 3.4, but now using the discrete propagation equations. In other words, we will assume that there are only three waves present: the pump 'p', the signal 's' fulfilling $\tilde{\omega}_\mathrm{s}<\tilde{\omega}_\mathrm{p}$ and the idler 'i' given by $\tilde{\omega}_\mathrm{i}=\tilde{\omega}_\mathrm{p}-\tilde{\omega}_\mathrm{s}$. We know from Chapter 5 that the assumption that these waves are the only waves present is a bad assumption *if the waves can up-convert.* But since we now will use the discrete propagation equations, as described in Equation (6.12), we are no longer limited to small frequencies and may place the pump close to the cutoff frequency, which will open up a band free of up-conversion as described in Section 6.1.

6.3.1 The propagation equations

We begin by reusing the assumption of small signal amplitude, $A_{\mathrm{s}0}\ll A_{\mathrm{p}0}$, which combined with a large pump frequency, $\omega_\mathrm{p}>\frac{1}{2}\omega_\mathrm{c}$, lets us assume a constant pump amplitude throughout the TWPA. Let us also reuse the definition for the phase mismatch, $\Delta\tilde{k}=\tilde{k}_\mathrm{p}-\tilde{k}_\mathrm{s}-\tilde{k}_\mathrm{i}$, then the propagation equations for the signal and the idler become

$$\begin{aligned}
&A_{\mathrm{s},n}\left(\tilde{\omega}_\mathrm{s}^2+\left(1-\tilde{C}\tilde{\omega}_\mathrm{s}^2\right)\left(\frac{A_{\mathrm{s},n+1}}{A_{\mathrm{s},n}}\mathrm{e}^{\mathrm{i}\tilde{k}_\mathrm{s}}-2+\frac{A_{\mathrm{s},n-1}}{A_{\mathrm{s},n}}\mathrm{e}^{-\mathrm{i}\tilde{k}_\mathrm{s}}\right)\right)\\
&=\frac{c_3}{2}\mathrm{e}^{\mathrm{i}\Delta\tilde{k}n}A_{\mathrm{p},n}\bar{A}_{\mathrm{i},n}\\
&\times\left[\left(\mathrm{e}^{\mathrm{i}\tilde{k}_\mathrm{p}}-1\right)\left(\frac{\bar{A}_{\mathrm{i},n+1}}{\bar{A}_{\mathrm{i},n}}\mathrm{e}^{-\mathrm{i}\tilde{k}_\mathrm{i}}-1\right)-\left(1-\mathrm{e}^{-\mathrm{i}\tilde{k}_\mathrm{p}}\right)\left(1-\frac{\bar{A}_{\mathrm{i},n-1}}{\bar{A}_{\mathrm{i},n}}\mathrm{e}^{\mathrm{i}\tilde{k}_\mathrm{i}}\right)\right],
\end{aligned}\tag{6.13a}$$

$$
\begin{aligned}
&A_{\mathrm{i},n}\left[\tilde{\omega}_{\mathrm{i}}^2+\left(1-\tilde{C}\tilde{\omega}_{\mathrm{i}}^2\right)\left(\frac{A_{\mathrm{i},n+1}}{A_{\mathrm{i},n}}\mathrm{e}^{\mathrm{i}\tilde{k}_{\mathrm{i}}}-2+\frac{A_{\mathrm{i},n-1}}{A_{\mathrm{i},n}}\mathrm{e}^{-\mathrm{i}\tilde{k}_{\mathrm{i}}}\right)\right]\\
&=\frac{c_3}{2}\mathrm{e}^{\mathrm{i}\Delta\tilde{k}n}A_{\mathrm{p},n}\bar{A}_{\mathrm{s},n}\\
&\times\left[\left(\mathrm{e}^{\mathrm{i}\tilde{k}_{\mathrm{p}}}-1\right)\left(\frac{\bar{A}_{\mathrm{s},n+1}}{\bar{A}_{\mathrm{s},n}}\mathrm{e}^{-\mathrm{i}\tilde{k}_{\mathrm{s}}}-1\right)-\left(1-\mathrm{e}^{-\mathrm{i}\tilde{k}_{\mathrm{p}}}\right)\left(1-\frac{\bar{A}_{\mathrm{s},n-1}}{\bar{A}_{\mathrm{s},n}}\mathrm{e}^{\mathrm{i}\tilde{k}_{\mathrm{s}}}\right)\right].
\end{aligned}
\tag{6.13b}
$$

6.3.2 Solving the propagation equations

To solve Equations (6.13a) and (6.13b), we take inspiration from Section 3.4 and use similar transformations,

$$A_{\mathrm{s},n}=B_{\mathrm{s}}\cdot\mathrm{e}^{\mathrm{i}\Delta\tilde{k}n/2}\cdot\mathrm{e}^{\mathrm{i}\lambda n}, \tag{6.14a}$$

$$A_{\mathrm{i},n}=\bar{B}_{\mathrm{i}}\cdot\mathrm{e}^{\mathrm{i}\Delta\tilde{k}n/2}\cdot\mathrm{e}^{\mathrm{i}\lambda n}. \tag{6.14b}$$

Here λ is very similar to the gain coefficient, with the relation $\lambda=-\mathrm{i}g$, *i.e.* a negative imaginary component of λ gives rise to exponential gain. This way of defining λ simplifies the calculations at a later point. With these transformations, the amplitude fractions become

$$\frac{A_{\mathrm{s},n+1}}{A_{\mathrm{s},n}}=\frac{B_{\mathrm{s}}\cdot\mathrm{e}^{\mathrm{i}\Delta\tilde{k}(n+1)/2}\cdot\mathrm{e}^{\mathrm{i}\lambda(n+1)}}{B_{\mathrm{s}}\cdot\mathrm{e}^{\mathrm{i}\Delta\tilde{k}n/2}\cdot\mathrm{e}^{\mathrm{i}\lambda n}}=\mathrm{e}^{\mathrm{i}\left(\lambda+\Delta\tilde{k}/2\right)}, \tag{6.15a}$$

$$\frac{A_{\mathrm{s},n-1}}{A_{\mathrm{s},n}}=\frac{B_{\mathrm{s}}\cdot\mathrm{e}^{\mathrm{i}\Delta\tilde{k}(n-1)/2}\cdot\mathrm{e}^{\mathrm{i}\lambda(n-1)}}{B_{\mathrm{s}}\cdot\mathrm{e}^{\mathrm{i}\Delta\tilde{k}n/2}\cdot\mathrm{e}^{\mathrm{i}\lambda n}}=\mathrm{e}^{-\mathrm{i}\left(\lambda+\Delta\tilde{k}/2\right)}, \tag{6.15b}$$

$$\frac{A_{\mathrm{i},n+1}}{A_{\mathrm{i},n}}=\frac{\bar{B}_{\mathrm{i}}\cdot\mathrm{e}^{\mathrm{i}\Delta\tilde{k}(n+1)/2}\cdot\mathrm{e}^{-\mathrm{i}\bar{\lambda}(n+1)}}{\bar{B}_{\mathrm{i}}\cdot\mathrm{e}^{\mathrm{i}\Delta\tilde{k}n/2}\cdot\mathrm{e}^{-\mathrm{i}\bar{\lambda}n}}=\mathrm{e}^{\mathrm{i}\left(\Delta\tilde{k}/2-\bar{\lambda}\right)}, \tag{6.15c}$$

$$\frac{A_{\mathrm{i},n-1}}{A_{\mathrm{i},n}}=\frac{\bar{B}_{\mathrm{i}}\cdot\mathrm{e}^{\mathrm{i}\Delta\tilde{k}(n-1)/2}\cdot\mathrm{e}^{-\mathrm{i}\bar{\lambda}(n-1)}}{\bar{B}_{\mathrm{i}}\cdot\mathrm{e}^{\mathrm{i}\Delta\tilde{k}n/2}\cdot\mathrm{e}^{-\mathrm{i}\bar{\lambda}n}}=\mathrm{e}^{-\mathrm{i}\left(\Delta\tilde{k}/2-\bar{\lambda}\right)}. \tag{6.15d}$$

Inserting these values of the fractions into Equations (6.13a) and (6.13b), they are simplified to

$$
\begin{aligned}
&B_{\mathrm{s}}\left[\tilde{\omega}_{\mathrm{s}}^2-4\left(1-\tilde{C}\tilde{\omega}_{\mathrm{s}}^2\right)\sin^2\left(\frac{\lambda+\Delta\tilde{k}/2+\tilde{k}_{\mathrm{s}}}{2}\right)\right]=\frac{c_3}{2}A_{\mathrm{p}}B_{\mathrm{i}}\\
&\times\left[\left(\mathrm{e}^{\mathrm{i}\tilde{k}_{\mathrm{p}}}-1\right)\left(\mathrm{e}^{\mathrm{i}\left(\lambda-\Delta\tilde{k}/2-\tilde{k}_{\mathrm{i}}\right)}-1\right)-\left(1-\mathrm{e}^{-\mathrm{i}\tilde{k}_{\mathrm{p}}}\right)\left(1-\mathrm{e}^{\mathrm{i}\left(\Delta\tilde{k}/2+\tilde{k}_{\mathrm{i}}-\lambda\right)}\right)\right]
\end{aligned}
\tag{6.16a}
$$

and

$$B_{\mathrm{i}}\left[\tilde{\omega}_{\mathrm{i}}^2 - 4\left(1-\tilde{C}\tilde{\omega}_{\mathrm{i}}^2\right)\sin^2\left(\frac{\lambda-\Delta\tilde{k}/2-\tilde{k}_{\mathrm{i}}}{2}\right)\right] = \frac{c_3}{2}A_{\mathrm{p}}B_{\mathrm{s}} \times\left[\left(\mathrm{e}^{-\mathrm{i}\tilde{k}_{\mathrm{p}}}-1\right)\left(\mathrm{e}^{\mathrm{i}\left(\lambda+\Delta\tilde{k}/2+\tilde{k}_{\mathrm{s}}\right)}-1\right)-\left(1-\mathrm{e}^{\mathrm{i}\tilde{k}_{\mathrm{p}}}\right)\left(1-\mathrm{e}^{-\mathrm{i}\left(\lambda+\Delta\tilde{k}/2+\tilde{k}_{\mathrm{s}}\right)}\right)\right]. \tag{6.16b}$$

Let us note that

$$\begin{aligned}\Delta\tilde{k}/2+\tilde{k}_{\mathrm{s}} &= \frac{1}{2}\left(\tilde{k}_{\mathrm{p}}-\tilde{k}_{\mathrm{s}}-\tilde{k}_{\mathrm{i}}\right)+\tilde{k}_{\mathrm{s}} = \frac{1}{2}\left(\tilde{k}_{\mathrm{p}}+\tilde{k}_{\mathrm{s}}-\tilde{k}_{\mathrm{i}}\right),\\ \Delta\tilde{k}/2+\tilde{k}_{\mathrm{i}} &= \frac{1}{2}\left(\tilde{k}_{\mathrm{p}}-\tilde{k}_{\mathrm{s}}-\tilde{k}_{\mathrm{i}}\right)+\tilde{k}_{\mathrm{i}} = \frac{1}{2}\Big(\tilde{k}_{\mathrm{p}}-\left(\tilde{k}_{\mathrm{s}}-\tilde{k}_{\mathrm{i}}\right)\Big),\end{aligned} \tag{6.17}$$

so by defining

$$\tilde{\kappa} = \tilde{k}_{\mathrm{s}}-\tilde{k}_{\mathrm{i}}-2\lambda, \tag{6.18}$$

we can write Equations (6.16a) and (6.16b) as

$$B_{\mathrm{s}}\left[\tilde{\omega}_{\mathrm{s}}^2 - 4\left(1-\tilde{C}\tilde{\omega}_{\mathrm{s}}^2\right)\sin^2\left(\frac{\tilde{k}_{\mathrm{p}}+\tilde{\kappa}}{4}\right)\right] = \frac{c_3}{2}A_{\mathrm{p}}B_{\mathrm{i}} \times\left[\left(\mathrm{e}^{\mathrm{i}\tilde{k}_{\mathrm{p}}}-1\right)\left(\mathrm{e}^{\mathrm{i}\left(\tilde{k}_{\mathrm{p}}-\tilde{\kappa}\right)/2}-1\right)-\left(1-\mathrm{e}^{-\mathrm{i}\tilde{k}_{\mathrm{p}}}\right)\left(1-\mathrm{e}^{\mathrm{i}\left(\tilde{k}_{\mathrm{p}}-\tilde{\kappa}\right)/2}\right)\right] \tag{6.19a}$$

and

$$B_{\mathrm{i}}\left[\tilde{\omega}_{\mathrm{i}}^2 - 4\left(1-\tilde{C}\tilde{\omega}_{\mathrm{i}}^2\right)\sin^2\left(\frac{\tilde{k}_{\mathrm{p}}-\tilde{\kappa}}{4}\right)\right] = \frac{c_3}{2}A_{\mathrm{p}}B_{\mathrm{s}} \times\left[\left(\mathrm{e}^{-\mathrm{i}\tilde{k}_{\mathrm{p}}}-1\right)\left(\mathrm{e}^{\mathrm{i}\left(\tilde{k}_{\mathrm{p}}+\tilde{\kappa}\right)/2}-1\right)-\left(1-\mathrm{e}^{\mathrm{i}\tilde{k}_{\mathrm{p}}}\right)\left(1-\mathrm{e}^{-\mathrm{i}\left(\tilde{k}_{\mathrm{p}}+\tilde{\kappa}\right)/2}\right)\right]. \tag{6.19b}$$

We can rewrite Equations (6.19a) and (6.19b) using the matrix format,

$$\underbrace{\begin{bmatrix}\mathcal{M}_{1,1} & \mathcal{M}_{1,2}\\ \mathcal{M}_{2,1} & \mathcal{M}_{2,2}\end{bmatrix}}_{\mathcal{M}}\begin{bmatrix}B_{\mathrm{s}}\\ B_{\mathrm{i}}\end{bmatrix} = \begin{bmatrix}0\\0\end{bmatrix} \tag{6.20}$$

where

$$\mathcal{M}_{1,1} = \tilde{\omega}_\mathrm{s}^2 - 4\left(1 - \tilde{C}\tilde{\omega}_\mathrm{s}^2\right)\sin^2\left(\frac{\tilde{k}_\mathrm{p} + \tilde{\kappa}}{4}\right), \tag{6.21a}$$

$$\mathcal{M}_{1,2} = -\frac{c_3}{2}A_\mathrm{p}\left[\left(\mathrm{e}^{\mathrm{i}\tilde{k}_\mathrm{p}} - 1\right)\left(\mathrm{e}^{-\mathrm{i}(\tilde{k}_\mathrm{p}-\tilde{\kappa})/2} - 1\right) - \left(1 - \mathrm{e}^{-\mathrm{i}\tilde{k}_\mathrm{p}}\right)\left(1 - \mathrm{e}^{\mathrm{i}(\tilde{k}_\mathrm{p}-\tilde{\kappa})/2}\right)\right], \tag{6.21b}$$

$$\mathcal{M}_{2,1} = -\frac{c_3}{2}A_\mathrm{p}\left[\left(\mathrm{e}^{-\mathrm{i}\tilde{k}_\mathrm{p}} - 1\right)\left(\mathrm{e}^{\mathrm{i}(\tilde{k}_\mathrm{p}+\tilde{\kappa})/2} - 1\right) - \left(1 - \mathrm{e}^{\mathrm{i}\tilde{k}_\mathrm{p}}\right)\left(1 - \mathrm{e}^{-\mathrm{i}(\tilde{k}_\mathrm{p}+\tilde{\kappa})/2}\right)\right], \tag{6.21c}$$

$$\mathcal{M}_{2,2} = \tilde{\omega}_\mathrm{i}^2 - 4\left(1 - \tilde{C}\tilde{\omega}_\mathrm{i}^2\right)\sin^2\left(\frac{\tilde{k}_\mathrm{p} - \tilde{\kappa}}{4}\right). \tag{6.21d}$$

Now, if $\det(\mathcal{M}) \neq 0$, the only solution to Equation (6.20) is $B_\mathrm{s} = B_\mathrm{i} = 0$, which does not agree with Equation (6.14a) if the initial signal amplitude is nonzero. Therefore we know that $\det(\mathcal{M}) = 0$, which gives us the equation

$$\mathcal{M}_{1,1}\mathcal{M}_{2,2} - \mathcal{M}_{1,2}\mathcal{M}_{2,1} = 0, \tag{6.22}$$

which we numerically solve for λ.

6.3.3 Comparison with the continuous model

In Figure 6.2 we compare the numerical solution of Equation (6.22) derived using the discrete theory for $g = -\mathrm{Im}(\lambda)$ with the solutions from the continuous equations, both for the nonlinear coupling coefficients as well as the approximated coupling factors, recall Equations (3.25a) and (3.25b). We note three key features in this figure:

1. In the small frequency limit, all solutions match. This is expected since the continuous equations are the approximation of the discrete equations in the small frequency limit, and the difference between linear coupling and nonlinear coupling goes to zero when the frequencies become small.

2. More importantly, we can see that neither of the continuous equations can predict the correct gain coefficient in the large frequency limit. More specifically, the nonlinear coupling equations overestimate the gain coefficient, while the linear coupling equations underestimate the gain coefficient.

3. Most importantly, it is theoretically possible to get exponential gain for a pump at large frequencies, *e.g.* $\omega_\mathrm{p} = 3\omega_\mathrm{c}/4 = 1.5\omega_0$ where we get 1/3 of the full band free of up-conversion (recall Figure 6.1), as long as the pump strength is large enough, $\chi \approx 0.1$. However, as we outline in Ref. [47] and paper [A], it does not seem possible to achieve such a large pump strength.

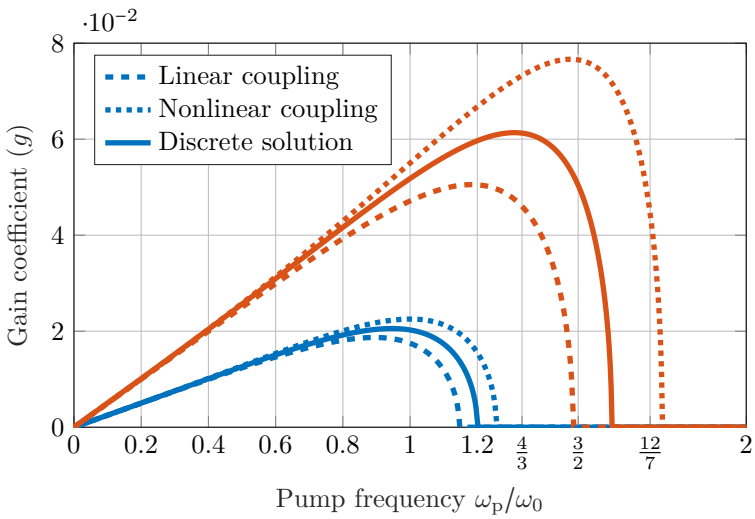

Figure 6.2: The gain coefficient $g = \mathrm{i}\lambda$ from numerically solving Equation (6.22) (solid) compared with the solution to Equation (3.24) with nonlinear coupling factors (dotted) and with linear coupling coefficients (dashed) for different pump strengths, $\chi = 0.05$ (blue) and $\chi = 0.1$ (orange). The solutions are found for $\tilde{C} = 0$, *i.e.* assuming that $\omega_\mathrm{pl} \gg \omega_0$, and $\delta = 0$, *i.e.* in the centre of the band.

6.4 Summary

In this chapter we noted that close to the cutoff frequency, there is a region free of up-conversion, and we investigated whether this could be utilised to retrieve the exponential gain originally predicted by Ref. [35]. A problem with this region is that we have a strongly nonlinear dispersion relation, and the wavelengths are on the order of the unitcell, so the continuous wave equation

previously used cannot be used any longer. Instead, we studied three-wave mixing in this region using the discrete equations. It turns out that it could theoretically be possible to use the TWPA in this regime. However, the phase mismatch is very large, and to overcome it, the pump strength also needs to be very large. We estimate that it is not possible to achieve a large enough pump strength to overcome the phase mismatch, although we do not prove this.

CHAPTER 7

Four-wave mixing

Until now, this work has been focused on three-wave mixing. The other commonly used mixing process for TWPAs is four-wave mixing (4WM). There are many similarities between three-wave mixing and four-wave mixing, but also some fundamental differences. In this chapter we outline the basic theory for four-wave mixing.

7.1 General four-wave mixing equations

For three-wave mixing, every mixing process is either an up-conversion process, $\omega_1 + \omega_2 \mapsto \omega_3$, or a down-conversion process, $\omega_3 \mapsto \omega_1 + \omega_2$. There are also degenerate processes which need to be treated slightly differently, $\omega_2 \leftrightarrow 2\omega_1$. This allowed us to express all mixing processes for a mode m as two sums, one corresponding to all down-conversion processes and one corresponding to all up-conversion processes, recall Equation (3.24). In general, any 3WM mixing process is captured by the frequency relation $\omega_c = \omega_a \pm \omega_b$.

For four-wave mixing, it is more complicated. In 4WM, there are four photons involved in every mixing process. Thus, the general frequency relation

for four-wave mixing is

$$\omega_d = \omega_a \pm \omega_b \pm \omega_c. \tag{7.1}$$

This gives us 3 distinct non-degenerate mixing transitions and 6 degenerate ones, or 9 in total. Writing the general propagation equations for 4WM, like an equivalent to Equation (3.24), would hence become very complicated. Instead, we will use a common simplification and limit the equations to the degenerate transitions involving at least two pump photons. This simplification is reasonable as long as we do not include up-conversion, since the signal and idler amplitudes are assumed to be much smaller than the pump amplitude. If up-conversion is to be included, the story quickly becomes more complicated, since we cannot assume that the pump harmonics are too small to ignore, so we would need to include the equations for all the transitions induced by pump harmonics as well.

7.2 The four-wave mixing single idler model

Let us study the single idler model for 4WM [15] where we only have 3 modes, the pump, the signal and the idler, and we ignore all up-conversion processes. With the 4WM idler defined as $\omega_\mathrm{i} = 2\omega_\mathrm{p} - \omega_\mathrm{s}$, the transitions involving at least two pump photons are

$$\omega_\mathrm{p} = \omega_\mathrm{p} + \omega_\mathrm{p} - \omega_\mathrm{p}, \tag{7.2a}$$

$$\omega_\mathrm{s} = \omega_\mathrm{s} + \omega_\mathrm{p} - \omega_\mathrm{p} = \omega_\mathrm{p} + \omega_\mathrm{p} - \omega_\mathrm{i}, \tag{7.2b}$$

$$\omega_\mathrm{i} = \omega_\mathrm{i} + \omega_\mathrm{p} - \omega_\mathrm{p} = \omega_\mathrm{p} + \omega_\mathrm{p} - \omega_\mathrm{s}. \tag{7.2c}$$

Now solving Equation (3.12) for $c_3 = 0$ and $c_4 \neq 0$, and using these transitions, we get the propagation equations

$$A_\mathrm{p}' = \mathrm{i}\frac{c_4}{8\tilde{\omega}_\mathrm{p}^2}\tilde{k}_\mathrm{p}^5 A_\mathrm{p}^2 \bar{A}_\mathrm{p}, \tag{7.3a}$$

$$A_\mathrm{s}' = \mathrm{i}\frac{c_4}{8\tilde{\omega}_\mathrm{s}^2}\left(2A_\mathrm{p}\bar{A}_\mathrm{p}A_\mathrm{s}\tilde{k}_\mathrm{p}^2\tilde{k}_\mathrm{s}^3 + A_\mathrm{p}^2\bar{A}_\mathrm{i}\tilde{k}_\mathrm{p}^2\tilde{k}_\mathrm{s}\tilde{k}_\mathrm{i}\left(2\tilde{k}_\mathrm{p} - \tilde{k}_\mathrm{i}\right)\mathrm{e}^{\mathrm{i}\Delta\tilde{k}_\mathrm{disp}\tilde{x}}\right), \tag{7.3b}$$

$$A_\mathrm{i}' = \mathrm{i}\frac{c_4}{8\tilde{\omega}_\mathrm{i}^2}\left(2A_\mathrm{p}\bar{A}_\mathrm{p}A_\mathrm{i}\tilde{k}_\mathrm{p}^2\tilde{k}_\mathrm{i}^3 + A_\mathrm{p}^2\bar{A}_\mathrm{s}\tilde{k}_\mathrm{p}^2\tilde{k}_\mathrm{s}\tilde{k}_\mathrm{i}\left(2\tilde{k}_\mathrm{p} - \tilde{k}_\mathrm{s}\right)\mathrm{e}^{\mathrm{i}\Delta\tilde{k}_\mathrm{disp}\tilde{x}}\right) \tag{7.3c}$$

where $\Delta\tilde{k}_{\mathrm{disp}} = 2\tilde{k}_{\mathrm{p}} - \tilde{k}_{\mathrm{s}} - \tilde{k}_{\mathrm{i}}$ is the dispersion-induced phase mismatch. We distinguish the dispersion-induced phase mismatch from the total phase mismatch here because, as we will soon see, for four-wave mixing there is an additional contribution to the total phase mismatch.

The solution to Equation (7.3a) is trivially found as

$$A_{\mathrm{p}} = A_{\mathrm{p0}} \mathrm{e}^{\mathrm{i}\alpha_{\mathrm{p}}\tilde{x}} \quad \text{where} \quad \alpha_{\mathrm{p}} = \frac{c_4 \tilde{k}_{\mathrm{p}}^5 A_{\mathrm{p0}} \bar{A}_{\mathrm{p0}}}{8\tilde{\omega}_{\mathrm{p}}^2}. \tag{7.4a}$$

Now, by defining

$$\begin{aligned} \kappa &= \frac{c_4}{8}\tilde{k}_{\mathrm{p}}^2 \left|A_{\mathrm{p0}}\right|^2, \quad \alpha_{\mathrm{s}} = \frac{2\tilde{k}_{\mathrm{s}}^3}{\tilde{\omega}_{\mathrm{s}}^2}\kappa, \quad \alpha_{\mathrm{i}} = \frac{2\tilde{k}_{\mathrm{i}}^3}{\tilde{\omega}_{\mathrm{i}}^2}\kappa, \\ \kappa_{\mathrm{s}} &= \frac{\tilde{k}_{\mathrm{s}}\tilde{k}_{\mathrm{i}}\left(2\tilde{k}_{\mathrm{p}} - \tilde{k}_{\mathrm{i}}\right)}{\tilde{\omega}_{\mathrm{s}}^2}\kappa, \quad \kappa_{\mathrm{i}} = \frac{\tilde{k}_{\mathrm{s}}\tilde{k}_{\mathrm{i}}\left(2\tilde{k}_{\mathrm{p}} - \tilde{k}_{\mathrm{s}}\right)}{\tilde{\omega}_{\mathrm{i}}^2}\kappa \end{aligned} \tag{7.4b}$$

the propagation equations can be reduced to the form

$$A_{\mathrm{s}}' = \mathrm{i}\alpha_{\mathrm{s}} A_{\mathrm{s}} + \mathrm{i}\kappa_{\mathrm{s}} \bar{A}_{\mathrm{i}} \mathrm{e}^{\mathrm{i}(\Delta\tilde{k}_{\mathrm{disp}} + 2\alpha_{\mathrm{p}})\tilde{x}}, \tag{7.5a}$$

$$A_{\mathrm{i}}' = \mathrm{i}\alpha_{\mathrm{i}} A_{\mathrm{i}} + \mathrm{i}\kappa_{\mathrm{i}} \bar{A}_{\mathrm{s}} \mathrm{e}^{\mathrm{i}(\Delta\tilde{k}_{\mathrm{disp}} + 2\alpha_{\mathrm{p}})\tilde{x}}. \tag{7.5b}$$

7.2.1 Solving the propagation equations

To solve Equations (7.5a) and (7.5b), we begin by making the transformation

$$A_{\mathrm{s}} = B_{\mathrm{s}} \mathrm{e}^{\mathrm{i}\alpha_{\mathrm{s}}\tilde{x}}, \tag{7.6a}$$

$$A_{\mathrm{i}} = B_{\mathrm{i}} \mathrm{e}^{\mathrm{i}\alpha_{\mathrm{i}}\tilde{x}} \tag{7.6b}$$

and introduce the four-wave mixing phase mismatch

$$\Delta\tilde{k} = \Delta\tilde{k}_{\mathrm{disp}} + 2\alpha_{\mathrm{p}} - \alpha_{\mathrm{s}} - \alpha_{\mathrm{i}}. \tag{7.7}$$

Then we can transform Equations (7.5a) and (7.5b) into

$$B_{\mathrm{s}}' = \mathrm{i}\kappa_{\mathrm{s}} \bar{B}_{\mathrm{i}} \mathrm{e}^{\mathrm{i}\Delta\tilde{k}\tilde{x}}, \tag{7.8a}$$

$$B_{\mathrm{i}}' = \mathrm{i}\kappa_{\mathrm{i}} \bar{B}_{\mathrm{s}} \mathrm{e}^{\mathrm{i}\Delta\tilde{k}\tilde{x}}. \tag{7.8b}$$

These equations have the same shape as Equations (3.27a) and (3.27b). We can hence use the same solution as in Section 3.4.2. After solving Equations (3.27a) and (3.27b) we can transform them back to the original amplitudes, and the solution is

$$A_\mathrm{s}(\tilde{x}) = \left[A_{\mathrm{s}0} \left(\cosh(g\tilde{x}) - \frac{\mathrm{i}\Delta\tilde{k}}{2g} \sinh(g\tilde{x}) \right) + \mathrm{i}\frac{\kappa_\mathrm{s}}{g} \bar{A}_{\mathrm{i}0} \sinh(g\tilde{x}) \right] \mathrm{e}^{\mathrm{i}(\alpha_\mathrm{s} + \Delta\tilde{k}/2)\tilde{x}}, \quad (7.9a)$$

$$A_\mathrm{i}(\tilde{x}) = \left[A_{\mathrm{i}0} \left(\cosh(g\tilde{x}) - \frac{\mathrm{i}\Delta\tilde{k}}{2g} \sinh(g\tilde{x}) \right) + \mathrm{i}\frac{\kappa_\mathrm{i}}{g} \bar{A}_{\mathrm{s}0} \sinh(g\tilde{x}) \right] \mathrm{e}^{\mathrm{i}(\alpha_\mathrm{i} + \Delta\tilde{k}/2)\tilde{x}}, \quad (7.9b)$$

where

$$g = \sqrt{\kappa_\mathrm{s}\bar{\kappa}_\mathrm{i} - \left(\frac{\Delta\tilde{k}}{2} \right)^2}. \quad (7.10)$$

7.2.2 Phase mismatch for purely linear dispersion

The propagation equations and the solution for four-wave mixing are very similar to the equations and the solution for three-wave mixing. There are however some key differences. One difference is that the gain band stretches from 0 to $2\omega_\mathrm{p}$. But another difference, of greater significance, is that of the phase mismatch. For three-wave mixing, there was only the dispersion-induced phase mismatch. For four-wave mixing, there are two contributions to the phase mismatch, recall Equation (7.7): the dispersion-induced one, and the Kerr-induced one,

$$\Delta\tilde{k} = \underbrace{2\tilde{k}_\mathrm{p} - \tilde{k}_\mathrm{s} - \tilde{k}_\mathrm{i}}_{\text{Dispersion-induced}} + \underbrace{2\alpha_\mathrm{p} - \alpha_\mathrm{s} - \alpha_\mathrm{i}}_{\text{Kerr-induced}}. \quad (7.11)$$

While the dispersion-induced phase mismatch can be made arbitrarily small, the Kerr-induced cannot. This becomes clear when we study the solution for purely linear dispersion, where $\tilde{k}_j = \tilde{\omega}_j$. Then the dispersion-induced phase mismatch disappears, $\Delta\tilde{k}_\mathrm{disp} = 0$, and the total phase mismatch becomes

$$\Delta\tilde{k} = 2\alpha_\mathrm{p} - \alpha_\mathrm{s} - \alpha_\mathrm{i} = 2\kappa\left(\tilde{\omega}_\mathrm{p} - \tilde{\omega}_\mathrm{s} - \tilde{\omega}_\mathrm{i}\right) = -2\tilde{\omega}_\mathrm{p}\kappa. \quad (7.12)$$

7.2.3 Gain in the purely linear dispersion regime

If we express the frequencies in terms of the four-wave mixing detuning

$$\tilde{\omega}_\mathrm{s} = (1+\delta)\tilde{\omega}_\mathrm{p}, \quad \tilde{\omega}_\mathrm{i} = (1-\delta)\tilde{\omega}_\mathrm{p}, \quad \delta = \frac{\tilde{\omega}_\mathrm{s} - \tilde{\omega}_\mathrm{p}}{\tilde{\omega}_\mathrm{p}} \in [-1, 1], \tag{7.13}$$

the gain coefficient becomes

$$g = \sqrt{\tilde{\omega}_\mathrm{s}\tilde{\omega}_\mathrm{i}\kappa^2 - \tilde{\omega}_\mathrm{p}^2\kappa^2} = \kappa\tilde{\omega}_\mathrm{p}\sqrt{-\delta^2} = \mathrm{i}\kappa\tilde{\omega}_\mathrm{p}\delta. \tag{7.14}$$

Now if we insert these simplified values of g and $\Delta\tilde{k}$ into Equation (7.9a), and use $A_{\mathrm{i}0} = 0$, we obtain the gain

$$G = \left|\frac{A_\mathrm{s}(\tilde{x})}{A_{\mathrm{s}0}}\right|^2 = \cos^2(\kappa\tilde{\omega}_\mathrm{p}\tilde{x}\delta) + \frac{1}{\delta^2}\sin^2(\kappa\tilde{\omega}_\mathrm{p}\tilde{x}\delta)\,. \tag{7.15}$$

As we can see, the gain oscillates between 1 and $1/\delta^2$, depending on the value of the effective length $\kappa\tilde{\omega}_\mathrm{p}\tilde{x}\delta$. In other words, not even when the dispersion-induced phase mismatch is completely neglected do we get exponential gain. This is because of the Kerr-induced phase mismatch, a phenomenon that does not exist for three-wave mixing, which ensures that there is always too much phase mismatch to get exponential gain.

7.2.4 Analysis of gain peaks and gain valleys

Since there is a detuning-dependency inside the parentheses of the gain formula, Equation (7.15), the maximum gain $1/\delta^2$ is not achieved for all frequencies simultaneously. Thus, for large values of $\kappa\tilde{\omega}_\mathrm{p}\tilde{x}$, there will be gain peaks and valleys at different frequencies, see Figure 7.1.

If one wants to avoid gain valleys, one can ensure that $\kappa\tilde{\omega}_\mathrm{p}\tilde{x} \le \pi$. However, then the maximum gain is limited to $1+\pi^2 \lesssim 10.87 \approx 10.36\,\mathrm{dB}$. More generally, the maximum gain is $1 + \kappa^2\tilde{\omega}_\mathrm{p}^2\tilde{x}^2$, and the width of the central gain peak is given by $|\delta| \le \frac{\pi}{\kappa\tilde{\omega}_\mathrm{p}\tilde{x}}$. Thus, if we can accept a smaller bandwidth of the central gain peak, we can get a larger maximum gain. If $\kappa\tilde{\omega}_\mathrm{p}\tilde{x} = n\pi$, the maximum gain is $1 + n^2\pi^2$ and the bandwidth 2δ is limited as $|\delta| \le \frac{1}{n}$.

For $|\delta| \le \frac{1}{2}$, the maximum gain is $1 + 4\pi^2 \approx 40 \approx 16\,\mathrm{dB}$. For $|\delta| \le \frac{1}{3}$, the maximum gain is $1 + 9\pi^2 \approx 90 \approx 19\,\mathrm{dB}$. As we can see, we have to heavily

reduce the bandwidth to increase the maximum gain with only a few decibel, see Figure 7.1.

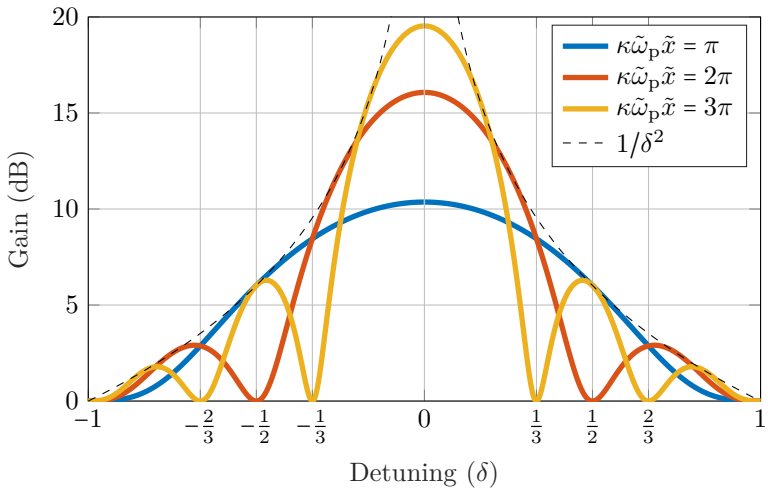

Figure 7.1: The gain for four-wave mixing in the linear dispersion regime.

7.3 A four-wave mixing single input study

In Section 7.2 we studied the single idler model for 4WM, and saw that 4WM has an additional component to the phase mismatch, compared to 3WM, due to Kerr effect. In the purely linear regime, the dispersion-induced phase mismatch was completely neglected, we saw that this additional phase mismatch prevents exponential gain.

A question one might now ask is: What happens when we include up-converted modes and the dispersion-induced phase mismatch? For 3WM, the up-converted modes made a fundamental difference. To try to answer this question, we turn to the case of a single input in the quasilinear regime. Here we present a shorter version of the work analysis done in Section 5.1, but now for 4WM. This work is also presented in paper [A].

As we discussed in Section 7.1, it is hard to cover all mixing processes for 4WM, even in the case of a single input. For only two harmonics of the pump, which for 4WM is the first harmonic and the third harmonic, the propagation

equations are

$$A_{\mathrm{p}}' = \mathrm{i}\frac{c_4}{8\tilde{\omega}_{\mathrm{p}}^2}\left(\tilde{k}_{\mathrm{p}}^5 A_{\mathrm{p}}^2 \bar{A}_{\mathrm{p}} - \tilde{k}_{3\mathrm{p}}\tilde{k}_{\mathrm{p}}^4 A_{3\mathrm{p}}\bar{A}_{\mathrm{p}}^2 \mathrm{e}^{\mathrm{i}(\tilde{k}_{3\mathrm{p}}-3\tilde{k}_{\mathrm{p}})\tilde{x}}\right), \tag{7.16a}$$

$$A_{3\mathrm{p}}' = \mathrm{i}\frac{c_4}{8\tilde{\omega}_{3\mathrm{p}}^2}\left(2\tilde{k}_{3\mathrm{p}}^3\tilde{k}_{\mathrm{p}}^2 A_{3\mathrm{p}}A_{\mathrm{p}}\bar{A}_{\mathrm{p}} - \frac{1}{3}\tilde{k}_{3\mathrm{p}}^2\tilde{k}_{\mathrm{p}}^3 A_{\mathrm{p}}^3 \mathrm{e}^{-\mathrm{i}(\tilde{k}_{3\mathrm{p}}-3\tilde{k}_{\mathrm{p}})\tilde{x}}\right). \tag{7.16b}$$

Now, assuming that we are in the quasilinear regime, where $\tilde{k}_j \approx \tilde{\omega}_j$ except for the phase mismatches where we use the next order approximation, and with similar transformations as the ones made in Section 5.1,

$$\xi(\tilde{x}) = \frac{c_4\tilde{\omega}_{\mathrm{p}}^3}{8}A_{\mathrm{p}0}^2\tilde{x}, \tag{7.17a}$$

$$a_{m\mathrm{p}}(\xi(\tilde{x})) = m\frac{A_{m\mathrm{p}}(\tilde{x})}{A_{\mathrm{p}0}}, \tag{7.17b}$$

$$\mu = 8\frac{\tilde{k}_{3\mathrm{p}} - 3\tilde{k}_{\mathrm{p}}}{c_4\tilde{\omega}_{\mathrm{p}}^3 A_{\mathrm{p}0}^2}, \tag{7.17c}$$

we can transform Equations (7.16a) and (7.16b) into

$$a_{\mathrm{p}}' = \mathrm{i}\left(a_{\mathrm{p}}^2\bar{a}_{\mathrm{p}} - 3a_{3\mathrm{p}}\bar{a}_{\mathrm{p}}^2\mathrm{e}^{\mathrm{i}\mu\xi}\right), \tag{7.18a}$$

$$a_{3\mathrm{p}}' = 3\mathrm{i}\left(2a_{3\mathrm{p}}a_{\mathrm{p}}\bar{a}_{\mathrm{p}} - \frac{1}{3}a_{\mathrm{p}}^3\mathrm{e}^{-\mathrm{i}\mu\xi}\right). \tag{7.18b}$$

Here we have only one parameter, μ, which corresponds to the effective dispersion-induced phase mismatch. As we can see in Figure 7.2, there is a fundamental difference between 3WM and 4WM for up-conversion into the next harmonic. For 3WM, when μ gets very small, more and more of the first harmonic gets up-converted, until it is completely up-converted.

However, for 4WM, the up-conversion is limited. Even for $\mu = 0$, which corresponds to the purely linear dispersion regime, only about 25 % of the pump is up-converted. By comparing it with the single input study for 3WM, we see that $\mu = 0$ for 4WM is very similar to $\mu = 3$ for 3WM. But if the Kerr-related terms are neglected from Equations (7.18a) and (7.18b), we get a similar behaviour as the one of 3WM. Thus we conclude, although not all of the pump harmonics are included in the equations, that up-conversion is much less of a problem for 4WM due to Kerr effect.

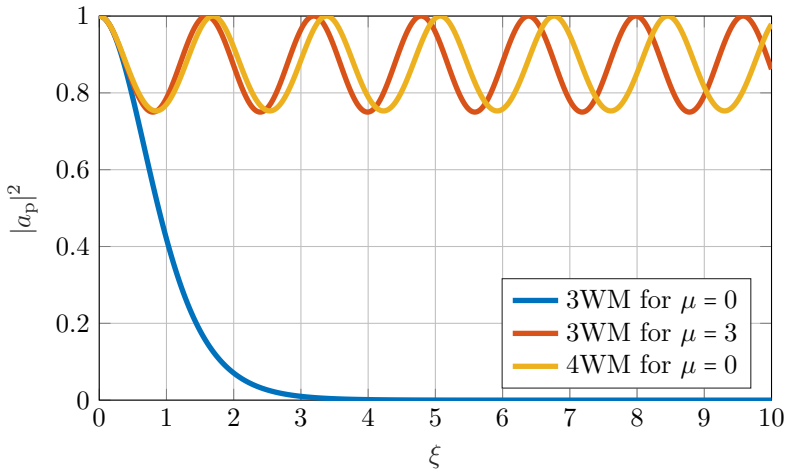

Figure 7.2: Comparison of the solutions for two harmonics for 3WM and 4WM.

7.4 Reversed Kerr

As we saw in Section 7.2, even for purely linear dispersion, the phase mismatch is too large to give exponential gain for 4WM. One way to solve this problem is with dispersion engineering, which we will discuss in Chapter 8. However, there is another solution that does not require any dispersion engineering, which is called 'reversed Kerr' [25].

The problem with the phase mismatch is that both contributions are negative. Now recall the definitions of $\alpha_p, \alpha_s, \alpha_i$, Equations (7.4a) and (7.4b). Note that all α:s include the factor κ, which in turn contains the mixing coefficient c_4. In other words, if we managed to change the sign of the 4WM coefficient, the Kerr-induced phase mismatch would change its sign, and we could make the two contributions to the phase mismatch cancel each other out:

$$\text{Regular Kerr:} \qquad \Delta\tilde{k} = \underbrace{\Delta\tilde{k}_{\text{disp}}}_{\leq 0} + \underbrace{\Delta\tilde{k}_{\text{Kerr}}}_{\leq 0} \leq 0, \tag{7.19a}$$

$$\text{reversed Kerr:} \qquad \Delta\tilde{k} = \underbrace{\Delta\tilde{k}_{\text{disp}}}_{\leq 0} + \underbrace{\Delta\tilde{k}_{\text{Kerr}}}_{\geq 0} \approx 0. \tag{7.19b}$$

Now recall Figures 4.4 and 4.7. As we can see, both the rf-SQUID and the SNAIL have the ability to provide a negative four-wave mixing coefficient within a range of fluxes. Especially, at half a flux quantum, the three-wave mixing coefficient is zero and we get pure 4WM with a negative mixing coefficient.

However, we do not want the Kerr-induced phase mismatch to be too large, we only want it to cancel the dispersion-induced phase mismatch. Furthermore, the Kerr-induced phase mismatch changes with pump power. In order to design a reversed Kerr amplifier, one hence needs to ensure that the Kerr-induced phase mismatch minimises the total phase mismatch for the desired frequencies at the pump power giving the desired gain.

7.5 Summary

In this chapter we have studied four-wave mixing (4WM). We first discussed how the general propagation equations are significantly more complicated for 4WM due to the 9 different kinds of conversion processes that can happen, compared with the 3 conversions that can happen for 3WM. Then we solved the propagation equations for the single idler model, and showed that even for purely linear dispersion, the phase mismatch is too large for 4WM to deliver an exponential gain due to Kerr effect. Next we looked at a single input for two harmonics, the first and the third, and showed that even for purely linear dispersion, the up-conversion is still limited due to Kerr effect. Kerr effect hence has both a positive and a negative effect. On the one hand, it prevents exponential gain. But on the other hand, it also suppresses up-conversion. If one can solve phase matching for the pump, the signal and the idler, without enabling up-conversion, one should hence get an exponential gain with small to no up-conversion. Finally we had a quick look at reversed Kerr, and noted that if the sign of the 4WM coefficient was changed, Kerr effect could start helping with phase matching.

CHAPTER 8

Dispersion engineering

Until now, we have looked at pure three-wave mixing and pure four-wave mixing for the standard TWPA structure, recall Figure 3.1. We have showed that neither 3WM nor 4WM can deliver an exponential gain using the standard TWPA structure, although for different reasons. In this chapter, we are going to look at how we can use dispersion engineering to get an exponential gain, both for 3WM and 4WM.

8.1 The phase mismatches

First let us outline what the phase mismatch is, so that we know what change is necessary. In Figure 8.1 we have plotted the phase mismatch as a function of detuning. Remember that the detuning is defined differently for the two processes, recall Equations (3.32) and (7.13). As can be seen, for 3WM the phase mismatch is always positive, while for 4WM it is always negative. For 3WM the phase mismatch is the largest at zero detuning, while for 4WM it is the largest at maximal detuning. For 4WM there is also the issue that Kerr effect increases the phase mismatch with the pump power. For small frequencies, the Kerr-induced phase mismatch shifts the whole phase mismatch

curve down, while for reversed Kerr the whole curve shifts up. The needed correction to the phase mismatch for 4WM is thus dependent on the pump power. To improve phase matching for 3WM we would need to add a negative number to the phase mismatch, while for 4WM with regular Kerr we would need to add a positive number.

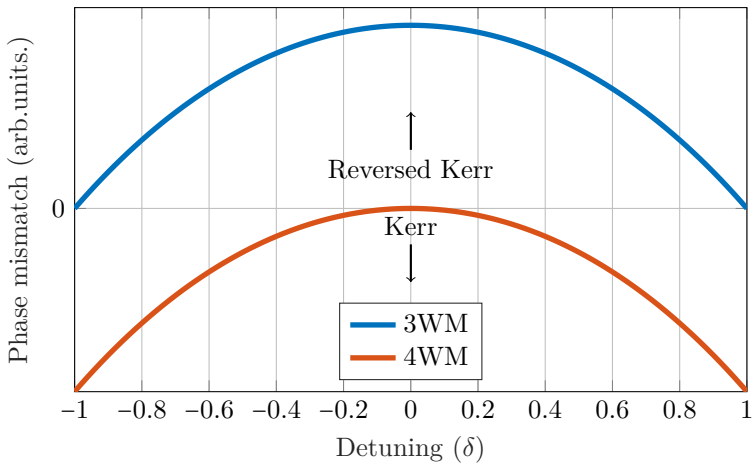

Figure 8.1: The phase mismatches in arbitrary units for 3WM and 4WM as a function of detuning δ at zero pump power. When the pump power is non-zero, Kerr effect will decrease the value of the 4WM phase mismatch, while reversed Kerr will increase it.

8.2 Resonant phase matching

One technique to give the needed correction to the phase mismatch is resonant phase matching (RPM) [19]. To implement RPM, we exchange the single shunt capacitor C_0 for a capacitor C_1 in parallel with a weakly coupled LC-oscillator, see Figure 8.2. Here the sum of the two capacitances is equal to the single capacitance in the standard unitcell, *i.e.* $C_0 = C_1 + C_c$, to ensure a similar unitcell impedance. By making this change, we open up a stopband around the resonance which we can use for phase matching.

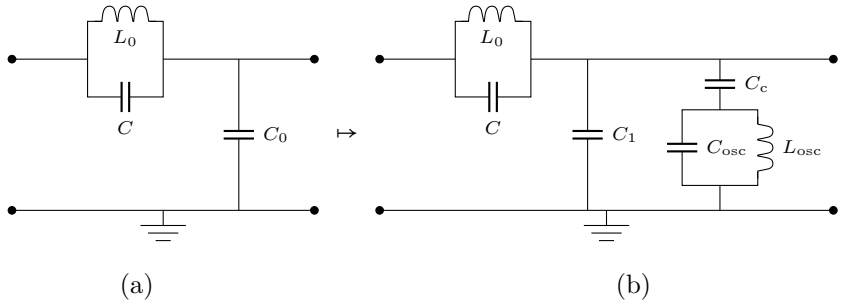

Figure 8.2: (a) The regular unitcell. (b) The RPM unitcell.

8.2.1 The dispersion relation

To find the dispersion relation of the RPM unitcell, we use $\cos\left(\tilde{k}\right) = \frac{A+D}{2}$ [52], where A and D are the elements (1,1) and (2,2) of the transmission matrix and $\tilde{k} = ka$ is the wave number normalised to the RPM unitcell. Then the dispersion relation for a TWPA with the RPM unitcell, Figure 8.2b, is given by

$$\begin{aligned}\cos\left(\tilde{k}\right) &= 1 - \frac{1}{2}\cdot\frac{\mathrm{i}\omega L_0}{1-\omega^2 L_0 C}\cdot\left(\mathrm{i}\omega C_1 + \frac{\mathrm{i}\omega C_c\left(1-\omega^2 L_{osc}C_{osc}\right)}{1-\omega^2 L_{osc}\left(C_c+C_{osc}\right)}\right)\\ &= 1 - \frac{1}{2}\cdot\frac{\omega^2/\omega_0^2}{1-\omega^2/\omega_{pl}^2}\cdot\frac{1-\nu\omega^2/\omega_r^2}{1-\omega^2/\omega_r^2}\end{aligned} \tag{8.1}$$

where

$$\omega_0^2 = \frac{1}{L_0 C_0}, \quad \omega_{pl}^2 = \frac{1}{L_0 C}, \quad \omega_r^2 = \frac{1}{L_{osc}\left(C_c + C_{osc}\right)}, \tag{8.2}$$

where ω_r is the resonance frequency of the RPM feature, and

$$\nu = 1 - \frac{C_c^2}{\left(C_1 + C_c\right)\left(C_c + C_{osc}\right)} = 1 - \frac{C_c}{C_0}\frac{C_c}{C_c + C_{osc}}. \tag{8.3}$$

Further simplification yields

$$4\sin^2\left(\frac{\tilde{k}}{2}\right) = \frac{\omega^2/\omega_0^2}{1-\omega^2/\omega_{pl}^2}\cdot\frac{1-\nu\omega^2/\omega_r^2}{1-\omega^2/\omega_r^2}. \tag{8.4}$$

Rearranging this equation in terms of ω yields a second degree polynomial with respect to ω^2,

$$\omega^4 \cdot \left[\frac{4\sin^2\left(\frac{\tilde{k}}{2}\right)}{\omega_{\mathrm{pl}}^2 \omega_{\mathrm{r}}^2} + \frac{\nu}{\omega_0^2 \omega_{\mathrm{r}}^2} \right] - \omega^2 \cdot \left[4\sin^2\left(\frac{\tilde{k}}{2}\right) \frac{\omega_{\mathrm{r}}^2 + \omega_{\mathrm{pl}}^2}{\omega_{\mathrm{r}}^2 \omega_{\mathrm{pl}}^2} + \frac{1}{\omega_0^2} \right] + 4\sin^2\left(\frac{\tilde{k}}{2}\right) = 0. \quad (8.5)$$

One can solve Equation (8.5) as it is, but we will simplify it first. The effect of the plasma frequency ω_{pl} is, similar to before (recall Figure 2.3), that it only pushes the bands to lower frequencies. We ignore this effect for now by letting $\omega_{\mathrm{pl}} \to \infty$, which is equivalent with setting $\tilde{C} = 0$. We also express Equation (8.5) in terms of normalised frequencies $\tilde{\omega} = \omega/\omega_0$ and multiply the equation with $\tilde{\omega}_{\mathrm{r}}^2$. Then it simplifies to

$$\nu\tilde{\omega}^4 - \tilde{\omega}^2 \cdot \left[\tilde{\omega}_{\mathrm{r}}^2 + 4\sin^2\left(\frac{\tilde{k}}{2}\right) \right] + 4\tilde{\omega}_{\mathrm{r}}^2 \sin^2\left(\frac{\tilde{k}}{2}\right) = 0 \quad (8.6)$$

which has two solutions,

$$\tilde{\omega}_{\pm}^2 = \frac{1}{2\nu} \left[\tilde{\omega}_{\mathrm{r}}^2 + 4\sin^2\left(\frac{\tilde{k}}{2}\right) \pm \sqrt{\left(\tilde{\omega}_{\mathrm{r}}^2 + 4\sin^2\left(\frac{\tilde{k}}{2}\right) \right)^2 - 16\nu\tilde{\omega}_{\mathrm{r}}^2 \sin^2\left(\frac{\tilde{k}}{2}\right)} \right]. \quad (8.7)$$

8.2.2 RPM phase corrections

Let us study the solutions of Equation (8.7) for different values of ν. For $\nu = 1$, corresponding to no coupling to the resonators, we retrieve the standard dispersion relation derived in Section 2.3. However, for $\nu < 1$ each resonator is coupled to each unitcell and a stopband opens up around the resonance frequency $\tilde{\omega}_{\mathrm{r}}$, see Figure 8.3. The $\tilde{\omega}_-$ solutions correspond to the lower band and the $\tilde{\omega}_+$ solutions correspond to the upper band. To get the frequency bands, we solve Equation (8.7) for the full range of wave numbers $\tilde{k} \in [0, \pi]$. While $\tilde{\omega}_{\pm}(\pi)$ gets a fairly long expression which we will not write down here, and $\tilde{\omega}_-(0)$ is trivially equal to 0, it is worth pointing out that $\tilde{\omega}_+(0) = \tilde{\omega}_{\mathrm{r}}/\sqrt{\nu}$.

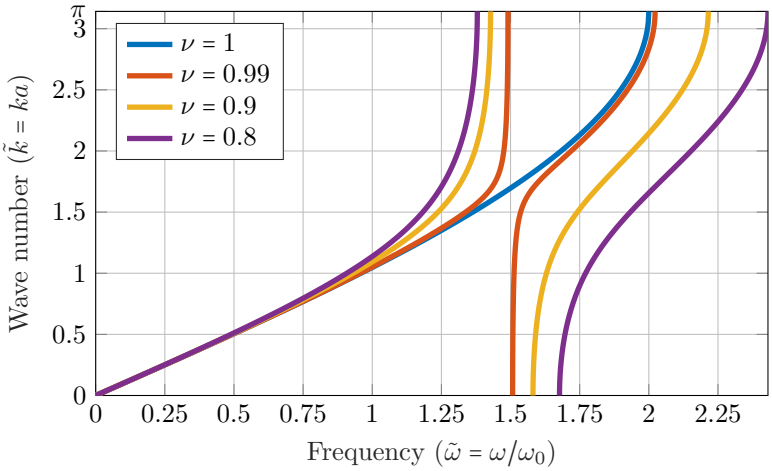

Figure 8.3: The dispersion relation, as given by Equation (8.7), for $\tilde{\omega}_r = 1.5$, $\omega_{pl} = \infty$ and different values of ν.

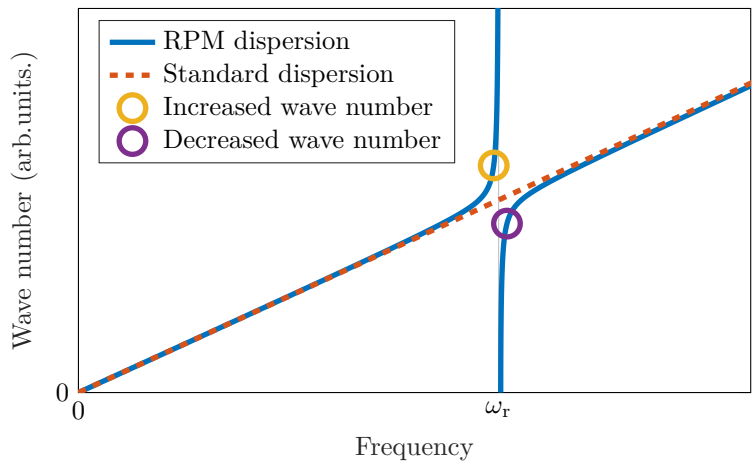

Figure 8.4: The RPM dispersion relation versus the standard dispersion relation. There are example marks for where the pump could be placed to get an increase of its wave number (yellow) or a decrease (purple), compared with the standard dispersion relation.

Now, assume a weakly coupled resonator, *e.g.* $\nu = 0.99$. Then the dispersion relation is unaffected for most frequencies, except the ones close to the resonance. By placing the pump below the resonance, one can hence get an increase in its wave number, and in turn the phase mismatch, see the yellow circle in Figure 8.4. This is what is needed for 4WM, and was demonstrated in Ref. [20]. But by placing the pump above the resonance, one can instead get a decrease in its wave number, and in turn the phase mismatch, see the purple circle in Figure 8.4. This is what is needed for 3WM.

8.2.3 Resonant phase matching for three-wave mixing

To use RPM for 4WM, one puts the pump slightly below the resonance, which gives an increase of the pump wave number, which can in turn both compensate for the Kerr effect and move the points of perfect phase matching away from zero detuning. This gives an exponential gain over a large band [19], [20].

For 3WM the picture is different. While minimising the phase mismatch is advantageous, the larger issue for 3WM is that of up-conversion, as shown in Chapter 5. Since the wave numbers, and in turn the propagation equations, are mostly unaffected by the resonance of the RPM, this issue still persists when using RPM. An approach to get around this is to place the pump, and in turn the resonance, close to the cutoff, as illustrated in Figure 6.1. Then the cutoff suppresses the up-conversion processes and the RPM minimises the phase mismatch in this regime. However, to verify that this would indeed work, one has to solve the discrete wave equation including the RPM feature, which is presented in paper [A].

8.2.4 Resonant phase matching with distributed resonators

An alternative approach to adding weakly coupled LC-oscillators, as proposed above, is to add distributed resonators instead [21]. The resonators have a similar impact on the dispersion relation, and can hence be used for the same purpose. The problem with distributed resonators, and the reason to why we have not taken this approach, is that they are physically much larger than lumped-element LC-oscillators, and they are needed in several of the unitcells. Therefore they are much harder to fit on the chip, making them impractical to use in an actual device.

8.3 Periodic modulation

An alternative approach to RPM is that of periodic modulation. In periodic modulation, we replace the regular unitcell with a supercell containing n subcells which are not all identical, see Figure 8.5. This will in turn create n bands in the dispersion relation, and $n-1$ stopbands, and the dispersion around the stopbands is similar to that of the RPM. This is shown experimentally for $n = 3$ subcells in paper [B].

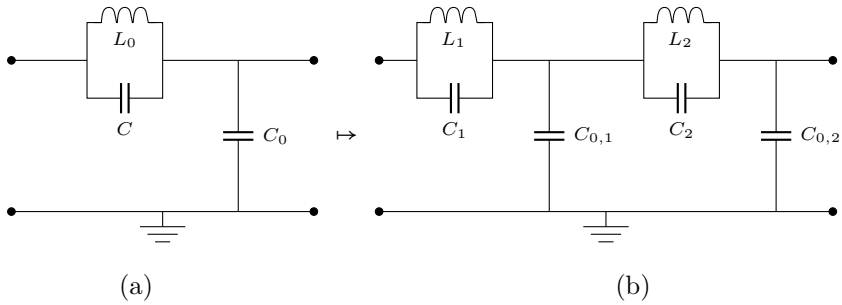

Figure 8.5: (a) The regular unitcell. (b) A supercell with 2 subcells.

8.3.1 The dispersion relation

To derive the dispersion relation for the modulated chain, let us make some simplifications. Let us assume $n = 2$ subcells, neglect the plasma frequencies $C_1 = C_2 = 0$ and identical shunt capacitances $C_{0,1} = C_{0,2} = C_0$. The only difference between the subcells is thus the inductances, L_1 and L_2. To find the dispersion relation, we first find the transmission matrix. The transmission matrix of the supercell is given by

$$\begin{aligned}\begin{bmatrix} A & B \\ C & D \end{bmatrix} &= \begin{bmatrix} 1-\omega^2 L_1 C_0 & \mathrm{i}\omega L_1 \\ \mathrm{i}\omega C_0 & 1 \end{bmatrix}\begin{bmatrix} 1-\omega^2 L_2 C_0 & \mathrm{i}\omega L_2 \\ \mathrm{i}\omega C_0 & 1 \end{bmatrix} \\ &= \begin{bmatrix} 1-\omega^2 C_0\left(2L_1+L_2\right)+\omega^4 L_1 L_2 C_0^2 & \mathrm{i}\omega L_1 + \mathrm{i}\omega L_2\left(1-\omega^2 L_1 C_0\right) \\ \mathrm{i}\omega C_0\left(2-\omega^2 L_2 C_0\right) & 1-\omega^2 L_2 C_0 \end{bmatrix}.\end{aligned} \tag{8.8}$$

Using $\cos\left(2\tilde{k}\right) = \frac{A+D}{2}$ [52], where $\tilde{k} = ka$ is the normalised wave number over a subcell, a is the length of a subcell and the factor 2 comes from having 2

subcells, we hence get

$$\cos\left(2\tilde{k}\right) = 1 - \omega^2 C_0 \left(L_1 + L_2\right) + \frac{1}{2}\omega^4 L_1 L_2 C_0^2. \tag{8.9}$$

Let us define

$$\omega_1^2 = \frac{1}{L_1 C_0}, \quad \omega_2^2 = \frac{1}{L_2 C_0}. \tag{8.10}$$

Then Equation (8.9) can be written as

$$4\sin^2\left(\tilde{k}\right) = 2\omega^2\left(\frac{1}{\omega_1^2} + \frac{1}{\omega_2^2}\right) - \frac{\omega^4}{\omega_1^2\omega_2^2}. \tag{8.11}$$

Rearranging this equation in terms of ω yields a second degree polynomial with respect to ω^2,

$$\omega^4 - \omega^2 \cdot 2\left(\omega_1^2 + \omega_2^2\right) + 4\omega_1^2\omega_2^2 \sin^2\left(\tilde{k}\right) = 0. \tag{8.12}$$

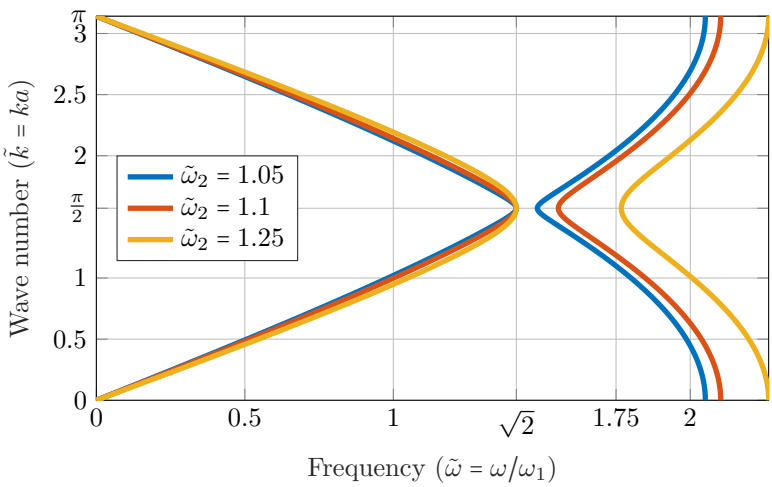

Figure 8.6: The dispersion relation for different values of $\tilde{\omega}_2 = \omega_2/\omega_1$. The stopband is in the frequency range $\tilde{\omega} \in \left(\sqrt{2}, \tilde{\omega}_2\sqrt{2}\right)$ and the cutoff frequency is at $\tilde{\omega} = \sqrt{2 + 2\tilde{\omega}_2^2}$.

The solutions are given by

$$\omega_{\pm}^2 = \omega_1^2 + \omega_2^2 \pm \sqrt{\left(\omega_1^2 + \omega_2^2\right)^2 - 4\omega_1^2\omega_2^2 \sin^2\left(\tilde{k}\right)}, \tag{8.13}$$

which are shown in Figure 8.6 for multiple values of $\tilde{\omega}_2 = \omega_2/\omega_1$. Note that we have plotted $\tilde{k}$, which is the wave number of *one subcell*, as a function of $\tilde{\omega} = \omega/\omega_1$. Solving Equation (8.13) for $\tilde{k} \in \left\{0, \frac{\pi}{2}, \pi\right\}$, and assuming that $\omega_2 > \omega_1$, we get that the frequency bands in terms of $\tilde{\omega} = \omega/\omega_1$ are

$$\tilde{\omega}_- \in \left[0, \sqrt{2}\right], \quad \tilde{\omega}_+ \in \left[\tilde{\omega}_2\sqrt{2}, \sqrt{2 + 2\tilde{\omega}_2^2}\right]. \tag{8.14}$$

8.3.2 Periodic modulation for three-wave mixing

Periodic modulation for three-wave mixing is a technique used in several different TWPA designs [28], [29], [33], [59], although for different reasons, and it is more common to modulate the shunt capacitances. Since periodic modulation has the possibility to create as many stopbands as desired, one can use it to create several stopbands with different purposes. The first stopband can be used to get the phase mismatch correction. The second stopband can be used to suppress up-conversion. If the second stopband is not wide enough, more stopbands at higher frequencies can further suppress the up-conversion processes.

What we did theoretically in paper [A] was instead to use only 2 subcells, and place the stopband close to the cutoff, similar to what we did with resonant phase matching. This way, the cutoff suppresses the up-conversion processes while the stopband is used to give the phase mismatch correction.

Since the phase mismatch for three-wave mixing is inherently small for small frequencies and the limiting factor for 3WM is the up-conversion processes, one can skip using a stopband to give the phase mismatch correction, and instead use the first stopband to suppress up-conversion. This is what we studied in paper [B].

8.3.3 Comparison with resonant phase matching

Periodic modulation and resonant phase matching have similarities and differences. The similarity is that they both can open up a stopband which gives a perturbation to the dispersion relation, which can be used for phase matching.

An advantage with periodic modulation is that it is easy to integrate it to the regular design: one simply adds a small change periodically to the unitcells. Another advantage is that it can easily be used to create many stopbands with more functions than the stopband of resonant phase matching. A disadvantage with periodic modulation is that the phase mismatch corrections are fairly small, while for resonant phase matching the wave number of the pump can in theory be any value between 0 and π. Thus, periodic modulation can only give phase mismatch corrections to an extent, while resonant phase matching can give a much larger range of corrections.

8.4 Summary

In this chapter we first looked at the phase mismatches for three-wave mixing as well as four-wave mixing. We noted that for four-wave mixing, an increase of the pump wave number is necessary to minimise the phase mismatch, while for three-wave mixing a decrease of the pump wave number is necessary. Then we presented two ways of achieving this: Either by adding weakly coupled oscillators/resonators, or by periodically modulating the chain. Both of these have the possibility to give corrections to the pump wave number, and in turn the phase mismatch, in order to enable exponential gain.

CHAPTER 9

Impedance matching, filters and frequency multiplexing

In this chapter we will look at the necessity of impedance matching and microwave filter theory. The filter theory will help us both with designing the necessary impedance matching networks that our TWPAs operating with frequencies close to the cutoff frequency will require, as well as designing frequency multiplexers which we will use in Chapter 10.

9.1 Impedance matching

When an electromagnetic field passes from one medium to another, there may occur reflections [52]. The reflection coefficient for a field going from medium 1 to medium 2 is given by

$$\Gamma = \frac{Z_2 - Z_1}{Z_2 + Z_1} \tag{9.1}$$

where Z_1 and Z_2 are the characteristic impedances of the two media, and Γ is equivalent to the scattering parameter S_{11}, recall Equation (2.24a). When the two media have the same impedances, there are no reflections. Then the two media are *impedance matched*.

Impedance matching is of high importance when designing amplifiers, since

if the amplifier is not impedance matched to its environment, reflections occur at the output and/or the input, which can make the amplifier unstable [52]. For the TWPA suggested in Chapter 8 and paper [A], using frequencies close to the cutoff frequency, three-wave mixing and resonant phase matching, we need impedance matching both in the signal range ($\sim \omega_c/4$ to $\sim 2\omega_c/4$) and at the pump frequency ($\sim 3\omega_c/4$).

We saw in Chapter 2 that it is easy to impedance match a discrete transmission line for frequencies well below the cutoff frequency. It is also possible to impedance match the discrete chain close to the cutoff frequency, but at the cost of an impedance mismatch at smaller frequencies, recall Section 2.4.3. Ensuring impedance matching in the full frequency range $\omega_c/4$ to $3\omega_c/4$ is hence going to be problematic.

9.2 Microwave filter theory

To be able to impedance match our TWPA prototype, it is instructive to look at microwave filter theory.

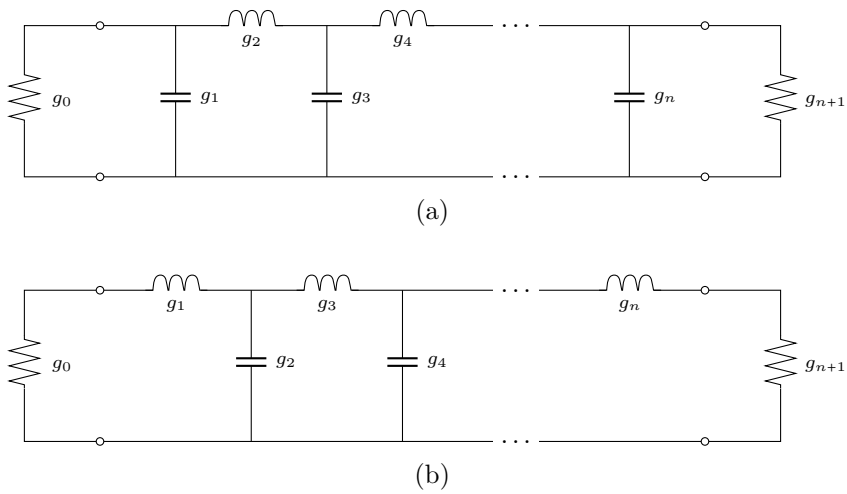

Figure 9.1: Definition of the prototype filter parameters for odd order filters. (a) A prototype with a π-structure. (b) A prototype with a T-structure.

Microwave filters are often synthesised using lumped-element low-pass filter prototypes, which are later transformed into the desired filter [60]. An n:th order prototype is described by its coefficients g_k for $k = \{0, 1, ..., n+1\}$, see Figure 9.1.

Here g_0 and g_{n+1} are the characteristic impedances of the source and the load, while g_k for $k = \{1, 2, ..., n\}$ are the values of the inductances and the capacitances of the filter. The filter prototype is defined this way because then the two prototypes in Figure 9.1a and Figure 9.1b have identical responses.

9.2.1 The Butterworth and Chebyshev filters

What the values of g_k should be depends on the filter design. Here we will not go through filter synthesising techniques as it is out of the scope of this thesis, but give concrete examples of two common filters, the Butterworth filter and the Chebyshev filter [60].

For a Butterworth filter of order n, the filter coefficients are

$$g_0 = g_{n+1} = 1, \quad g_k = 2\sin\left(\pi\frac{2k-1}{2n}\right) \quad \text{for} \quad k \in [1, n] \cap \mathbb{N}. \tag{9.2}$$

This is also known as a *maximally flat* filter, because its frequency response is as flat as possible.

A Chebyshev filter is not maximally flat, but has a transmission that stays within a desired ripple level, and instead a higher attenuation in the stopband. To design a Chebyshev filter, we hence need to decide a desired ripple level. For a ripple level ε in dB, one first computes

$$\begin{aligned} \beta &= \ln\left(\coth\frac{\varepsilon\ln(10)}{40}\right), \quad \gamma = \sinh\left(\frac{\beta}{2n}\right), \\ a_k &= 2\sin\left(\pi\frac{2k-1}{2n}\right), \quad b_k = \gamma^2 + \sin^2\left(\frac{k\pi}{n}\right). \end{aligned} \tag{9.3a}$$

Then the filter coefficients can be computed as

$$\begin{aligned} g_0 &= 1, \quad g_1 = \frac{2a_1}{\gamma}, \\ g_k &= \frac{4a_{k-1}a_k}{b_{k-1}g_{k-1}} \quad \text{for} \quad k \in [2, n] \cap \mathbb{N}, \\ g_{n+1} &= \begin{cases} 1, & \text{if } n \text{ odd}, \\ \coth^2\left(\frac{\beta}{4}\right), & \text{if } n \text{ even}. \end{cases} \end{aligned} \tag{9.3b}$$

See examples of the filter coefficients in Figure 9.2a, and the corresponding transmission of these filters in Figure 9.2b.

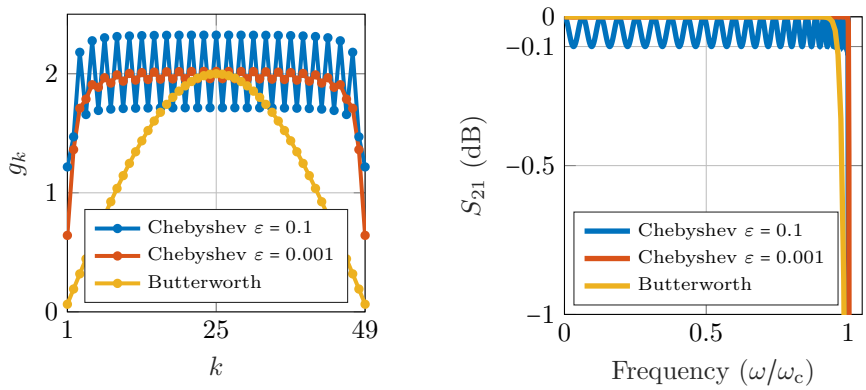

(a) **(b)**

Figure 9.2: Examples of filters. (**a**) The g_k coefficients for filters with order $n = 49$. (**b**) The transmission of the filters.

9.2.2 Filter transformations

Once the filter prototype is determined, one transforms it into either a lowpass, bandpass, highpass or bandstop filter [61]. To make a lowpass filter with the cutoff frequency ω_c, one sets the inductances and capacitances according to

$$L_k = g_k \frac{Z_0}{\omega_c}, \quad C_k = g_k \frac{Y_0}{\omega_c} \tag{9.4a}$$

where ω_c is the cutoff frequency, Z_0 the characteristic impedance of the filter and $Y_0 = Z_0^{-1}$ is the characteristic admittance.

To make a highpass filter, one changes the order of the inductances and capacitances such that the filter has series capacitors and shunt inductors, with the values

$$L_k = \frac{1}{g_k}\frac{Z_0}{\omega_c}, \quad C_k = \frac{1}{g_k}\frac{Y_0}{\omega_c}. \tag{9.4b}$$

To make a bandpass filter, one first determines the desired band ω_1 and ω_2. Then one calculates

$$\omega_{12} = \sqrt{\omega_1\omega_2}, \quad \alpha = \frac{\omega_{12}}{\omega_2 - \omega_1}. \tag{9.4c}$$

Finally, each series inductor is replaced by a series LC-oscillator with the inductance L_{k1} and the capacitance C_{k1}, and each shunt capacitor is replaced by a parallel LC-oscillator with the inductance L_{k2} and the capacitance C_{k2}, where the inductances and capacitances are given by

$$L_{k1} = \alpha g_k \frac{Z_0}{\omega_{12}}, \quad C_{k1} = \frac{1}{\alpha g_k}\frac{Y_0}{\omega_{12}}, \quad L_{k2} = \frac{1}{\alpha g_k}\frac{Z_0}{\omega_{12}}, \quad C_{k2} = \alpha g_k \frac{Y_0}{\omega_{12}}. \tag{9.4d}$$

To make a bandstop filter, one calculates the same α and ω_{12} as for the bandpass filter, see Equation (9.4c). Then each series inductor is replaced by a parallel LC-oscillator with the inductance L_{k1} and the capacitance C_{k1}, and each shunt capacitor is replaced by a series LC-oscillator with the inductance L_{k2} and the capacitance C_{k2}, where the inductances and capacitances are given by

$$L_{k1} = \frac{g_k}{\alpha}\frac{Z_0}{\omega_{12}}, \quad C_{k1} = \frac{\alpha}{g_k}\frac{Y_0}{\omega_{12}}, \quad L_{k2} = \frac{\alpha}{g_k}\frac{Z_0}{\omega_{12}}, \quad C_{k2} = \frac{g_k}{\alpha}\frac{Y_0}{\omega_{12}}. \tag{9.4e}$$

9.3 Impedance matching networks

As mentioned in Section 9.1, we need to solve the issue of impedance matching to prevent our TWPA prototype from being unstable. The aim is to amplify the frequency band $\omega_c/4$ to $2\omega_c/4$, which would be free of up-conversion using a pump at $3\omega_c/4$. Therefore we need to impedance match the full $\omega_c/4$ to $3\omega_c/4$ band.

The TWPA has the structure of the discrete transmission line, recall Chapter 2. The asymmetric discrete transmission line has the structure of an even

order low-pass filter with $n = 2N$ where $g_k = 2$ for all $k \in [1, 2N] \cap \mathbb{N}$, and N is the number of unitcells. The symmetric discrete transmission line has the structure of an odd order low-pass filter with $n = 2N + 1$ where $g_1 = g_{2N+1} = 1$ and $g_k = 2$ for all $k \in [2, 2N] \cap \mathbb{N}$.

We see in Figure 9.2a that appropriately designed filters in general have smaller g_k-values at the edges compared to the middle. Especially a Chebyshev filter with a small ε has approximately constant g_k-values in the middle of the filter, and only different and smaller g_k-values at the edges. Thus, taking inspiration from the Chebyshev filter using $n = 1000$ and $\varepsilon = 10^{-5}$, we determine the g_k-values of the impedance matching networks as

$$\begin{aligned} g_1 &= 0.44, \quad g_2 = 1.10, \quad g_3 = 1.48, \quad g_4 = 1.67, \\ g_5 &= 1.78, \quad g_6 = 1.84, \quad g_7 = 1.89. \end{aligned} \tag{9.5}$$

Then we build the TWPA by using 3, 5 or all 7 of these values, followed by the TWPA itself using $g_k = 2$ for both the inductances and the capacitances, followed by the same g_k-values as at the input, but in reverse order. The full structure of a TWPA with N unitcells and 3 additional impedance matching components would hence have the g_k-values

$$\begin{aligned} g_1 = 0.44, \quad g_2 = 1.10, \quad g_3 = 1.48, \quad g_j = 2.00, \\ g_{2N+3} = 1.48, \quad g_{2N+4} = 1.10, \quad g_{2N+5} = 0.44. \end{aligned} \tag{9.6}$$

for $j \in [4, 2N + 2] \cap \mathbb{N}$. When adding these additional impedance matching components the transmission, and in turn the impedance matching, quickly becomes better, see the transmission curves in Figure 9.3.

However, this is only the impedance without the pump and the gain. Once we start pumping the TWPA, there is an additional impedance mismatch arising. To understand this impedance mismatch, it is instructive to study the pumpistor model [42], [62]. When we pump the TWPA, the nonlinear inductive elements no longer act as regular linear inductors, but can be modelled as a linear inductor in parallel with a complex-valued impedance, the 'pumpistor', see Figure 9.4. It is the impedance of the pumpistor that explains the gain-induced impedance mismatch. The real part of the pumpistor impedance is negative, *i.e.* it behaves as a resistor with a negative resistance, which explains the gain.

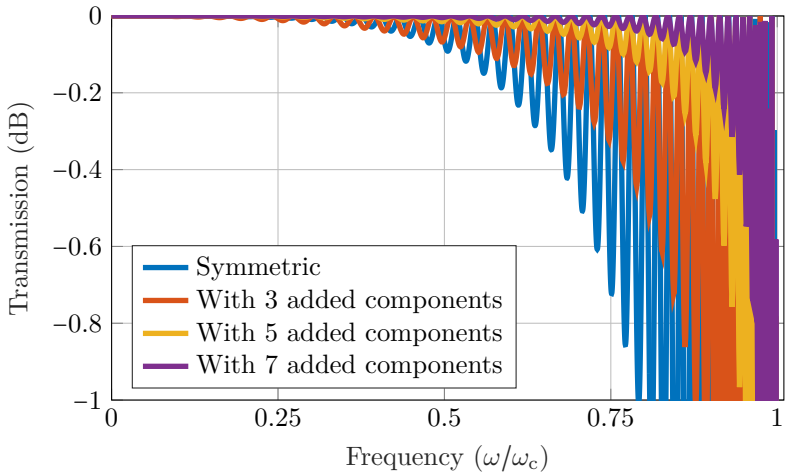

Figure 9.3: The transmission of the symmetric discrete transmission line with 49 unitcells and the discrete transmission line with different number of impedance matching components added.

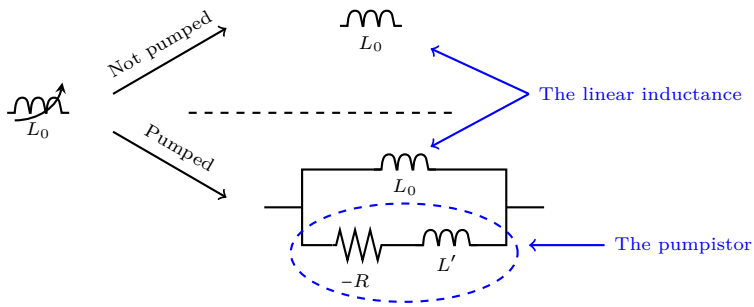

Figure 9.4: An illustration of the pumpistor model. When the nonlinear inductor is not pumped, it acts as a regular inductor. When the nonlinear inductor is pumped, it acts a the same inductor in parallel with a complex-valued impedance.

We can see in Figure 9.5 that the impedance mismatch arising from the pumpistor is symmetric around the origin in a Smith chart. This means that the impedance is highly frequency-dependent, and shows both a capacitive

and an inductive behaviour. Therefore we cannot simply solve this impedance mismatch by adjusting the inductances or capacitances of the TWPA. Nor can it be solved by adding more units to the impedance matching networks, since adding a component to adjust the impedance at one particular frequency will make it worse for a frequency at the opposite side of the Smith chart. To solve the issue of this impedance mismatch, we must implement more complicated techniques, which we discuss in Chapter 10 and paper [C].

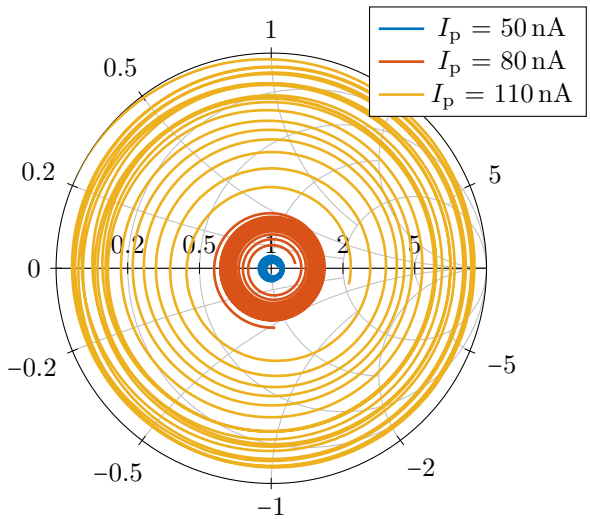

Figure 9.5: A Smith chart of the simulated reflection and impedance of a pumped TWPA, with 100 unitcells and a pump at 12 GHz, for signal frequencies in the range 4 to 8 GHz. For small pump currents, corresponding to a small gain, the TWPA is approximately impedance matched. For large pump currents, corresponding to a large gain, the impedance mismatch becomes large and the TWPA becomes unstable.

9.4 Frequency multiplexing

Another useful concept from microwave filter theory is frequency multiplexing. A frequency multiplexer [60] is an $n + 1$ port device that combines several filters into one, see Figure 9.6, $n \geq 2$ is the number of frequency bands. The multiplexer has one 'common' port and n ports associated with each filter.

Ideally, when a signal enters at the common port, it is fully transmitted to the port associated with its frequency. When a signal enters at one of the filter ports, it should ideally get transmitted to the common port only if it is within the appropriate frequency range of the filter, and otherwise get reflected.

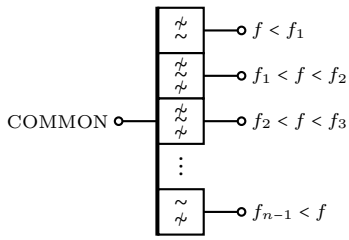

Figure 9.6: A generic frequency multiplexer with n frequency bands. A microwave with frequency f that enters at the common port is transmitted to the appropriate filter port associated with its frequency. A microwave with frequency f that enters at one of the filter ports is transmitted to the common port if it is within the band associated with the filter port, otherwise it is reflected.

If $n = 2$ we get what is called a diplexer. The diplexer has three ports: (1) the common port, (2) a low-pass port and (3) a high-pass port, see Figure 9.7.

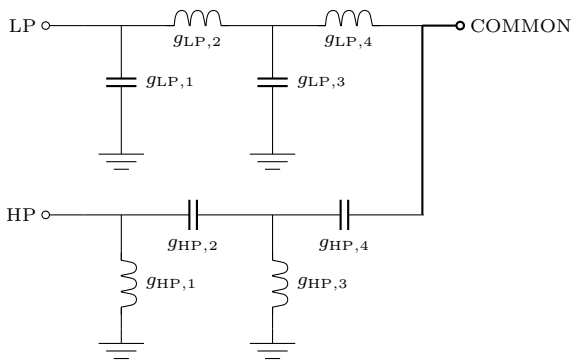

Figure 9.7: A generic 4th order diplexer schematic.

The scattering matrix of the ideal diplexer is

$$\boldsymbol{S} = \begin{bmatrix} 0 & F & 1-F \\ F & 1-F & 0 \\ 1-F & 0 & F \end{bmatrix} \tag{9.7}$$

where F is equal to 1 when $f < f_1$ and 0 when $f > f_1$. If $n = 3$ we instead get what is called a triplexer, which has a second transition frequency f_2 and a bandpass port.

A naive approach to make a frequency multiplexer is to simply connect several regular filters to each other in parallel. This is not a good approach, however, since the filters will interact with each other giving a very poor performance [60]. We need to modify the equations for the g_k coefficients to generate $g_{n+1} = \infty$, and then we connect the side associated with g_{n+1} to the common port[1]. For a Butterworth filter, one first computes

$$a_k = \sin\left(\pi \frac{2k-1}{2n}\right), \quad c_k = \cos^2\left(\frac{\pi k}{2n}\right). \tag{9.8}$$

Then the filter coefficients are

$$g_1 = a_1, \quad g_{n+1} = \infty, \quad g_k = \frac{a_k a_{k-1}}{c_{k-1} g_{k-1}}. \tag{9.9}$$

For a Chebyshev filter with ripple level ε in dB, one first computes the same β and γ as in Equation (9.3a), but now also

$$a_k = \sin\left(\pi \frac{2k-1}{2n}\right), \quad d_k = \left[\gamma^2 + \sin^2\left(\frac{\pi k}{2n}\right)\right] \cos^2\left(\frac{\pi k}{2n}\right). \tag{9.10}$$

Then the filter coefficients are

$$g_1 = \frac{a_1}{\gamma}, \quad g_{n+1} = \infty, \quad g_k = \frac{a_k a_{k-1}}{d_{k-1} g_{k-1}}. \tag{9.11}$$

9.5 Summary

In this chapter we briefly touched on the necessity of impedance matching for an amplifier, we summarised some main points from microwave filter theory,

[1] The n in g_{n+1} refers to the filter order n, and not to the number of frequency bands.

and showed two important applications.

Firstly, we can take inspiration from microwave filters to design impedance matching networks for our TWPAs. By adding a few additional cells to the TWPA input and the TWPA output, with smaller values of the inductances and capacitances than those of the TWPA itself, we can make the TWPA impedance matched both in the frequency band $0.25\omega_c$ to $0.5\omega_c$ and at the pump frequency $0.75\omega_c$ *simultaneously*. The exact number of required additional cells depends on the tolerance of the impedance mismatch, but in general only a few, approximately 5, additional cells are needed.

Secondly, we can use microwave filter theory to build frequency multiplexers. These are components that we will use a lot in Chapter 10.

CHAPTER 10

Peripheral circuits for ideal performance

The TWPA prototype we have outlined in the previous chapters uses magnetically flux-biased SNAILs as inductive elements, a small cutoff frequency to prevent up-conversion, resonant phase matching to get phase matching and impedance matching networks to get impedance matching. This makes an amplifier with several good properties: wideband amplification, ideally quantum-limited noise performance and a high gain per unitcell which limits the impact of signal loss.

However, it does not fulfill all the desired properties of the ideal low-noise amplifier, as outlined in Chapter 1. It has gain ripples, due to the impedance mismatch that occurs when there is gain, as mentioned in Chapter 9. But more importantly, it has leakage of all unwanted modes: reflections of the pump, the signal and the idler, and it transmits more than one mode per signal. Furthermore, it does not isolate either.

In this chapter we will look at different peripheral circuitry that can be added to the TWPA that can, in theory, make it the ideal low-noise amplifier. We also discuss peripheral circuits for ideal performance in paper [C].

10.1 Frequency-multiplexed TWPAs

In this section we will look at how frequency multiplexers can be used with TWPAs, recall Section 9.4. First we will look at how the pump leakage can be removed using diplexers. Then we will look at a technique we call *halfband idler filtering* can be achieved using triplexers.

10.1.1 The diplexed TWPA

As outlined in Section 9.4, a diplexer separates frequencies below a certain transition frequency f_1 from frequencies above it. For three-wave mixing, the pump frequency is typically well detuned from the signal. It is thus suitable to use diplexers before and after the TWPA to remove the pump leakage, see Figure 10.1. Since no diplexer is ideal, there will be some leakage from the lowpass to the highpass port of the diplexer, and thus some leakage of the pump. The leakage between the ports is typically the largest when we are close to the diplexer transition frequency. For that reason, we put the diplexer transition frequency as close as possible to the signal band.

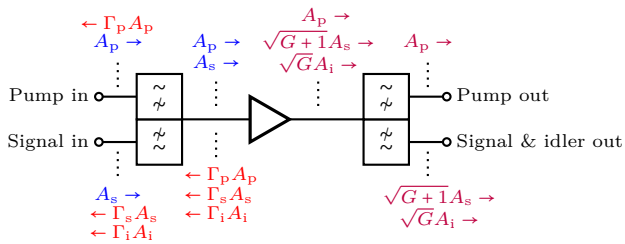

Figure 10.1: The schematic of a diplexed 3WM TWPA: The incoming waves (blue), the reflected waves (red) and the transmitted waves (purple).

For four-wave mixing the pump is in the middle of the gain band. Therefore one cannot use the regular lowpass-highpass-diplexer. However, if one constructs a bandpass-bandstop-diplexer, diplexers can be used for four-wave mixing as well. This was not discussed in Section 9.4, but one can use the filter equations, together with the bandpass and bandstop transformations outlined in Section 9.2.2. The hard part for four-wave mixing is to build a diplexer with high enough attenuation of the pump, without losing too much of the gain band.

10.1.2 The triplexed TWPA

As outlined in Section 9.4, a triplexer is similar to a diplexer, but it has three frequency bands, and thus one more port than the diplexer. This can be used to not only separate the signal and idler from the pump, but also to separate the signal and idler from each other, which is useful for creating isolation as discussed in Section 1.6.3.

If we add triplexers to each side of a TWPA, we get a 6-port device, see Figure 10.2. Let us assume that the first triplexer transition frequency matches the middle of the gain band, *i.e.* that $f_1 = f_p/2$, and that the second one is right above the gain band, *e.g.* $f_2 = 3f_p/4$. If we terminate the bandpass input port, the lowpass output port and the highpass output port, and read out at the idler frequency, we get an amplifier that is *mostly* free of leakage while it also isolates, see Figure 10.3a. This works since the idler contains the same information as the signal. The reflected and transmitted pump is filtered out at the highpass ports, the reflected idler is terminated at the bandpass input port, and the transmitted signal is terminated at the lowpass output port. Furthermore, if any unwanted wave enters at the bandpass output port, it gets terminated at the bandpass input port.

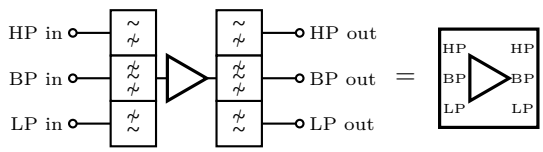

Figure 10.2: The schematic of a triplexed TWPA and its symbol.

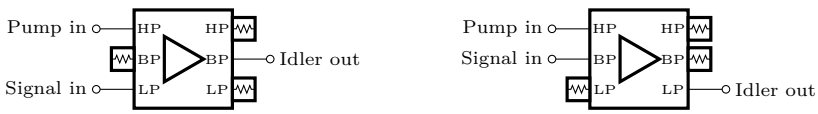

Figure 10.3: Setups for halfband idler filtering using the triplexed TWPA. (**a**) The signal is in the lower half of the gain band and the outputted idler is in the upper half of the gain band. (**b**) The signal is in the upper half of the gain band and the outputted idler is in the lower half of the gain band.

To be able to use the upper half of the gain band, we simply swap the connections between the lowpass and the bandpass ports, compare Figures 10.3a and 10.3b.

The triplexed TWPA has some clear advantages. However, we are still not free of signal reflection and gain ripples, and we have to sacrifice half of the gain band. It is hence not the ideal low-noise amplifier.

10.2 The balanced TWPA

Another important setup is the balanced amplifier setup [63]. A necessary building block for a balanced amplifier is the 90° hybrid coupler. The 90° hybrid coupler is a 4 port device which splits an input into two outputs of equal amplitude, but with a 90° phase shift, see Figure 10.4.

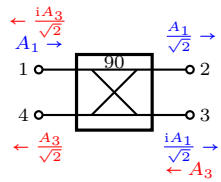

Figure 10.4: A 90° hybrid coupler. An input at port 1 (blue) exits at port 2 and port 3. An input at port 3 (red) exits at port 1 and port 4.

The scattering matrix of the hybrid coupler is hence

$$\boldsymbol{S} = \frac{1}{\sqrt{2}} \begin{bmatrix} 0 & 1 & \mathrm{i} & 0 \\ 1 & 0 & 0 & \mathrm{i} \\ \mathrm{i} & 0 & 0 & 1 \\ 0 & \mathrm{i} & 1 & 0 \end{bmatrix}. \tag{10.1}$$

In a balanced amplifier setup, we use two identical amplifiers connected to each other via two 90° hybrid couplers, where one port of each hybrid coupler is terminated with a matched load, see Figure 10.5. Since the amplifiers are identical, they have the same transmission coefficient T and the same reflection coefficient Γ. In reality a hybrid coupler may have some amplitude and phase imbalances, meaning that the outputs do not have the same amplitudes or exactly 90° phase difference, and the amplifiers may not be completely

identical. But for now, let us assume ideal components, *i.e.* that the hybrid couplers have zero amplitude and phase imbalance in the full band and that the amplifiers are fully identical. Then the reflections towards the input port will destructively interfere, while the reflections towards the left load in Figure 10.5 constructively interfere,

$$\frac{1}{\sqrt{2}} \cdot \frac{\Gamma A_0}{\sqrt{2}} + \frac{\mathrm{i}}{\sqrt{2}} \cdot \frac{\mathrm{i}\Gamma A_0}{\sqrt{2}} = \frac{\Gamma A_0}{2} - \frac{\Gamma A_0}{2} = 0, \tag{10.2a}$$

$$\frac{\mathrm{i}}{\sqrt{2}} \cdot \frac{\Gamma A_0}{\sqrt{2}} + \frac{1}{\sqrt{2}} \cdot \frac{\mathrm{i}\Gamma A_0}{\sqrt{2}} = \frac{\mathrm{i}\Gamma A_0}{2} + \frac{\mathrm{i}\Gamma A_0}{2} = \mathrm{i}\Gamma A_0. \tag{10.2b}$$

Simultaneously, the transmitted modes will constructively interfere towards the output port, while they destructively interfere towards the right load,

$$\frac{\mathrm{i}}{\sqrt{2}} \cdot \frac{T A_0}{\sqrt{2}} + \frac{1}{\sqrt{2}} \cdot \frac{\mathrm{i}T A_0}{\sqrt{2}} = \frac{\mathrm{i}T A_0}{2} + \frac{\mathrm{i}T A_0}{2} = \mathrm{i}T A_0, \tag{10.2c}$$

$$\frac{1}{\sqrt{2}} \cdot \frac{T A_0}{\sqrt{2}} + \frac{\mathrm{i}}{\sqrt{2}} \cdot \frac{\mathrm{i}T A_0}{\sqrt{2}} = \frac{T A_0}{2} - \frac{T A_0}{2} = 0. \tag{10.2d}$$

Therefore, the balanced amplifier completely eliminates reflections without losing any gain.

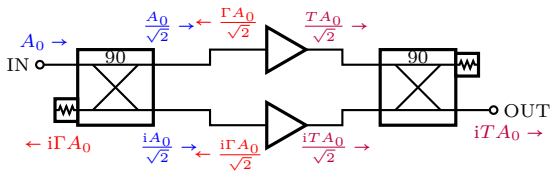

Figure 10.5: The schematic of a balanced amplifier: any incoming wave (blue) gets split in two, the reflections (red) constructively interfere towards the left load, while the transmitted waves (purple) constructively interfere towards the output.

If we now add diplexers to both couple the pump and to filter out any leakage from nonideal couplers, we get what we call the diplexed & balanced TWPA, see Figure 10.6. One might think we are now free of leakage. However, the idler phase is given by $\varphi_\mathrm{i} = \varphi_\mathrm{p} - \varphi_\mathrm{s}$. Therefore, the phase of the idler in the upper arm is $0° - 0° = 0°$ and the phase in the lower arm is also $90° - 90° = 0°$, or in other words: the idlers in the two arms are in phase with each other.

Calculating the reflected idler travelling towards the input we get

$$\frac{1}{\sqrt{2}} \cdot \frac{\Gamma_\mathrm{i} A_\mathrm{i}}{\sqrt{2}} + \frac{\mathrm{i}}{\sqrt{2}} \cdot \frac{\Gamma_\mathrm{i} A_\mathrm{i}}{\sqrt{2}} = \frac{\Gamma_\mathrm{i} A_\mathrm{i}}{2} + \frac{\mathrm{i}\Gamma_\mathrm{i} A_0}{2} = \frac{1+\mathrm{i}}{2}\Gamma_\mathrm{i} A_\mathrm{i}, \tag{10.3}$$

or in other words: half of the reflected idler leaks back towards the input. The same applies for the transmitted idler. In summary, the diplexed & balanced TWPA solves the issues of pump leakage and signal reflection, but not the issues of idler leakage or isolation.

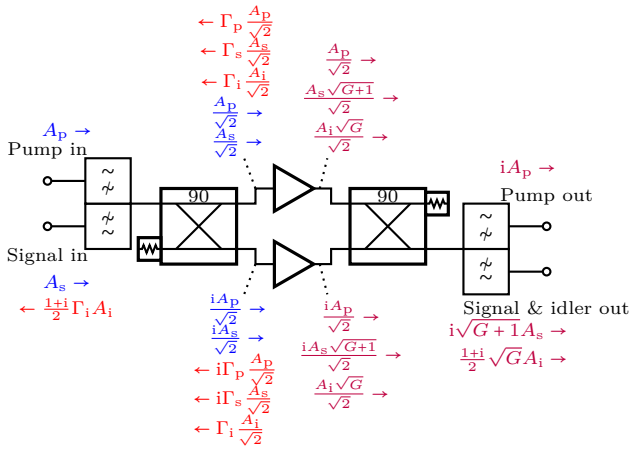

Figure 10.6: The schematic of a balanced TWPA with diplexers: the incoming waves (blue), the reflected waves (red) and the transmitted (purple).

10.3 The single layered WIF-TWPA

A slightly more complicated setup than the diplexed & balanced TWPA is the single layered wideband idler filtering (WIF) TWPA, where we instead add the hybrid couplers to two diplexed TWPAs, see Figure 10.7. Now we have two pumps but also two degrees of freedom: the phases of the two pumps.

Without loss of generality we can assume that the signal phase and the phase of the first pump are all zero, and that the phase difference between the pumps is in the phase of the second pump, $\Delta\theta_\mathrm{p}$. By studying the reflected and the transmitted idler, we get two equations for the idler leakage. To eliminate

the idler leakage, we must fulfill

$$\text{no reflected idler:} \qquad 1 + e^{i\Delta\theta_p} = 0, \tag{10.4a}$$

$$\text{no transmitted idler:} \qquad i + e^{i(\Delta\theta_p - \pi/2)} = 0. \tag{10.4b}$$

Unfortunately, these two equations cannot be fulfilled simultaneously. The first one yields the solution $\Delta\theta_p = \pi$, while the second one yields $\Delta\theta_p = 0$. We thus conclude that the single layered WIF-TWPA can only filter out one of the idler leakages, but not both simultaneously.

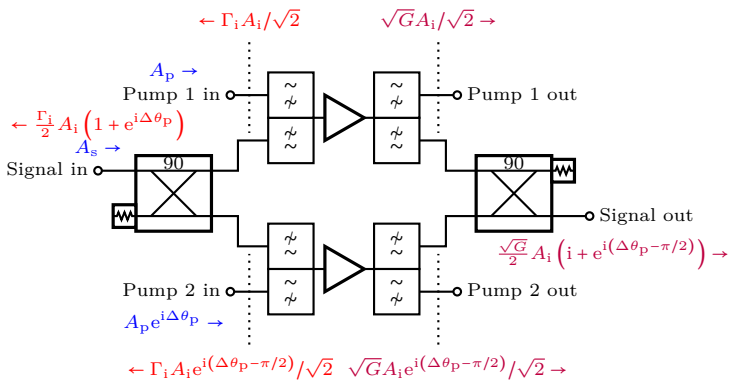

Figure 10.7: The single layered wideband idler filtering TWPA: The incoming signal and pump (blue), the reflected idler (red) and the transmitted idler (purple).

10.4 The double layered WIF-TWPA

To be able to fully filter out both the reflected and the transmitted idler, we turn to the double layered WIF-TWPA. In the double layered WIF-TWPA, we connect two single layered WIF-TWPAs in parallel to each other via yet another layer of couplers, see Figure 10.8. Now the expressions for the idlers become a bit complicated, but one can show that if one uses the pump phases $0, \pi, 0, \pi$, the reflected idler is terminated at node 2 in Figure 10.8, while the transmitted idler is separated from the signal and exits at 'idler out'.

If one now terminates the 'idler out' port, we hence have an amplifier fully

free of leakage. We call this setup the 'transhybrid', as the signal path resembles that of a transisomer of a molecule. However, this setup does not isolate. If we instead terminate the 'signal out', and read out the idler at the idler port, any unwanted mode entering at the output port will become terminated at node 1. We have thus both eliminated the leakage and we get isolation. We call this setup the 'cishybrid', as the signal path resembles that of a cisisomer of a molecule.

We study the limiting factors of the isolation, how to generate the correct pumps, effects of nonidealities, *etc*, in paper [C].

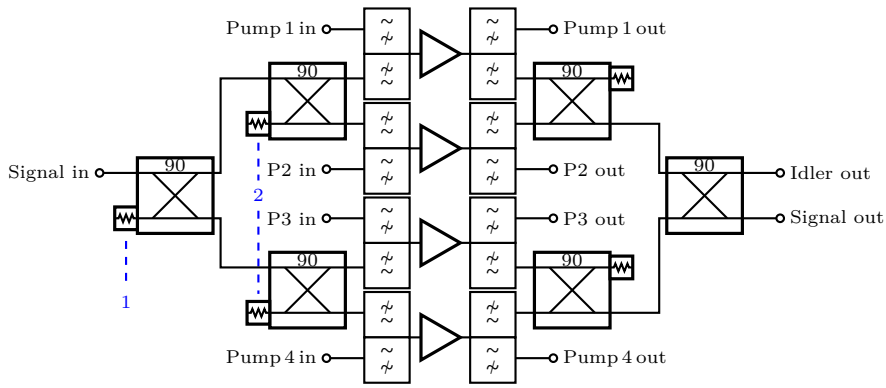

Figure 10.8: The double layered wideband idler filtering TWPA. 'P2' and 'P3' are abbreviations for 'pump 2' and 'pump 3'.

10.5 Summary

In this chapter we have looked at different peripheral circuits, see Table 10.1, and how to achieve what we call 'ideal performance', especially how to get rid of leakage and get isolation. Adding diplexers to a TWPA can solve the issue of pump leakage. Adding triplexers to a TWPA can solve the issue of pump leakage, idler leakage and get isolation, but not that of signal reflection. Making a diplexed & balanced TWPA solves both the issue of pump leakage and signal leakage, but not that of idler leakage. The single layered WIF-TWPA can achieve that of the diplexed & balanced TWPA, and also eliminate *either* the reflected idler *or* the transmitted one, but not both. Only the double layered WIF-TWPA can solve all issues simultaneously.

Table 10.1: A summary of the TWPA performance using the different peripheral circuits. The presented isolation numbers are for the approximately lowest simulated isolation when our TWPA model delivers at least 20 dB gain in the full 4-8 GHz band. For the triplexed TWPA, the isolation depends on the triplexer.

	Signal reflection	Pump leakage	Idler leakage	Isolation	Readout frequency
No peripheral circuits	Yes	Yes	Yes	-	f_s
Balanced	No	Yes	Yes	-	f_s
Diplexed	Yes	No	Yes	-	f_s
Triplexed	Yes	No	No	Yes	f_i
Diplexed & balanced	No	No	Yes	-	f_s
Single layered WIF ($\Delta\phi_p = 0$)	No	No	Backwards	10 dB	f_i
Single layered WIF ($\Delta\phi_p = \pi$)	No	No	Forwards	-	f_s
Double layered WIF (transhybrid)	No	No	No	-	f_s
Double layered WIF (cishybrid)	No	No	No	10 dB	f_i
Two cascaded cishybrids	No	No	No	30 dB	f_s
The ideal case	No	No	No	∞	f_s

CHAPTER 11

Simulations, fabrication and experiments

In this chapter we will outline the last part of this work: How we simulate our devices, how we fabricate them and how we measure them.

11.1 Harmonic balance simulations

Previously, we have investigated how the TWPA works with the help of the wave equations, recall Equations (3.6) and (3.12), the propagation equations, recall Equation (3.24) and the discrete matrix equation, recall Equation (6.22). However, to reach these equations, many assumptions and approximations were made. For example, we neglected higher order mixing when going from Equation (3.4) to Equation (3.6). We assumed continuous waves and we neglected higher order derivatives in Section 3.2. We neglected non-resonant contributions when dropping the time dependence in Sections 3.3.2 and 6.2.2, *etc.*

Thus, before concluding too much from the solutions found in the previous chapters, we also took a numerical approach to simulate the full system and compare the results with the analytically found solutions. We built nonlinear black box models for the Josephson junction and elements based on it,

e.g. the SQUID and the SNAIL, using "Symbolically Defined Devices" (SDD) in Keysight PathWave Advanced Design System (ADS). These models were used in simulation of the TWPAs in time domain, S-parameters and harmonic balance analysis. The harmonic balance method captures the nonlinear large signal effects related to wave propagation in the TWPA and does not need incurring any approximation like Taylor expansion of the Josephson junction or the SNAIL nonlinearity. It faithfully recreates what the propagation equations and experiments predict about the effect of pump harmonics on the gain of the TWPA, but it also captures other effects, *e.g.* signal reflection and gain ripples. Details about the nonlinear modelling, simulation of TWPAs, harmonic balance analysis, *etc*, are presented in paper [D].

11.2 Nanofabrication

Once we have decided on a design, we need to fabricate it. This is done at the Nanofabrication Laboratory (NFL) at Chalmers University of Technology. To amplify signals in the 4 to 8 GHz band, we design the unitcell parameters to have the cutoff frequency of the TWPA at 16 GHz. This requires the inductance and the capacitance of each unitcell to be on the order of ~ 1 nH and ~ 400 fF, respectively. Simultaneously, we want each unitcell to be very small, so that the full footprint of the TWPA does not become too large.

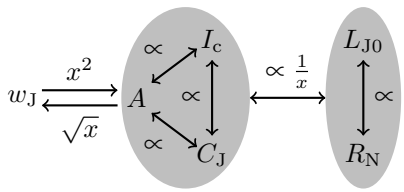

Figure 11.1: The relations between the junction width w_J (assuming square junctions), the junction area A, the critical current I_c, the intrinsic capacitance C_J, the normal resistance R_N and the junction zero-bias inductance L_J0. The expressions with x explain the mathematical relations when following certain arrows.

To get large inductances with a small footprint, we use small Josephson junctions, since the junction inductance scales with the reciprocal of the junction area, see Figure 11.1, or arrays of inductive elements connected in series,

recall Section 4.5. The junctions are fabricated using shadow evaporation and the Manhattan technique to ensure that the resist thickness has a small impact on the junction size [64].

To make large capacitances with a small footprint, we use the parallel-plate geometry capacitors with a very thin aluminium nitride film of 40 nm as the dielectric, see Figure 11.2. Aluminium nitride has a relative permittivity of $\varepsilon_r \sim 7$ [65]. Using the capacitance formula

$$C = \varepsilon_r \varepsilon_0 \frac{lw}{d} \quad \Longrightarrow \quad l = \frac{Cd}{\varepsilon_r \varepsilon_0 w}, \tag{11.1}$$

with the capacitance $C = 400\,\text{fF}$, the thickness $d = 40\,\text{nm}$ and the width $w = 5\,\mu\text{m}$, we get that the length l of the capacitor does not need to exceed $52\,\mu\text{m}$.

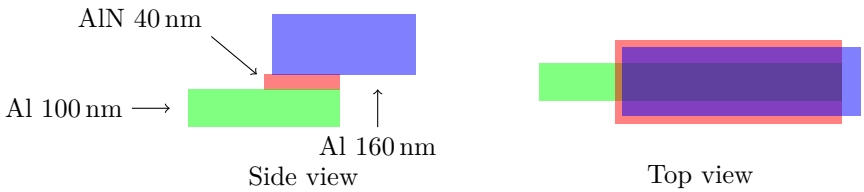

Figure 11.2: Our parallel plate capacitors from the side and from above. The capacitor plates are made with aluminium, while the dielectric is made of a thin film of aluminium nitride.

11.3 Experiments

Experiments on our fabricated devices were performed in our dilution refrigerators from BlueFors. We have used two different setups, depending on whether the TWPA is placed in the old sample box or the new one.

In the first setup, see Figure 11.3, we put our TWPAs on a cryogenic switch in parallel with a regular $50\,\Omega$ coaxial cable to use as a reference. We place a large coil next to the TWPAs to provide the magnetic flux-bias. We also have some *device under test* (DUT) which typically is a qubit chip. We do not want the pump to interact with the DUT, therefore we have a directional coupler in the fridge, so that only the signal inserted at 'Signal in 1' interacts with the DUT.

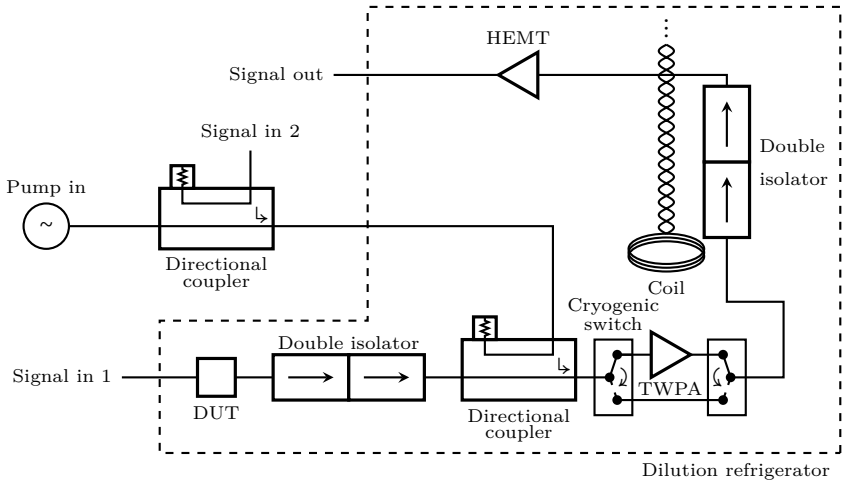

Figure 11.3: The first experimental setup. The magnetic flux-bias is applied via a large coil. The pump is coupled to the signal via a directional coupler.

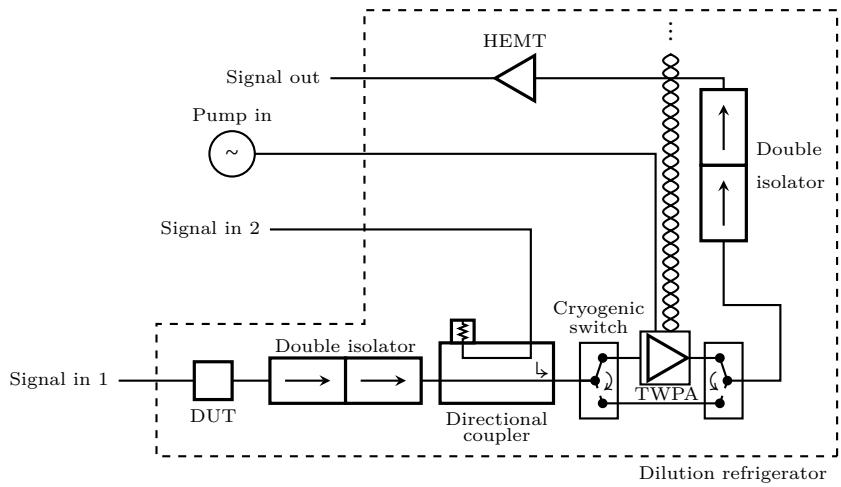

Figure 11.4: The second experimental setup using the new box. The magnetic flux-bias is applied via an integrated coil inside the box. The pump is coupled to the signal via integrated diplexers.

Sometimes we wish that the signal does not interact with the DUT either, therefore we also have a directional coupler at room temperature and then we insert the signal at 'Signal in 2'.

The second setup, see Figure 11.4, is very similar to the original setup, but with two key differences. Firstly, the box has a coil integrated into it, with its own DC-connectors. Thus, the DC-connectors now go directly to the box instead of the large coil. When using several TWPAs in one cooldown, we connect the boxes in series. Secondly, it has diplexers integrated. The pump input cable is thus connected directly to the box. The pump output from the box is terminated with a 50 Ω cryogenic load.

To measure the gain profile, we connect a vector network analyser (VNA) to 'Signal 2 in' and 'Signal out'. Then we measure S_{21} while we sweep different values of flux bias, pump power and pump frequency. By comparing the transmission of the TWPA with the pump on versus with the pump off, we get what we call the *parametric gain*. This is the gain that the theory we have done may predict. However, when we do theory we assume zero losses, but in reality the TWPA has losses. A more important metric is thus the *effective* gain, which is the gain we get when the losses are included. To measure the effective gain, we measure the transmission of the pumped TWPA and compare it to the transmission of the cable.

To measure the signal-to-noise ratio (SNR), we instead use a signal generator and a spectrum analyser. We insert a signal with the signal generator at some frequency f_s, and sweep frequencies within a 1 MHz range around f_s. The SNR is determined by comparing the signal power to that of the noise floor, see Figure 11.5. The signal-to-noise ratio improvement (ΔSNR) is determined by comparing the SNR of the TWPA with the SNR of the reference.

The gain and the ΔSNR for one of our devices in presented in Figure 11.6. This is a SNAIL-based device with 200 unitcells, resonant phase matching and a low cutoff. There were several fabrication issues with this device. Firstly, there was an impedance matching problem. Secondly, there was a flux-biasing issue. Thirdly, as a result of the previous two points, all frequencies were shifted down, so instead of having a pump with $f_p = 12$ GHz, the sweet spot ended up at $f_p = 11.27$ GHz. Our HEMT bandwidth is 4-12 GHz, therefore we cannot measure the gain below 4 GHz properly. Yet, the device has a good performance, with an average effective gain around 15 dB over a 3 GHz bandwidth, and an average effective ΔSNR of 10 dB. More data and information

about the device in Figure 11.6 is presented in paper [E].

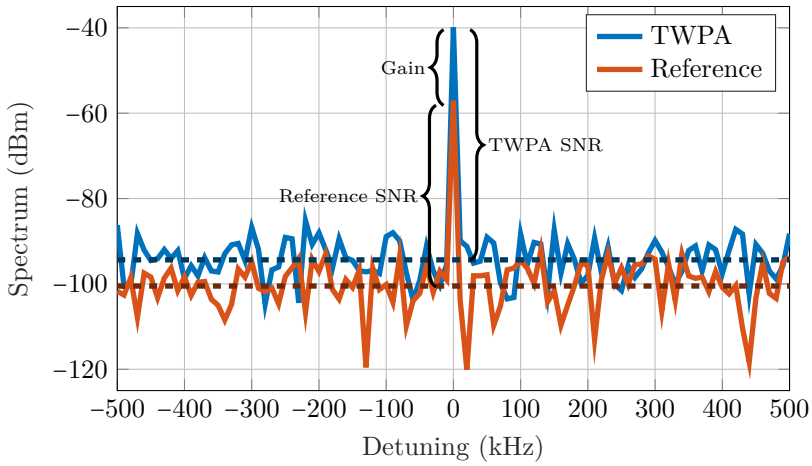

Figure 11.5: The spectrum in 1 MHz around a signal for a pumped TWPA and the reference. The noise floor (dashed) is determined as the average value of the points at non-zero detuning. The SNR is determined as the difference between the signal peak and the noise floor.

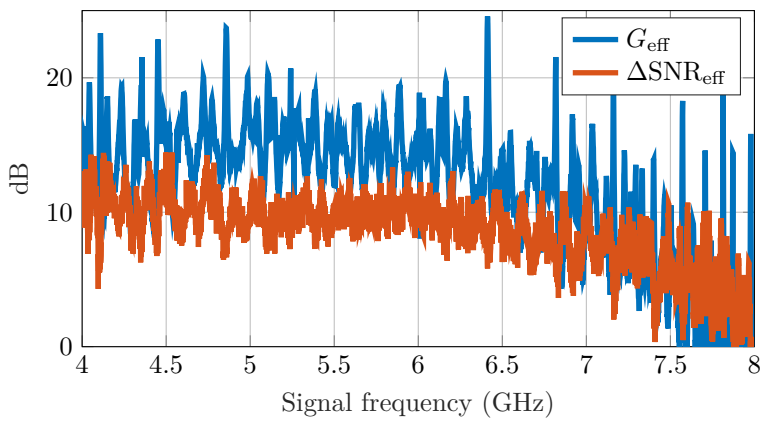

Figure 11.6: The effective gain and the effective signal-to-noise ratio improvement (ΔSNR) for one of our devices. The gain is measured with a VNA and the ΔSNR is measured with a spectrum analyser.

CHAPTER 12

Conclusions and future work

In this chapter we revisit all the main conclusions from this work. Firstly we will go through the conclusions about how to make a travelling-wave parametric amplifier based on three-wave mixing. Secondly we will comment on the difference when designing a travelling-wave parametric amplifier based on four-wave mixing. Then we will go through how we can make the ideal low-noise amplifier by adding peripheral circuitry to several identical TWPAs. Finally we will summarise all of this work and briefly discuss future work to be done.

12.1 Building a three-wave mixing travelling-wave parametric amplifier

To build a travelling-wave parametric amplifier based on three-wave mixing, several criteria need to be fulfilled, see Figure 12.1. We need impedance matching to the amplifier's environment to prevent the amplifier from becoming unstable. We need phase matching for the down-conversion process to get any gain. But we also need phase mismatching for the up-conversion

processes, otherwise they will deteriorate the gain, as shown in Chapter 5 and paper [A].

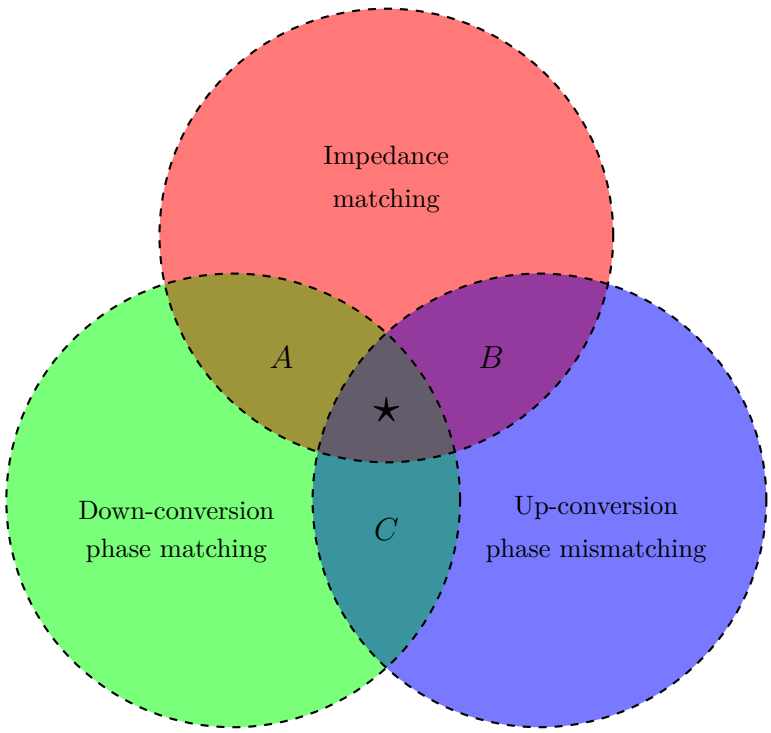

Figure 12.1: A Venn diagram over the different requirements and regions for a travelling-wave parametric amplifier.

In Figure 12.1 we see several different regions: A, B, C and $\star$. The only region with the possibility for a stable exponential gain is the $\star$ region. However, when designing a TWPA, one typically ends up in one of the other regions.

When using small frequencies in the standard dispersion, *i.e.* a large cut-off frequency in comparison to the signal and the pump, the TWPA is approximately impedance matched for all relevant frequencies and the phase mismatches become negligible. In other words, we get impedance matching and down-conversion phase matching. However, we also get phase matching for the up-conversion processes, and we thus end up in region A. By using

periodic modulation, we can create a phase mismatch for the up-conversion processes, and thus reach the $\star$-region. We use this approach in paper [B].

When using large frequencies in the standard dispersion, *i.e.* a small cut-off frequency in comparison to the signal and the pump, the TWPA is no longer impedance matched and the phase mismatches are large. By using resonant phase matching, we get down-conversion phase matching and end up in region C. We discuss this in paper [A]. Then, by adding the impedance matching networks outlined in Chapter 9, we can also ensure impedance matching, and thus reach the $\star$-region. We discuss in paper [C], based on the simulation models from paper [D], and experimentally demonstrate the device in paper [E].

In conclusion, to build a travelling-wave parametric amplifier based on three-wave mixing, one has to either: (1) work with small frequencies and dispersively engineer a phase mismatch for the up-conversion processes, or (2) work with large frequencies and dispersively engineer phase matching for the down-conversion process. In the latter, gain per unitcell becomes larger, but one also has to add impedance matching networks to get impedance matching.

12.2 Building a four-wave mixing travelling-wave parametric amplifier

When designing a travelling-wave parametric amplifier based on four-wave mixing, Figure 12.1 and its regions are still valid, but the premise is different: By using small frequencies with the standard dispersion, one has impedance matching and, due to Kerr effect, a phase mismatch for both the down-conversion process as well as the up-conversion processes. We are thus in region B. The only problem to solve is hence phase matching for the down-conversion. This can be done either with reversed Kerr, as described in Section 7.4, or with dispersion engineering, *e.g.* resonant phase matching as described in Section 8.2.

12.3 Peripheral circuits for ideal performance

The travelling-wave parametric amplifier fulfills many of the criteria of the ideal low-noise amplifier. It has a potential for quantum-limited amplification in a wide band, potentially with a large saturation power and low signal distortion.

However, it has leakage of more modes than just the amplified signal, both in the forward and the backward directions, and it does not isolate. The leakage can interfere with the signal sources as well as what may come after the amplifier, and the lack of isolation lets the noise entering at the output reach the signal sources as well.

We showed in Chapter 10, and in paper [C], that all of these issues can be solved by adding peripheral circuitry to four identical TWPAs. The peripheral circuitry is based on a combination of superconducting diplexers and hybrid couplers. Then the interference between the TWPAs ensures that all reflections constructively interfere towards cryogenic loads, while the signal gets separated from the idler. One can either read out at the idler frequency or cascade two of these amplifier setups, which then retrieves the signal frequency and improves the isolation.

12.4 Summary

In Chapter 1 we outlined properties of the ideal low-noise amplifier. It should have quantum-limited noise performance and a high enough gain to suppress the noise of the subsequent amplifiers. Its transfer function should be insensitive to the signal properties: its frequency, amplitude, phase and shape (signal envelope). It should have no leakage of any other mode than the desired one, it should provide isolation and be physically small. Throughout this work, we have addressed how to achieve most of these properties.

By building a travelling-wave parametric amplifier, as outlined in both Sections 12.1 and 12.2, we get a wideband phase-insensitive quantum-limited amplifier with a high gain. In other words, we get a high-gain amplifier with quantum-limited noise performance that is relatively insensitive to the signal frequency and signal phase. By using a TWPA design using three-wave mixing and small cutoff frequency, the TWPA is also physically very small. By adding peripheral circuitry as discussed in Section 12.3, we can additionally

solve the issues of leakage and isolation.

What remains to be studied and solved is insensitivity to signal amplitude, *i.e.* how to get a large saturation power without getting a large pump leakage, and signal shape, *i.e.* the transient response. We will discuss this briefly in Section 12.5.

12.5 Future work

In this section we will discuss what can be done to build on this work.

Firstly, we suggest to try building the proposed setup in Section 10.4, the double layered WIF-TWPA, since it is just a theoretical proposal at the moment. While the setup could in theory create the ideal low-noise amplifier, there are many practical things that could go wrong, such as having nonidealities in the peripheral circuitry or nonidentical TWPAs. Therefore it is a big project on its own to realise this circuit.

Secondly, once the double layered WIF-TWPA has been realised, we propose to try building two cascaded double layered WIF-TWPAs. This would not only retrieve the original signal frequency while also having isolation, but by using different TWPAs in the second WIF-TWPA setup, we could also solve the issue of insensitivity to signal amplitude, *i.e.* we could increase the saturation power. We discussed how to increase the saturation power briefly in Sections 4.4 and 4.5, by using either kinetic inductors or arrays of inductive elements, but there is a tradeoff. These inductive elements have weaker nonlinearities, so the pump power would need to be increased to compensate for the weaker nonlinearity. When the pump power is increased, so is the pump leakage. By using high saturation power TWPAs in the second WIF-TWPA setup, one can get both a high saturation power and a small pump leakage *simultaneously*. The pump leakage from the first WIF-TWPA setup would be small since it uses Josephson junctions, and thus a small pump, and the pump leakage from the second WIF-TWPA setup would be small since it gets filtered by the first WIF-TWPA. Simultaneously the saturation power would be high.

Thirdly, we propose to study the sensitivity to the signal shape, *i.e.* how the different TWPA designs may distort pulse shapes. The distortion could be done by the TWPA itself, but also by the impedance matching networks. To study these effects, simulations of transients for different kinds of pulses

and TWPA designs would be advantageous.

Another project could be an investigation into pulsed pumping. When the pump is on, there is both pump leakage and heating of the cryostat. A way to reduce this problem could be to only pump when there is a signal to amplify, and keep the pump off at all other times. However, to implement this, it would be important to characterise the time it takes from that the pump is turned on until the gain has stabilised. It could also be worth investigating what effect different shapes of the pump pulses has.

Another project that could be done would be making the TWPAs smaller. The biggest components in the TWPAs today are the capacitors, measuring around $\sim 500\,\mu m^2$, compared to the SNAILs measuring around $\sim 100\,\mu m^2$. In theory the capacitors can easily be made smaller simply by making a thinner dielectric. However, when the dielectric gets thinner, variations in thickness have a bigger impact. An interesting study would hence be to see how thin the dielectric can be made, without facing problems from the variations in dielectric thickness.

References

[1] H. Renberg Nilsson, A. Fadavi Roudsari, D. Shiri, P. Delsing, and V. Shumeiko, "High-gain traveling-wave parametric amplifier based on three-wave mixing," *Physical Review Applied*, vol. 19, 044 056, 2023.

[2] A. Fadavi Roudsari, D. Shiri, H. Renberg Nilsson, G. Tancredi, A. Osman, I.-M. Svensson, M. Kudra, M. Rommel, J. Bylander, V. Shumeiko, and P. Delsing, "Three-wave mixing traveling-wave parametric amplifier with periodic variation of the circuit parameters," *Applied Physics Letters*, vol. 122, 052 601, 2023.

[3] H. Renberg Nilsson, D. Shiri, R. Rehammar, A. Fadavi Roudsari, and P. Delsing, "Peripheral circuits for ideal performance of a traveling-wave parametric amplifier," *Physical Review Applied*, vol. 21, 064 062, 2024.

[4] D. Shiri, H. Renberg Nilsson, P. Telluri, A. F. Roudsari, V. Shumeiko, C. Fager, and P. Delsing, *Modeling and harmonic balance analysis of parametric amplifiers for qubit read-out*, 2023. arXiv: `2306.05177 [quant-ph]`.

[5] H. Renberg Nilsson, L. Chen, G. Tancredi, R. Rehammar, D. Shiri, F. Nilsson, A. Osman, V. Shumeiko, and P. Delsing, *A small footprint travelling-wave parametric amplifier with a high signal-to-noise ratio improvement in a wide band*, 2024. arXiv: `2408.16366 [physics.app-ph]`.

[6] C. M. Caves, "Quantum limits on noise in linear amplifiers," *Physical Review D*, vol. 26, 1817, 1982.

[7] T. Yamamoto, K. Inomata, M. Watanabe, K. Matsuba, T. Miyazaki, W. D. Oliver, Y. Nakamura, and J. S. Tsai, "Flux-driven Josephson parametric amplifier," *Applied Physics Letters*, vol. 93, 042 510, 2008.

[8] N. Bergeal, F. Schackert, M. Metcalfe, R. Vijay, V. E. Manucharyan, L. Frunzio, D. E. Prober, R. J. Schoelkopf, S. M. Girvin, and M. H. Devoret, "Phase-preserving amplification near the quantum limit with a Josephson ring modulator," *Nature*, vol. 465, 64, 2010.

[9] N. Roch, E. Flurin, F. Nguyen, P. Morfin, P. Campagne-Ibarcq, M. H. Devoret, and B. Huard, "Widely tunable, nondegenerate three-wave mixing microwave device operating near the quantum limit," *Physical Review Letters*, vol. 108, 147 701, 2012.

[10] A. Roy and M. Devoret, "Introduction to parametric amplification of quantum signals with Josephson circuits," *Comptes Rendus Physique*, vol. 17, 740, 2016.

[11] J. Aumentado, "Superconducting parametric amplifiers: The state of the art in Josephson parametric amplifiers," *IEEE Microwave Magazine*, vol. 21, 45, 2020.

[12] R. J. Schoelkopf and S. M. Girvin, "Wiring up quantum systems," *Nature*, vol. 451, 664, 2008.

[13] A. A. Clerk, M. H. Devoret, S. M. Girvin, F. Marquardt, and R. J. Schoelkopf, "Introduction to quantum noise, measurement, and amplification," *Reviews of Modern Physics*, vol. 82, 1155, 2010.

[14] C. S. Macklin, "Quantum feedback and traveling-wave parametric amplification in superconducting circuits," Ph.D. dissertation, University of California, Berkeley, 2015.

[15] O. Yaakobi, L. Friedland, C. Macklin, and I. Siddiqi, "Parametric amplification in Josephson junction embedded transmission lines," *Physical Review B*, vol. 87, 144 301, 2013.

[16] V. Sivak, N. Frattini, V. Joshi, A. Lingenfelter, S. Shankar, and M. Devoret, "Kerr-free three-wave mixing in superconducting quantum circuits," *Physical Review Applied*, vol. 11, 054 060, 2019.

[17] A. Miano and O. A. Mukhanov, "Symmetric traveling wave parametric amplifier," *IEEE Transactions on Applied Superconductivity*, vol. 29, 1, 2019.

[18] M. Perelshtein, K. Petrovnin, V. Vesterinen, S. Hamedani Raja, I. Lilja, M. Will, A. Savin, S. Simbierowicz, R. Jabdaraghi, J. Lehtinen, L. Grönberg, J. Hassel, M. Prunnila, J. Govenius, G. Paraoanu, and P. Hakonen, "Broadband continuous-variable entanglement generation using a Kerr-free Josephson metamaterial," *Physical Review Applied*, vol. 18, 024 063, 2022.

[19] K. O'Brien, C. Macklin, I. Siddiqi, and X. Zhang, "Resonant phase matching of Josephson junction traveling wave parametric amplifiers," *Physical Review Letters*, vol. 113, 157 001, 2014.

[20] C. Macklin, K. O'Brien, D. Hover, M. E. Schwartz, V. Bolkhovsky, X. Zhang, W. D. Oliver, and I. Siddiqi, "A near quantum-limited Josephson traveling-wave parametric amplifier," *Science*, vol. 350, 307, 2015.

[21] T. C. White, J. Y. Mutus, I.-C. Hoi, R. Barends, B. Campbell, Y. Chen, Z. Chen, B. Chiaro, A. Dunsworth, E. Jeffrey, J. Kelly, A. Megrant, C. Neill, P. J. J. O'Malley, P. Roushan, D. Sank, A. Vainsencher, J. Wenner, S. Chaudhuri, J. Gao, and J. M. Martinis, "Traveling wave parametric amplifier with Josephson junctions using minimal resonator phase matching," *Applied Physics Letters*, vol. 106, 242 601, 2015.

[22] M. T. Bell and A. Samolov, "Traveling-wave parametric amplifier based on a chain of coupled asymmetric squids," *Physical Review Applied*, vol. 4, 024 014, 2015.

[23] L. Planat, A. Ranadive, R. Dassonneville, J. Puertas Martínez, S. Léger, C. Naud, O. Buisson, W. Hasch-Guichard, D. M. Basko, and N. Roch, "Photonic-crystal Josephson traveling-wave parametric amplifier," *Physical Review X*, vol. 10, 021 021, 2020.

[24] A. B. Zorin, "Josephson traveling-wave parametric amplifier with three-wave mixing," *Physical Review Applied*, vol. 6, 034 006, 2016.

[25] A. Ranadive, M. Esposito, L. Planat, E. Bonet, C. Naud, O. Buisson, W. Guichard, and N. Roch, "Kerr reversal in Josephson meta-material and traveling wave parametric amplification," *Nature Communications*, vol. 13, 1737, 2022.

[26] A. B. Zorin, "Flux-driven Josephson traveling-wave parametric amplifier," *Physical Review Applied*, vol. 12, 044 051, 2019.

[27] B. Ho Eom, P. K. Day, H. G. LeDuc, and J. Zmuidzinas, "A wideband, low-noise superconducting amplifier with high dynamic range," *Nature Physics*, vol. 8, 623, 2012.

[28] C. Bockstiegel, J. Gao, M. Vissers, M. Sandberg, S. Chaudhuri, A. Sanders, L. Vale, K. Irwin, and D. Pappas, "Development of a broadband NbTiN traveling wave parametric amplifier for mkid readout," *Journal of Low Temperature Physics*, vol. 176, 1, 2014.

[29] M. R. Vissers, R. P. Erickson, H.-S. Ku, L. Vale, X. Wu, G. C. Hilton, and D. P. Pappas, "Low-noise kinetic inductance traveling-wave amplifier using three-wave mixing," *Applied Physics Letters*, vol. 108, 012 601, 2016.

[30] S. Chaudhuri, D. Li, K. D. Irwin, C. Bockstiegel, J. Hubmayr, J. N. Ullom, M. R. Vissers, and J. Gao, "Broadband parametric amplifiers based on nonlinear kinetic inductance artificial transmission lines," *Applied Physics Letters*, vol. 110, 152 601, 2017.

[31] R. P. Erickson and D. P. Pappas, "Theory of multiwave mixing within the superconducting kinetic-inductance traveling-wave amplifier," *Physical Review B*, vol. 95, 104 506, 2017.

[32] S. Goldstein, N. Kirsh, E. Svetitsky, Y. Zamir, O. Hachmo, C. E. M. de Oliveira, and N. Katz, "Four wave-mixing in a microstrip kinetic inductance travelling wave parametric amplifier," *Applied Physics Letters*, vol. 116, 152 602, 2020.

[33] M. Malnou, M. Vissers, J. Wheeler, J. Aumentado, J. Hubmayr, J. Ullom, and J. Gao, "Three-wave mixing kinetic inductance traveling-wave amplifier with near-quantum-limited noise performance," *PRX Quantum*, vol. 2, 010 302, 2021.

[34] D. J. Parker, M. Savytskyi, W. Vine, A. Laucht, T. Duty, A. Morello, A. L. Grimsmo, and J. J. Pla, "Degenerate parametric amplification via three-wave mixing using kinetic inductance," *Physical Review Applied*, vol. 17, 034 064, 2022.

[35] P. K. Tien, "Parametric amplification and frequency mixing in propagating circuits," *Journal of Applied Physics*, vol. 29, 1347, 1958.

[36] A. L. Cullen, "A travelling-wave parametric amplifier," *Nature*, vol. 181, 332, 1958.

[37] T. Duty, G. Johansson, K. Bladh, D. Gunnarsson, C. Wilson, and P. Delsing, "Observation of quantum capacitance in the Cooper-pair transistor," *Physical Review Letters*, vol. 95, 206 807, 2005.

[38] M. A. Sillanpää, T. Lehtinen, A. Paila, Y. Makhlin, L. Roschier, and P. J. Hakonen, "Direct observation of Josephson capacitance," *Physical Review Letters*, vol. 95, 206 806, 2005.

[39] P. K. Tien and H. Suhl, "A traveling-wave ferromagnetic amplifier," *Proceedings of the IRE*, vol. 46, 700, 1958.

[40] A. L. Grimsmo and A. Blais, "Squeezing and quantum state engineering with Josephson travelling wave amplifiers," *npj Quantum Information*, vol. 3, 20, 2017.

[41] J. A. Armstrong, N. Bloembergen, J. Ducuing, and P. S. Pershan, "Interactions between light waves in a nonlinear dielectric," *Physical Review*, vol. 127, 1918, 1962.

[42] K. Sundqvist, S. Kintas, M. Simoen, P. Krantz, M. Sandberg, C. Wilson, and P. Delsing, "The pumpistor: A linearized model of a flux-pumped superconducting quantum interference device for use as a negative-resistance parametric amplifier," *Applied Physics Letters*, vol. 103, 102 603, 2013.

[43] H. Takahasi, "Information theory of quantum-mechanical channels," in ser. Advances in Communication Systems, A. Balakrishnan, Ed., vol. 1, Elsevier, 1965, 227.

[44] M. T. Raiford, "Degenerate parametric amplification with time-dependent pump amplitude and phase," *Physical Review A*, vol. 9, 2060, 1974.

[45] M. Simoen, "Parametric interactions with signals and the vacuum," Ph.D. dissertation, Chalmers University of Technology, 2015.

[46] T. Dixon, J. Dunstan, G. Long, J. Williams, P. Meeson, and C. Shelly, "Capturing complex behavior in Josephson traveling-wave parametric amplifiers," *Physical Review Applied*, vol. 14, 034 058, 2020.

[47] H. Renberg Nilsson, *Three-wave mixing in Josephson travelling-wave parametric amplifiers*, Licentiate thesis, Chalmers University of Technology, 2022.

[48] M. J. Feldman, P. T. Parrish, and R. Y. Chiao, "Parametric amplification by unbiased Josephson junctions," *Journal of Applied Physics*, vol. 46, 4031, 1975.

[49] J. D. Kraus, *Radio astronomy*. McGraw-Hill, 1966.

[50] M. Malnou, B. T. Miller, J. A. Estrada, K. Genter, K. Cicak, J. D. Teufel, J. Aumentado, and F. Lecocq, *A traveling-wave parametric amplifier and converter*, 2024. arXiv: 2406.19476 [quant-ph].

[51] A. Ranadive, B. Fazliji, G. L. Gal, G. Cappelli, G. Butseraen, E. Bonet, E. Eyraud, S. Böhling, L. Planat, A. Metelmann, and N. Roch, *A traveling wave parametric amplifier isolator*, 2024. arXiv: 2406.19752 [quant-ph].

[52] D. M. Pozar, *Microwave Engineering*. Chichester, 2012.

[53] P. H. Smith, "Transmission line calculator," *Electronics*, vol. 12, 29, 1939.

[54] N. E. Frattini, V. V. Sivak, A. Lingenfelter, S. Shankar, and M. H. Devoret, "Optimizing the nonlinearity and dissipation of a SNAIL parametric amplifier for dynamic range," *Physical Review Applied*, vol. 10, 054 020, 2018.

[55] A. B. Zorin, "Quasi-phasematching in a poled Josephson traveling-wave parametric amplifier with three-wave mixing," *Applied Physics Letters*, vol. 118, 222 601, 2021.

[56] A. Kamal, A. Marblestone, and M. Devoret, "Signal-to-pump back action and self-oscillation in double-pump Josephson parametric amplifier," *Physical Review B*, vol. 79, 184 301, 2009.

[57] A. Barone and G. Paternò, *Physics and applications of the Josephson effect*. John Wiley & Sons, Inc., 1982.

[58] N. Maleeva, L. Grünhaupt, T. Klein, F. Levy-Bertrand, O. Dupre, M. Calvo, F. Valenti, P. Winkel, F. Friedrich, W. Wernsdorfer, A. V. Ustinov, H. Rotzinger, A. Monfardini, M. V. Fistul, and I. M. Pop, "Circuit quantum electrodynamics of granular aluminum resonators," *Nature Communications*, vol. 9, 3889, 2018.

[59] V. Gaydamachenko, C. Kissling, R. Dolata, and A. B. Zorin, "Numerical analysis of a three-wave-mixing Josephson traveling-wave parametric amplifier with engineered dispersion loadings," *Journal of Applied Physics*, vol. 132, 154 401, 2022.

[60] G. L. Matthaei, L. Young, and E. M. T. Jones, *Microwave filters, impedance-matching networks, and coupling structures*. Norwood: McGraw-Hill Book Company, Inc., 1964.

[61] M. Steer, *Microwave and RF Design IV: Modules*. North Carolina State University, 2024.

[62] K. Sundqvist and P. Delsing, "Negative-resistance models for parametrically flux-pumped superconducting quantum interference devices," *EPJ Quantum Technology*, vol. 1, 6, 2014.

[63] R. Engelbrecht and K. Kurokawa, "A wide-band low noise l-band balanced transistor amplifier," *Proceedings of the IEEE*, vol. 53, 237, 1965.

[64] P. de Groot, "Cmos compatible fabrication methods for submicron Josephson junction qubits," English, *IEE Proceedings - Science, Measurement and Technology*, vol. 148, 225, 2001.

[65] K. Khor, K. Cheng, L. Yu, and F. Boey, "Thermal conductivity and dielectric constant of spark plasma sintered aluminum nitride," *Materials Science and Engineering: A*, vol. 347, 300, 2003.